

Coupling of the Yeast Metabolic Cycle and the Cell
Division Cycle in Populations and Single Cells

by

Anthony James Burnetti

University Program in Genetics and Genomics
Duke University

Date: _____

Approved:

Nicolas Buchler, Supervisor

Paul Magwene, Chair

Philip Benfey

Amy Schmid

Dissertation submitted in partial fulfillment of the requirements for the degree of
Doctor of Philosophy in the University Program in Genetics and Genomics
in the Graduate School of Duke University
2017

ABSTRACT

Coupling of the Yeast Metabolic Cycle and the Cell Division
Cycle in Populations and Single Cells

by

Anthony James Burnetti

Univeristy Program in Genetics and Genomics
Duke University

Date: _____

Approved:

Nicolas Buchler, Supervisor

Paul Magwene, Chair

Philip Benfey

Amy Schmid

An abstract of a dissertation submitted in partial fulfillment of the requirements for
the degree of Doctor of Philosophy in the University Program in Genetics and
Genomics
in the Graduate School of Duke University
2017

Copyright © 2017 by Anthony James Burnetti
All rights reserved except the rights granted by the
Creative Commons Attribution-Noncommercial Licence

Abstract

Biological oscillators are ubiquitous in living systems. They allow cellular processes to anticipate and act in synchrony with regular events in the outside world (such as the day/night cycle), or they ensure that processes occur in a particular order. Living things typically contain multiple oscillators, which can often couple to each other and influence each other's timing and function. The purpose of this thesis has been to investigate the relationship between two coupled oscillators in *Saccharomyces cerevisiae*: the yeast metabolic cycle and the cell division cycle. I have focused on two key questions: what is the biological significance of their coupling, and is one oscillator dominant in its interaction with the other?

First, I investigated the temporal relationship between the cell division cycle and metabolic shifts that occur during the metabolic cycle across diverse yeast strains. I showed that a particular cell cycle event (DNA replication) was consistently delayed relative to a metabolic event (entry into the high oxygen consumption phase). This suggested that an earlier cell cycle event (Start and commitment to the cell cycle) was tied to the onset of high oxygen consumption. Second, I used fluorescent probes to examine the relationship between the metabolic cycle and the commitment to cell cycle progression at single-cell resolution. This revealed that cells enter high oxygen consumption phase of the metabolic cycle before passing Start, supporting a model of metabolic cycle/cell division cycle coupling in which the shorter metabolic cycle controls cell cycle commitment, likely via modulation of cell size thresholds.

Contents

Abstract	iv
List of Tables	ix
List of Figures	x
List of Abbreviations and Symbols	xii
Acknowledgements	xiv
1 Introduction	1
1.1 Overview and Significance	1
1.2 Background	3
1.2.1 The Yeast Metabolic Cycle	3
1.2.2 Cell to Cell Coupling Versus Cell-Autonomous Behavior	8
1.2.3 Coupling Between the Yeast Metabolic Cycle and Cell Division Cycle	9
1.2.4 Regulation of the Cell Division Cycle and Potential Mecha- nisms of YMC/CDC Coupling	11
2 Relationship Between the YMC and CDC Across Strains and Growth Rates	16
2.1 Introduction	16
2.1.1 Strains	17
2.1.2 Determining a Universal Growth Medium	19
2.1.3 Chemostat Operation	20

2.1.4	Calibrating Chemostat pO_2 Measurements	21
2.1.5	pO_2 Reflects the Instantaneous Rate of Oxygen Consumption	24
2.1.6	YMC Sampling and Data Collection	25
2.1.7	Data Analysis	27
2.2	Results	29
2.2.1	Effects of Growth Rate on the Yeast Metabolic Cycle	29
2.2.2	Timing of DNA Replication	37
2.3	Discussion	42
2.3.1	Biological Significance of the Yeast Metabolic Cycle	42
2.3.2	Response of the YMC to Growth Rate	44
2.3.3	Similarity of YMC Dynamics to Bacterial Growth Laws	46
2.3.4	Potential Reasons for Metabolic Cycling in Yeast	47
2.3.5	Timing of DNA Replication	48
2.4	Contributions and Publications	49
3	Timing of Cell Cycle Start During the YMC at Single Cell Resolution	51
3.1	Introduction	51
3.1.1	Measuring Cell Cycle Start in Single Cells	53
3.1.2	Cell Size and Replicative Age	53
3.1.3	Strains and Genotypes	55
3.1.4	Chemostat Sampling and Microscopy	57
3.1.5	Microscopy Image Analysis	59
3.1.6	pHluorin Flow Cytometry	61
3.2	Results	62
3.2.1	Measurement of Metabolic State With pHluorin	62
3.2.2	Cell Size and Replicative Age	64

3.2.3	Timing of Cell Cycle Start Relative to HOC entry	65
3.2.4	Artificial Induction of HOC	68
3.2.5	Numerical Analysis of Cell Cycle Start Timing in Subpopulations of Cells	71
3.2.6	Timing Analysis	74
3.2.7	Rate of Commitment and Fraction of Cells Committing	76
3.3	Discussion	79
3.3.1	Cell cycle Start Occurs <i>After</i> Entry into HOC	79
3.3.2	Standard Models of Cell Size Control May Explain Observed YMC/CDC Coupling	81
3.3.3	Short-Period Oscillators Dominate Long-Period Oscillators in Coupled Systems	86
3.3.4	YMC/CDC Crosstalk May Lead to Mutual Coupling	88
3.4	Contributions	91
4	Conclusions	93
4.1	The Yeast Metabolic Cycle Segregates Cell Growth/Division Into Pulses	93
4.2	The YMC Drives Cell Cycle Commitment	94
4.3	Potential Mutual Coupling of the YMC and CDC	94
5	Additional Materials and Methods	96
5.1	Strains	96
5.2	Chemostat Equipment	97
5.3	Growth Medium	100
5.4	Chemostat Culture and Sampling for DNA Replication Analysis	100
5.5	Data Analysis - DNA Replication Timing and Yeast Metabolic Cycle Analysis	102
5.6	Chemostat Culture and Sampling for Cell Cycle Start Analysis	103
5.7	Microscopy and Image Segmentation	104

5.8	Data Analysis - Cell Cycle Start	105
5.9	Measurement of Cytosolic pH With pHluorin Via Flow Cytometry . .	107
A	Quantification of CDC Commitment	109
	Bibliography	112
	Biography	121

List of Tables

2.1	YMC Parameter Fits	33
2.2	DNA Replication Timing	44
5.1	Yeast Strains - Cell Cycle Start Analysis	97
5.2	Oligonucleotides Used for Transformation and Confirmation of Yeast.	98
5.3	Plasmids Used for Transformation of Yeast.	98
A.1	DBY12007 Natural Oscillations	109
A.2	GZ240/241 Natural Oscillations	110
A.3	GZ240/241 Artificial HOC Induction	111

List of Figures

1.1	Chemostat Growth Conditions	5
1.2	Genetically and Metabolically Defined YMC Phases	6
1.3	Yeast Size Homeostasis	12
1.4	Cell Cycle Start Network	13
2.1	Typical Chemostat Setup.	21
2.2	Chemostat Parameter Analysis	24
2.3	Metabolic Cycle Phases.	27
2.4	Strain-Specific YMC Waveforms.	29
2.5	Effect of Growth Rate on YMC.	31
2.6	YMC Behavior for All Strains - Period	33
2.7	Mixed Model Minimizes Residuals	34
2.8	YMC Behavior for All Strains - Frequency	35
2.9	HOC Occupancy Vs Growth Rate	36
2.10	HOC Saturates at Maximum Aerobic Respiration Rate	37
2.11	DNA Replication Across Strains	39
2.12	DNA Replication Across Growth Rates	40
2.13	DBY12007 - DNA replication data	41
2.14	YPS670 - DNA replication data	42
2.15	Timing of DNA Replication Tied to HOC Entry	43
3.1	Observing Start	54

3.2	Cell Cycle Start Observed via Microscopy	56
3.3	Sampling of Chemostat Chambers for Cell Cycle Start Measurements	58
3.4	Automatic Identification of Division-Committed Cells	60
3.5	Cytosolic pH As A Proxy for Energy State During the YMC	63
3.6	Size Distribution of Mother, Daughter Cells	65
3.7	HOC Entry and Start	66
3.8	Natural Oscillations	67
3.9	Artificial Induction - Metabolic Effects	69
3.10	Artificial Induction - Start	70
3.11	Artificial Induction - Subpopulations	71
3.12	Spline Interpolation	73
3.13	Behavior of Subpopulations	74
3.14	Oscillation - T_c	75
3.15	Induction - T_c	76
3.16	Oscillation - F_{max}	77
3.17	Oscillation - R_{max}	77
3.18	Induction - F_{max}	78
3.19	Induction - R_{max}	78
3.20	Carbon Metabolism and Cell Cycle Start	80
3.21	Size Control of Cell Cycle Start	82
3.22	Size Control and the YMC	84
3.23	Growth of Cells During HOC	85
3.24	Possible YMC/CDC Feedback Loop	89
3.25	Artificial HOC Induction and CDC to YMC Coupling	91

List of Abbreviations and Symbols

Abbreviations

CDC	Cell Division Cycle
YMC	Yeast Metabolic Cycle
HOC	High Oxygen Consumption phase of the yeast metabolic cycle, in which the lower 65% of the range of observed dissolved oxygen levels occurs.
LOC	Low Oxygen Consumption phase of the yeast metabolic cycle, in which the upper 35% of the range of observed dissolved oxygen levels occurs.
CV	Coefficient of Variation, the standard deviation of a value in a population divided by the mean of the value. CV of the Whi5-Tomato pixel intensity in yeast cell images is used to determine commitment to the cell division cycle.

Symbols - Chemostat Culture

D	Dilution rate of a chemostat culture, in volumes per hour.
pO_2	Actual partial pressure of O_2 in a chemostat chamber as a fraction of saturation.
pO_{2m}	Measured partial pressure of O_2 in a chemostat chamber as a fraction of saturation
pO_2^*	Equilibrium partial pressure of O_2 in a chemostat chamber which pO_2 approaches over time via diffusion of O_2 from air
τ_{ymc}	Length of the yeast metabolic cycle
f_{ymc}	Frequency of the yeast metabolic cycle

τ_{cdc}	Population/biomass doubling time ()
f_{cdc}	Average frequency of cell division cycle ($1/\tau_{cdc}$)
τ_{hoc}	Length of high oxygen consumption phase of the yeast metabolic cycle
τ_{loc}	Length of low oxygen consumption phase of the yeast metabolic cycle
Δ	Interval between entry into HOC phase of the yeast metabolic cycle and the time at which half of cells that will enter S/G2/M phase of the cell division cycle have done so
Δ_s	Interval between entry into HOC phase of the yeast metabolic cycle and the time at which the maximum fraction of cells are in S phase
ϕ_{hoc}	Fraction of time that a yeast culture spends in high oxygen consumption phase of the yeast metabolic cycle
τ_r	Response time of pO2 probe
k	Oxygen mass-transfer coefficient of chemostat chamber
QCO_2	Average rate of production of CO_2 during chemostat growth
QO_2	Average rate of consumption of O_2 during chemostat growth

Symbols - Cell Cycle Start analysis

T_c	Commitment time at which half of a population of cells that will commit to cell cycle progression have committed.
R_{max}	Maximum rate of commitment of a population of cells to cell cycle progression.
F_{max}	Maximum fraction of a population of cells that will commit to cell cycle progression during a metabolic cycle or artificial metabolic cycle induction.
p	Spline fitting parameter. Larger values of p will result in smoothing splines that are less smooth but more closely fit the data-points provided.

Acknowledgements

I would like to thank Professor Nicolas Buchler, my advisor, for the opportunity and freedom to choose a unique direction and focus when I joined his group. He has provided support and guidance over the course of my project and helped me improve my science communication skills. Mert Aydin, Shiyu Liu, Selcan Aydin, and all other Buchler laboratory members and collaborators have provided valuable assistance and advice that has allowed me to accomplish what I have, and made this a great place to work.

I am thankful for the time and advice of my thesis committee members: Professor Amy Schmid, Professor Paul Magwene, and Professor Philip Benfey. Their advice and ideas have helped shape this project since its beginning. I have also had the good fortune to obtain vital materials for my work from David Botstein, Benjamin Tu, Bruce Futcher, David Isom, and Daniel Lew, among others. Without them I could not have pursued this work as far as I have. The Strahl laboratory at UNC have been ongoing collaborators on additional projects, and I welcome the possibility of continuing to work with them.

I could not have accomplished this work without support from the DARPA Biochronicity Grant, the NIH Directors New Innovator Award, the Burroughs Wellcome Fund, and the Duke Graduate School. I'd like to thank Dr. Stephen Mount, Dr. Raman Sood, Dr. William Pavan, Dr. Kyungjae Myung, and Professor Debra Silver for giving me my first golden opportunities to get involved in research, and

Mr. Bunday for all his encouragement in high school. I finally want to thank all my friends I have made in Durham and all my old friends from the Blue House who have gone through this adventure with me, and my family who have been there from the beginning at a moment's notice.

Introduction

1.1 Overview and Significance

Biological oscillators and clocks are present in many living organisms, often serving multiple functions. They anticipate environmental changes, allowing an organism to pre-adapt to periodic shifts. They also coordinate internal processes that must be separated in time from each other or must occur in a particular order. The abundance of biological oscillators ensures that several of them co-exist in cells and organisms. The interaction of those biological oscillators influences processes of fundamental importance as diverse as metabolism, day/night cycles, and cell division.

My dissertation seeks to understand the connection between two biological oscillators in budding yeast: the yeast metabolic cycle in which cultures grown in chemostat conditions alternate between the buildup and consumption of carbon stores in synchrony with each other, and the cell division cycle by which cells coordinate growth with replication and segregation of DNA before cell division. Specifically, I seek to understand the relationship between the timing of a cell's commitment to the cell cycle at a well-studied checkpoint known as "Start" and the sudden metabolic shifts

that occur during the yeast metabolic cycle. Have these two oscillators evolved to coordinate specific metabolic events with cell cycle Start or, as proposed by others, to separate cell cycle events from incompatible metabolic processes? In order to answer this question, I have pursued multiple lines of research to measure cell cycle and metabolic events in *populations* and at the *single cell* level.

In Chapter 2, I describe a *systematic analysis* of the relationship between the phase of the metabolic cycle and the onset of DNA replication at the population level in a cycling chemostat. I measured the relative timing of metabolic and cell cycle events across four genetically diverse yeast strains at multiple rates of growth in the same growth medium. Previous work on the yeast metabolic cycle focused on two different laboratory strains of yeast, grown in different media at different growth rates. All previous studies observed pulses of cell division occurring once per metabolic cycle, but they arrived at a contradictory set of conclusions regarding whether DNA replication was strictly separated from the high oxygen consumption (HOC) phase of the metabolic cycle and the biological meaning of the coupling. By comparing the timing of DNA replication and the behavior of the metabolic cycle in multiple strains and at multiple growth rates in the same medium, I uncovered a *fixed length of time* between the metabolic shift from low oxygen consumption phase to high oxygen consumption phase and the later onset of DNA replication. This relationship suggests a close connection between the onset of HOC phase and cell cycle ‘Start’ - the tightly regulated commitment to cell cycle progression that occurs before DNA replication. This is significant because it demonstrates coordination between a *single event* in each cycle. I also discovered a linear relationship between growth rate and the ratio of time spent in low and high oxygen consumption phases of the metabolic cycle itself. This suggests a biological reason for the YMC to exist - yeast may control their average metabolic rate by altering the frequency of pulses of maximal metabolism rather than smoothly ramping metabolism as bacteria do.

In Chapter 3, I examined *individual cells* during coupled metabolic and cell division cycles in a chemostat. In order to determine the relationship between Start and onset of high oxygen consumption, I fused a fluorescent protein to Whi5, a critical regulator of cell cycle Start. Its subcellular localization is one of the most reliable indicators of cell cycle Start, and is the point in the cell division cycle which is closely regulated by checkpoints and signaling pathways. I measured the timing of cell cycle commitment during metabolic cycles and the properties (size, age) of those cells which do and do not divide during a given cycle. This has allowed me to conclude that for yeast cells in a synchronized chemostat population, the cell cycle is driven by metabolism in a manner consistent with increased metabolic carbon flux during HOC phase triggering the production of Cln3, a factor which pushes forward cell cycle Start by lowering the size threshold for division to commence.

My results demonstrate that cell cycle Start is preceded and likely driven by the onset of high oxygen consumption phase that occurs once per metabolic cycle. This opens new avenues of research on the detailed mechanisms of coupling between them, which I describe at the end of Chapter 3. Before describing my results in detail, the remainder of this chapter provides an introduction to previous research on both of these biological cycles.

1.2 Background

1.2.1 *The Yeast Metabolic Cycle*

The yeast metabolic cycle, or YMC, occurs in slow-growing aerobic cultures of *Saccharomyces cerevisiae* [Kaspar von Meyenburg, 1969]. This phenomenon is also called the yeast respiratory oscillation or ultradian metabolic oscillations. The YMC is a synchronous population behavior observed in well-mixed fully aerobic cultures. The rates of numerous metabolic processes are observed to oscillate with a period between 45 minutes and several hours during this cycle depending on the strains and

growth rates examined [Kaspar von Meyenburg, 1969; Tu et al., 2005; Slavov and Botstein, 2011; Keulers et al., 1996; Satroutdinov et al., 1992]. The dissolved oxygen in the culture medium is most clearly observed to oscillate, switching between a high oxygen consumption (HOC) state and a low oxygen consumption (LOC) state, and a single large pulse of cell division is observed to occur once per cycle.

The YMC is most readily observed in chemostat culture. A chemostat is a form of continuous-flow bioreactor, in which a flow of fresh media is constantly added to a growth chamber at the same rate that depleted media and cells are removed (Fig. 1.1). Under these conditions cells grow to a steady state concentration at which rate of uptake of the limiting reagent in the fresh media is equal to its rate of addition, with the average population doubling time inversely proportional to the dilution rate. Growth rate and the rate of cell division can thus be closely controlled by regulating the rate of media flow. The average doubling time of a chemostat culture, τ_{cdc} , is equal to:

$$\tau_{cdc} = \ln(2)/D \tag{1.1}$$

where D represents the dilution rate of the chamber in volumes per unit time. The average frequency of cell division f_{cdc} represents the inverse of τ_{cdc} . Once steady state is reached, media composition is relatively constant compared to batch growth without the temporal structure of diauxic shifts from one nutrient to another or the onset of stationary phase. This allows detailed metabolic and genetic studies of cells in particular metabolic states without confounding dynamic factors [Brauer et al., 2005].

For chemostat studies of the YMC, carbon is generally maintained as the limiting reagent either in the form of glucose or ethanol. After cells are grown to saturation, the YMC will either slowly begin to spontaneously appear during constant flow or

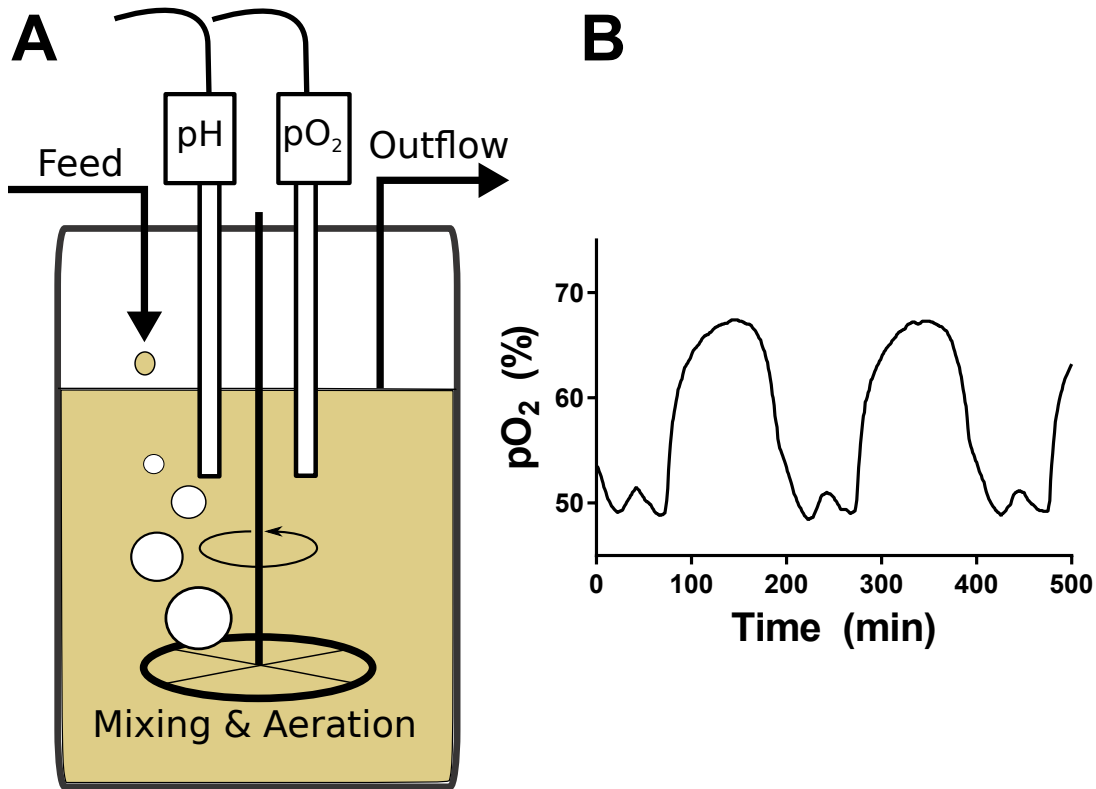


FIGURE 1.1: Chemostat growth. In a chemostat chamber (A), a yeast culture is stirred and aerated while fed fresh media at a constant dilution rate (D , volumes/hr). Depleted media and cells are removed at the same rate via an outflow tube. Cell growth reaches an equilibrium in which media composition is roughly constant and the rate of growth equals the dilution rate of the media. Probes constantly measure pH and pO_2 . (B) During continuous growth, metabolic oscillations are detectable by rhythmic changes in pO_2 .

quickly appear in response to a sudden shock to growth rate or media composition. While chemostat conditions are necessary to observe the YMC using glucose as a carbon source, it can also be observed during batch growth on nonfermentable ethanol [Slavov et al., 2011] or the slowly-consumed disaccharide trehalose [Jules et al., 2005] as a sole carbon source. It can also be observed transiently during a diauxic shift from glucose to ethanol during batch growth [Mochan and Pye, 1973]. As such, while chemostat conditions are the most common context in which synchronous yeast metabolic oscillations are induced and observed, the YMC is not an

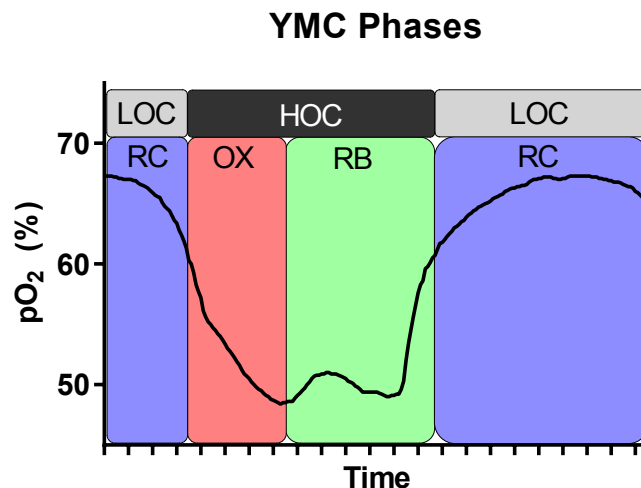


FIGURE 1.2: Phases of the yeast metabolic cycle, defined both according to oxygen metabolism and gene expression. Metabolism defines two phases. Low oxygen consumption phase (LOC, gray) is characterized by the buildup of storage carbohydrates trehalose and glycogen, while high oxygen consumption phase (HOC, black) is characterized by the aerobic consumption of storage carbohydrates, production of ethanol/acetate/acetaldehyde in early HOC, and consumption of these metabolites in late HOC. Gene expression defines three phases [Tu et al., 2005]. Oxidative phase (OX, red) is characterized by expression of ribosome biogenesis genes and amino acid anabolism genes. Reductive building phase (RB, green) is characterized by expression of cell cycle genes, mitochondrial biogenesis and mitoribosome genes. Reductive charging (RC, blue) is characterized by expression of fatty acid catabolism and stress response genes. HOC phase corresponds roughly to the combined OX and RB phases, LOC phase corresponds roughly to RC phase. Model from Tu et al., 2005, with pO_2 data from my work.

artifact of chemostat conditions.

Oxygen consumption is the most easily measured of many cellular processes that are known to oscillate as part of the YMC. However, intracellular levels of numerous substances rise and fall in a predictable phase relationship [Lloyd and Murray, 2005]. NAD(P)H reproducibly reaches a minimal value at the shift from low oxygen consumption to high oxygen consumption, rising thereafter [Lloyd et al., 2002; Lloyd and Murray, 2007; Tu et al., 2007]. Cellular redox state, as measured by

glutathione cycles, exhibits large-scale oxidation during periods of high oxygen consumption [Murray et al., 2001, 1999]. Cellular acetyl-coA levels rise dramatically during HOC, as does the global level of chromatin acetylation [Tu et al., 2007; Shi and Tu, 2013a]. The levels of the storage carbohydrates trehalose and glycogen rise continuously over the course of LOC phase before being rapidly consumed during HOC phase [Shi et al., 2010]. These storage carbohydrates provide much of the carbon that is consumed aerobically and contributes to the acetyl-coA and NAD(P)H pool [Tu et al., 2007; Cai et al., 2011]. Yeast unable to produce trehalose exhibit an extremely unstable YMC [Xu and Tsurugi, 2007]. Yeast appear to temporally segregate high rates of metabolic carbon flux into HOC phase, and accumulate storage carbohydrates over the course of LOC phase to help fuel this high flux.

Large numbers of genes are expressed cyclically during the YMC. Transcriptome and chromatin analysis timecourses have revealed a number of reproducible clusters of genes expressed over the course of the YMC, broadly separable into three clusters - see Fig. 1.2 [Tu et al., 2005; Machné and Murray, 2012; Kuang et al., 2014]. The first cluster, termed ‘oxidative’, is expressed during the initial increase in oxygen consumption rate of early HOC phase. This cluster includes many genes involved in ribosome biogenesis and amino acid anabolism. The second cluster, termed ‘reductive building’, is expressed during late HOC phase until the sudden drop in oxygen consumption at the beginning of LOC phase. This cluster includes large numbers of DNA-replication and mitotic genes, as well as genes involved in mitochondrial biogenesis and mitoribosome production. The third cluster, termed ‘reductive charging’, is expressed during the majority of LOC phase, and includes lipid catabolism genes and stress response pathways. This cyclical gene expression appears to produce a ‘just-in-time’ supply chain, building cellular elements at exactly the time they are used during the YMC [Kuang et al., 2014] and concentrating the production of growth-associated genes into the period in which there is ample metabolic carbon flux to

support anabolism [Slavov et al., 2012].

1.2.2 Cell to Cell Coupling Versus Cell-Autonomous Behavior

One of the most striking aspects of the YMC is its stability and robustness. Once a cycle is initiated, the oscillation can continue uninterrupted for weeks if media flow is maintained. Cell to cell differences in YMC or CDC period fail to lead to a loss of synchrony, unlike artificially synchronized cell division cycles which rapidly fall out of phase with each other during batch growth. This self-organizing synchrony is due to metabolic coupling between cells via small molecule metabolite signals. The two-carbon products of anaerobic or aerobic glycolysis - ethanol, acetate, and acetaldehyde - have all been observed to phase-shift the metabolic cycle when added to a cycling chamber [Martegani et al., 1990; Murray et al., 2003; Robertson et al., 2008; Cai et al., 2011]. These metabolites induce an early HOC phase when added during LOC, and phase-advance the next cycle in late HOC but delay it when added during early LOC [Robertson et al., 2008; Cai et al., 2011; Shi and Tu, 2013b]. Two-carbon metabolites are produced during early HOC/oxidative phase and later consumed during late HOC/reductive building phase [Murray et al., 2003; Porro et al., 1988; Martegani et al., 1990]. They thus represent an extremely important synchronizing signal along with H₂S, which is produced during early LOC and causes respiratory chain inhibition [Sohn et al., 2000].

Chemostat growth is quite different from the natural environment of yeast. The well-mixed fluid environment allows diffusible signals to couple the entire population on very short timescales. It has been suggested that the YMC is an artifact of the unnatural conditions that these cells were placed under, where large pulses of metabolite production built up in dense culture are thought to drive behavior that would not naturally occur in individual cells [Porro et al., 1988; Martegani et al., 1990]. However, recent research supports the conclusion that the YMC is both nat-

ural and cell-autonomous. A study of yeast from *non-oscillating* chemostat cultures by the Botstein laboratory [Silverman et al., 2010] examined the levels of mRNAs in individual cells by single-molecule FISH, focusing on genes that had been previously shown to oscillate in chemostat cultures undergoing a YMC. It was found that the levels of mRNAs expressed during different YMC phases in oscillating cultures were still anticorrelated in non-oscillating cultures. mRNAs from the same YMC phase were tightly correlated in the same cultures. This led them to conclude that, “the yeast metabolic cycle is an intrinsic property of yeast metabolism and does not depend on either synchronization or external limitation of growth by the carbon source” [Silverman et al., 2010]. More recently, the Heinemann laboratory has shown that individual yeast cells in non-chemostat conditions exhibit a regular metabolic oscillation over a wide range of growth rates [Papagiannakis et al., 2016]. Using live-cell microscopy, they observed cycles in NAD(P)H and ATP levels in single cells similar to those observed in synchronous chemostat populations. These metabolic oscillations couple to the cell division cycle at a similar phase and timeframe. It has thus been proposed that this metabolic cycle represents a vital intrinsic rhythm in the life of the cell, which coordinates alternating periods of rapid growth and quiescence with each other [Slavov et al., 2012] and coordinates the biosynthesis versus breakdown of important cellular components [Papagiannakis et al., 2016].

1.2.3 Coupling Between the Yeast Metabolic Cycle and Cell Division Cycle

The coupling between the YMC and the cell division cycle (CDC) has been noted since its first descriptions [Kaspar von Meyenburg, 1969; Porro et al., 1988]. In all cases examined, a single pulse of DNA replication occurs per metabolic cycle. In strain IFO0233, studied by the Kuriyama and Murray laboratories, DNA replication was observed only during LOC/reductive charging phase [Keulers et al., 1996; Klevecz et al., 2004]. It was first proposed by these groups that DNA replication

was segregated into this phase of the YMC in order to reduce oxidative damage to DNA during replication. Subsequent work from the McKnight laboratory supported the hypothesis using strain CEN.PK. The authors found that DNA replication was relegated to the transcriptionally-defined ‘reductive building’ phase of the YMC, which was interpreted as a period of low oxidative stress [Tu et al., 2005]. Follow-up work [Chen et al., 2007] showed that yeast bearing mutations in cell cycle genes had shorter metabolic cycles, less synchronous waves of cell division, greater spread in the timing of DNA replication during the YMC, and elevated mutation rates in oscillatory conditions.

Subsequent work by the Botstein laboratory showed that in strain DBY12007, a wave of DNA replication occurs during early LOC phase at high growth rates [Slavov and Botstein, 2011]. However, when varying the growth rate of their culture they observed this wave of DNA replication occurring in mid HOC phase at lower growth rates. Not only could DNA replication occur in a phase of the YMC deemed mutagenic by previous research, but growth rate was capable of resetting the apparent phase relationship between the YMC and CDC. This showed that the relative phase relationship of the YMC and CDC is more complicated than had been previously appreciated.

A previous model of YMC/CDC coupling suggested that there was no autonomous YMC at all, and that secreted metabolites maintained a synchronized cell division cycle alone in which metabolic shifts reflect the differences in metabolic behavior between different cell cycle phases [Porro et al., 1988; Martegani et al., 1990]. However, experiments from the Botstein laboratory have investigated the ability of cells to undergo metabolic oscillations in the absence of progression of the cell division cycle [Slavov et al., 2012]. By growing yeast in phosphate-limited batch culture with ethanol as a sole carbon source they completely arrested division, but still observed a regular YMC with metabolic and gene expression profiles similar to that observed in

chemostat growth. This indicates that while YMC and CDC are normally coupled, the YMC can occur in the absence of cell division.

It has been widely hypothesized that there could be an ancestral relationship between the YMC and circadian rhythms [Lloyd and Murray, 2005, 2007; Causton et al., 2015]. Circadian rhythms share a strong redox-state oscillation with the yeast metabolic cycle [O'Neill and Reddy, 2011; Edgar et al., 2012; Wang et al., 2012], and they also couple to the cell division cycle with a single pulse of cell division occurring once per day in mammalian tissue and tissue culture [Scheving et al., 1978; Matsuo et al., 2003; Gérard and Goldbeter, 2012]. The yeast metabolic cycle also behaves in a temperature compensated fashion in some strains, much like the circadian rhythm [Murray et al., 2001]. However, the true mechanistic and evolutionary relationship between the YMC and circadian cycles remains uncertain. Whatever the case, the phenomenon of coupled oscillators is widespread in living systems and the relationships between multiple oscillators which coexist in the same cell are relevant to nearly every process in biology.

1.2.4 Regulation of the Cell Division Cycle and Potential Mechanisms of YMC/CDC Coupling

Control of cell division has been studied for decades in *Saccharomyces cerevisiae*. In the 1970s, the Hartwell laboratory demonstrated that cells arrested in the cell division cycle were able to continue growing without progression through the CDC. They also showed that accumulating the required biomass to divide was usually the slowest, rate-limiting step for cell division rather than the mechanics of progression through S, G2, or M phases of the cell division cycle [Johnston et al., 1977]. This meant that yeast must have a size homeostasis mechanism to ensure they divide at a rate appropriate for their biomass accumulation.

The Jagadish and Lord groups later proposed that a minimal size threshold for

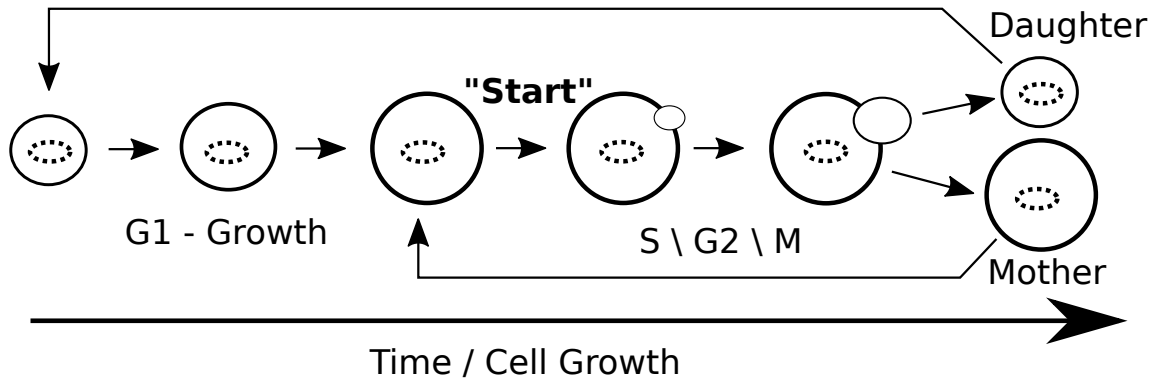


FIGURE 1.3: Growth, size, and cell cycle Start in mother and daughter cells. Large mothers are able to re-divide rapidly after a small amount of growth, while daughters must grow significantly before reaching the critical size threshold required for division.

commitment to progression of the cell division cycle - known as “Start” in yeast - could explain the persistent difference in cell cycle duration between subpopulations of yeast cells in culture [Carter and Jagadish, 1978; Tyson and Lord, 1979]. Yeast cells divide asymmetrically with large ‘mother’ cells budding to produce small ‘daughters’ once per cell division cycle, and these daughters require significantly more time to grow and become competent to commit to the cell cycle - see Fig. 1.3.

Size homeostasis is a very important process in the reproduction of yeast, as division must be coordinated with biomass production. Cells must neither be allowed to accumulate excessive biomass before division (which leads to ever-increasing cell sizes), nor divide more frequently than biomass doubles (which leads to decreasing cell size) [Turner et al., 2012].

Study of the molecular mechanisms of cell cycle regulation in yeast has led to a reliable model of cell cycle Start control which has informed the study of the same process in other organisms. The cyclin dependent kinase, Cdk1, is the primary coordinator of cell cycle progression acting in response to the levels of oscillating

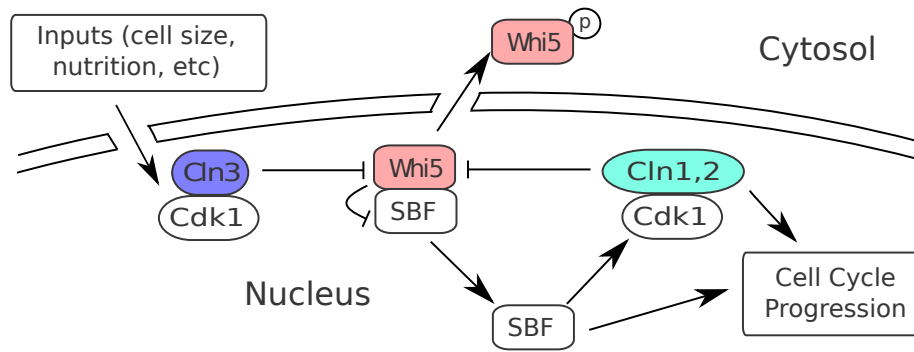


FIGURE 1.4: The cell cycle Start network in *Saccharomyces cerevisiae*. Whi5 binds to and inhibits SBF, a primary G1/S transition transcription factor, during G1 phase. Active Cln3-Cdk1 complex phosphorylates Whi5, causing its export from the nucleus. When nuclear Whi5 level drops below a critical threshold, Cln1p and Cln2p are produced, further phosphorylating and exporting Whi5 until it is entirely cytosolic. Whi5 returns to the nucleus at the M/G1 transition. Cellular nutrition and environment influence the progression of cell cycle Start, as does cell growth/size.

proteins known as cyclins, which direct its activity towards different substrates. The commitment to cell cycle Start, after which an attempt to replicate DNA and divide is assured, is regulated by a network of G1 cyclins, transcription factors, and inhibitors (Fig. 1.4). The G1/S cyclin Cln3 controls the progression through Start by triggering the phosphorylation and inactivation of Whi5, an inhibitor of the transcription factor SBF [Costanzo et al., 2004; De Bruin et al., 2004]. Phosphorylated Whi5 is exported from the nucleus and SBF is disinhibited, leading to the expression of S phase genes including the cyclins Cln1 and Cln2 [Nasmyth and Dirick, 1991; Ogas et al., 1991; Sidorova and Breeden, 1993]. These additional G1/S cyclins further inhibit Whi5 leading to a switch-like transition at the beginning of the cell cycle [Skotheim et al., 2008]. Regulation of this event at Start by Cln3 is the primary mechanism by which yeast control when commitment to the cell cycle occurs, and size is sensed. Whi5 remains delocalized during the entirety of S/G2/M phase of the cell division cycle, and relocalizes to the nuclear compartment upon return to G1 (Fig. 1.3).

Recent work by the Skotheim laboratory has developed a molecular model of cell

cycle Start (involving Cln3 and Whi5) and yeast size homeostasis. They demonstrate that size is sensed through the differential level of expression of Cln3 and the cell cycle inhibitor Whi5. As a cell grows, the total Cln3 expression level is seen to scale with cell size while the total level of Whi5 per cell is size-independent. As cells grow the Cln3 to Whi5 ratio increases until the Cln3 overwhelms Whi5 at some critical threshold [Schmoller et al., 2015]. This provides a molecular mechanistic basis for yeast size control, which can be integrated with other cellular processes.

Size control has been proposed as a mechanism of coupling between the YMC and CDC [Porro et al., 1988; Martegani et al., 1990]. The authors proposed that growth rate changes as a result of oscillating media composition during the YMC. This in turn changes the critical size threshold at which division occurs and the rate at which cells reach it. For example, during LOC the media contains very little glucose, and the mobilization of storage carbohydrates and the production of ethanol or other two-carbon metabolites during HOC may allow faster biomass production, which causes cells to pass their critical Start size at a faster rate. However, cell-autonomous mechanisms of coupling the YMC and CDC have also been proposed.

There are two proposed molecular mechanisms by which the cyclin/CDK oscillator could be tied to the YMC, which have very different implications. The first is based on recent work by the Tu laboratory that has identified the changing cellular level of acetyl-coA during the YMC as a major determinant of chromatin acetylation, driving much cyclical gene expression [Cai et al., 2011; Kuang et al., 2014]. This metabolically-driven gene expression pulse during reductive building and reductive charging phase triggers the expression of large numbers of genes, including Cln3 [Shi and Tu, 2013b]. According to this model, this expression of a positive regulator of cell cycle Start forces a number of cells forward through Start each metabolic cycle. Thus, YMC controls timing of the CDC in oscillating populations.

A second model is centered on the ability of the cyclin dependent kinase to phos-

phorylate and activate metabolic enzymes involved in the YMC. The Futcher and Skotheim laboratories have recently demonstrated that S phase cyclins phosphorylate and activate the trehalose degrading enzyme Nth1 and glycogen-degrading enzyme Gph1, increasing the metabolic carbon flux [Ewald et al., 2016; Zhao et al., 2016]. According to this model, it is the commitment to cell cycle progression that initially triggers metabolic events. Thus, it is the CDC that drives the YMC rather than vice versa in this model. To resolve these hypotheses, this dissertation seeks to test the relationship between the YMC and CDC via population-level and single-cell analysis of the timing of metabolic and cell cycle events.

Relationship Between the YMC and CDC Across Strains and Growth Rates

2.1 Introduction

As discussed in Chapter 1 the segregation of DNA replication and high oxygen consumption does not appear to be a reliable feature of the YMC, with different groups reporting different patterns of coupling. Upon closer examination, however, it becomes clear that these contradictory results are not necessarily directly comparable to each other. Differing chemostat settings/equipment and growth media were used by these groups. The Botstein laboratory used synthetic defined media with 0.1% glucose as a carbon source [Slavov and Botstein, 2011; Slavov et al., 2012] while the Murray, McKnight, and later Tu laboratories used rich media with yeast extract and 1%-2% glucose [Klevecz et al., 2004; Tu et al., 2005; Kuang et al., 2014], and early experiments in the Kuriyama laboratory used ethanol as a sole carbon source [Keulers et al., 1996]. Oxygen flow rates used in these chemostat experiments also varied greatly. Perhaps more importantly, different strain backgrounds were used in different laboratories. DBY12007 (used by the Botstein laboratory) is closely related

to the standard S288C laboratory strain [Silverman et al., 2010], CEN.PK (used by the McKnight and Tu laboratories) is a strain developed in Europe for high biomass yield [Entian and Kötter, 2007; van Dijken JP et al., 2000], and IFO0233 (used by the Murray and Kuriyama laboratories) is a distiller’s strain [Keulers et al., 1996; Satroutdinov et al., 1992]. Oscillations were observed with YMC periods ranging between 45 minutes and 5 hours. In this chapter, we sought to distinguish the effects of environment and genotype on the YMC. Does the relationship between the YMC and cell division cycle (CDC) represent an *exclusion* of DNA replication from a particular point or state during the metabolic oscillation, or does it represent a *coordination* between DNA replication and YMC events such as periods of maximal energy availability?

By systematically investigating the growth of genetically diverse yeast strains grown at different growth rates in the same chemostat and growth medium, we were able to isolate invariant aspects of the YMC and its coupling to the CDC. Different strains were observed to initiate DNA replication in different metabolic states, but all strains showed a constant delay between *entry into* high oxygen consumption phase and DNA replication. Thus, while DNA replication is not explicitly excluded from or coordinated with any particular metabolic state, its onset is tied to the *shift* from low oxygen consumption (LOC) to high oxygen consumption (HOC) phase. All strains showed an increasing length of LOC as growth rate decreases and the relative fraction of time spent in HOC phase during the YMC rises linearly with growth rate, suggesting a biological role for the YMC in the regulation of yeast metabolism.

2.1.1 Strains

To clarify the relationship between the yeast metabolic cycle and the cell division cycle, we examined the YMC of multiple strains at multiple growth rates. The period of an individual YMC oscillation varied from 1-5 hours depending on growth rate,

and multiple oscillations at a given growth rate were required in order to ensure that an oscillation was regular. Four strains were chosen to survey in detail, as only six chemostat growth chambers were available at a time and a large number of several week long chemostat experiments were required.

We included the two strains studied in the greatest detail in the existing YMC literature. First, CEN.PK (specifically, CEN.PK 122) has been studied extensively by the Tu and McKnight laboratories [Chen et al., 2007; Tu et al., 2005; Kuang et al., 2014]. This strain is the result of a European program aimed to create yeast which grow well in models of industrial fermentation processes [Nijkamp et al., 2012; Entian and Kötter, 2007], and has a robust growth phenotype under industrially-relevant conditions [van Dijken JP et al., 2000]. It bears mutations in the CYR1 gene and other components of the cAMP-PKA pathway, leading to altered carbohydrate metabolism, higher biomass production in fermentation tanks, and reduced mobilization of storage carbohydrates in response to activation of PKA by glucose addition. The metabolic cycle of CEN.PK is significantly longer than that of other strains examined in the past, sometimes exceeding 5 hours in length during growth in rich media at $D=0.1 \text{ hr}^{-1}$. Mating-type a and type α CEN.PK 122 strains [Tu et al., 2005; Shi et al., 2010] were generously provided by the Tu laboratory, and we mated them to produce a diploid CEN.PK strain used in all experiments.

DBY12007 was the second strain. This is one of the primary strains examined by the Botstein laboratory [Slavov and Botstein, 2011; Slavov et al., 2012]. DBY12007 is closely related to the standard laboratory reference strain S288C. However, the normal auxotrophies present in S288C were repaired by the Botstein laboratory so as to remove any disruptions to the cell's metabolic pathways, a necessary step due to the potential for auxotrophies to disrupt central carbon metabolism [Brauer and Huttenhower, 2008]. DBY12007 also bears a repaired HAP1 gene. Hap1 is an oxygen and heme-sensing transcription factor and is mutated in the standard

S288C background, leading to disrupted mitochondrial function. Thus, the aerobic respiration properties of DBY12007 are closer to that of most wild isolates. Diploid DBY12007 yeast was generously provided by the Botstein laboratory.

Both CEN.PK and DBY12007 are highly domesticated laboratory strains. They have been grown in rich media for a very large number of generations with very different selective pressures on central carbon metabolism compared to wild yeast. They also sample a very small fraction of the genetic diversity of *Saccharomyces cerevisiae*. Recent work on metabolic variation between domesticated laboratory strains and a wild strain [Breunig et al., 2014] uncovered extensive genetic differences that affect metabolic pathways such as glucose uptake, ethanol secretion, and sulfur assimilation which are functionally relevant pathways for the metabolic cycle. In order to better sample the available genetic diversity of yeast and ensure that laboratory selection and domestication have not altered the behavior of the YMC, the wild isolates YPS670 and YJM128 were chosen. YPS670 was first isolated from oak tree exudate [Murphy et al., 2006]. YJM128 is a clinical lung isolate from an immunocompromised patient [McCusker et al., 1994].

2.1.2 Determining a Universal Growth Medium

Previous work on the yeast metabolic cycle used a variety of growth media. For example, the McKnight and Tu laboratories [Tu et al., 2005; Kuang et al., 2014] used complex media containing yeast extract and 1% glucose, while the Botstein lab used fully defined synthetic media with essential vitamins instead of yeast extract and 0.1% glucose [Slavov and Botstein, 2011; Slavov et al., 2012]. In order to compare the behavior of multiple strains, we needed to use the same medium and growth conditions for all of them. We tested growth of all four strains in our chemostat with a variety of growth media, varying the glucose concentration and the use of vitamins versus yeast extract for trace nutrients. This allowed us to find a growth medium

in which all four strains grew robustly and exhibited metabolic oscillations over an overlapping range of media feed rates. This synthetic defined medium used essential vitamins and contained 0.25% glucose, and is described in detail in Materials and Methods.

2.1.3 Chemostat Operation

A 6-chamber Multifors bioreactor was used for chemostat growth. These 1L chambers contained a pO₂ probe, thermocouple, and pH probe to measure the continuous state of the chamber. Culture pH was maintained by pumps that added 1M NaOH and 1M H₂PO₄ into each chamber as needed. The controller maintained a pH of 4 ± 0.1 for all strains except YJM128, which was maintained at a pH of 5 ± 0.1 because it did not tolerate acidic synthetic media. Temperature was maintained at 30 ° C at all times. Filtered room air was bubbled through the chamber at 1L per minute, and all chambers were stirred at 550 RPM to increase the rate of oxygen diffusion. See Materials and Methods for additional details of chemostat equipment, setup, and calibration.

All yeast were inoculated into chambers containing 1L of synthetic media with 0.25% glucose and grown in batch growth mode until all carbon sources were exhausted. After carbon was exhausted and pO_2 rose to near saturation, cells were allowed to starve for six hours. Fresh media was then fed into the chamber at a dilution rate of $D=0.1$ volumes per hour (100 mL per hour) and chamber contents removed at the same rate to maintain chemostat conditions. After several hours of transient behavior, regular metabolic oscillations would begin. Strains DBY12007 and YPS670 occasionally exhibited longstanding transient behavior or lack of synchronous oscillations. If this continued for more than one day, the chamber was re-starved for another six hours and the feed pump was reactivated. Fig. 2.1 illustrates a typical inoculation, batch growth period, starvation, refeeding, and oscillation initiation for

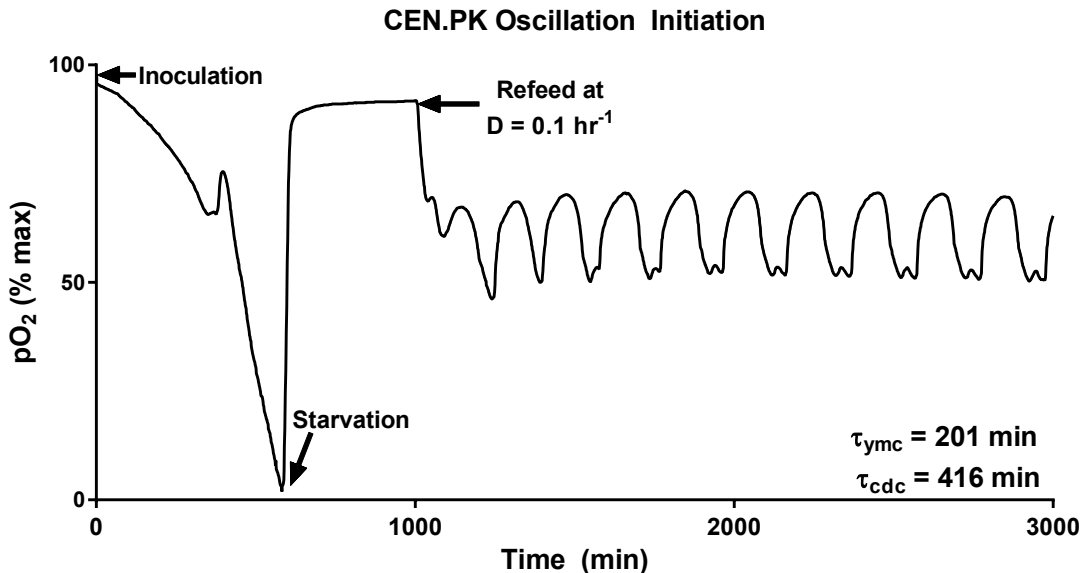


FIGURE 2.1: Typical initiation of oscillations for strain CEN.PK. Inoculation of yeast into a chemostat chamber is defined as $T=0$ minutes. As cells grow to saturation pO_2 falls while cell density increases, except for a brief diauxic shift as carbon metabolism is remodeled to consume secondary metabolites rather than glucose. Upon consumption of all media carbon, cells are allowed to starve for 6 hours before refeeding at $D=0.1$ volumes per hour. An oscillation begins and after brief irregular transient behavior settles down into a regular pattern.

strain CEN.PK.

2.1.4 Calibrating Chemostat pO_2 Measurements

In previous YMC literature [Tu et al., 2005; Kuang et al., 2014], the *rate of change* of pO_2 was used in part to subdivide the metabolic cycle into phases alongside gene expression data. Oxidative phase was interpreted as the time period in which maximal aerobic respiration was occurring. This was due to a negative *slope* in pO_2 readings, interpreted as representing the culture consuming a large stock of dissolved oxygen which was slow to reach equilibrium with the atmosphere. Here, we show that dissolved oxygen in the chemostat growth medium equilibrates quickly and that pO_2 rather than its rate of change closely reflects the underlying rate of oxygen

consumption by yeast.

During chemostat operation, the dissolved oxygen content of the growth medium is constantly measured as a readout of the average metabolic rate of the culture. This readout is indirect, and it was important to confirm that the level of dissolved oxygen in a chemostat chamber (pO_2) tracks the oxygen uptake rate of yeast cells in the chamber to accurately examine the relationship between the YMC and CDC. The rate of oxygen consumption of yeast represents a flow of oxygen out of the growth media, which necessarily reaches equilibrium some finite time *after* the change in metabolic rate occurs. An analysis of the oxygen diffusion characteristics of the chemostat and the response time of the pO_2 probe was performed to confirm that the relevant indicator of metabolic state is pO_2 rather than its derivative.

We measured the oxygen probe response time τ_r and the oxygen mass-transfer coefficient k of our chemostat using the dynamic method described by Garcia-Ochoa and Gomez [Garcia-Ochoa and Gomez, 2009]. The response time depends on the chemistry and permeability of the dissolved oxygen probe, and the oxygen mass-transfer coefficient depends on the rate of gas flow, impeller geometry, rotation speed, and temperature of the chemostat chamber. The probe response to a change in pO_2 , and pO_2 changes in response to shifts in oxygen flux, are described by the following differential equations. pO_{2m} represents the measured dissolved oxygen level, pO_2 represents the actual dissolved oxygen level, and pO_2^* represents the equilibrium steady-state level that the system approaches with all gas flow rates in and out of the system left constant:

$$\frac{dpO_{2m}}{dt} = \frac{pO_2 - pO_{2m}}{\tau_r} \quad (2.1)$$

$$\frac{dpO_2}{dt} = k \cdot (pO_2^* - pO_2) \quad (2.2)$$

We determined τ_r and k by experimentally switching gas-line inputs to a chemostat chamber filled with one liter of synthetic chemostat media without sugar or vitamins. We switched the input from nitrogen gas ($pO_2^* = 0\%$) to room air ($pO_2^* = 100\%$). The dynamics of reaching the new steady state are described by the following equation:

$$pO_{2m}(t) = 100\% \cdot \left[1 + \frac{\tau_r \cdot k \cdot e^{-\frac{-(t-t_0)}{\tau_r}} - e^{-k \cdot (t-t_0)}}{1 - \tau_r \cdot k} \right] \quad (2.3)$$

when $t > t_0$ and where t_0 is a variable time lag that represents the travel time of gas in supply lines between the gas source and the chemostat chamber after switching sources at $t=0$. We fitted eq. 2.3 to experimental pO_{2m} from the same chemostat conditions used in our YMC experiments. Our best fit to multiple datasets gives a response time $\tau_r \approx 0.19$ min and an oxygen mass-transfer coefficient $k \approx 1.2$ min⁻¹. See Fig. 2.2a for a representative fit.

By manipulating eq. 2.1 and eq. 2.2 we derive the time-varying steady-state $pO_2^*(t)$ from $pO_{2m}(t)$, and associated first derivative $pO'_{2m}(t)$ and second derivative $pO''_{2m}(t)$:

$$pO_2^*(t) = pO_{2m}(t) + \tau_r \cdot pO'_{2m}(t) + \left[\frac{\tau_r \cdot pO''_{2m}(t) + pO'_{2m}(t)}{k} \right] \quad (2.4)$$

The value of $pO_2^*(t)$ in eq. 2.4 represents what $pO_{2m}(t)$ would be if the chemostat had an infinite oxygen mass-transfer coefficient and zero probe response time. We used eq. 2.4 and our best fit k and τ_r parameters to convert actual measured $pO_{2m}(t)$ data into $pO_2^*(t)$. The measured dissolved oxygen levels are nearly identical to the imputed values in a chamber without the errors introduced by oxygen diffusion and probe response - see Fig. 2.2b. Thus, throughout the remainder of this work we use pO_2 , pO_{2m} , and pO_2^* interchangeably.

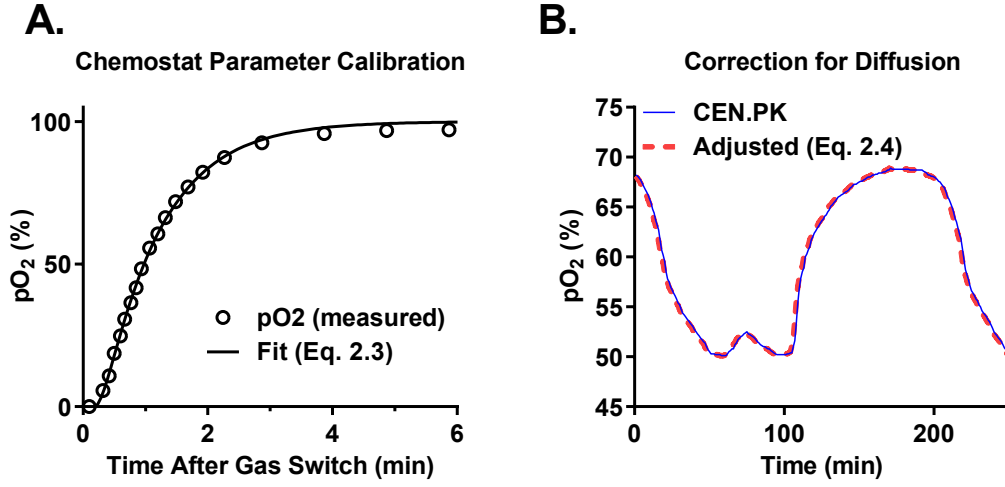


FIGURE 2.2: (A) Fit of eq. 2.3 to measured pO_2 from a chemostat chamber, after switching aeration from 100% nitrogen to room air. The values of the oxygen mass-transfer coefficient k and the probe response time τ_r are determined from this fit. (B) Calculation of imputed $pO_2^*(t)$ from measured $pO_{2m}(t)$ during the yeast metabolic cycle using eq. 2.4. The effect of oxygen diffusion and probe response time is negligible.

2.1.5 pO_2 Reflects the Instantaneous Rate of Oxygen Consumption

The pO_2 of a chemostat chamber with yeast growing inside represents a balance between the rate of oxygen transfer from the gas bubbled through it to the liquid media, and the yeast oxygen uptake rate (OUR). Mathematically, the rate of change of pO_2 in response to yeast OUR is given by the following equation:

$$\frac{dpO_2}{dt} = k \cdot (pO_2^* - pO_2) - OUR \tag{2.5}$$

where pO_2^* is the saturation level of dissolved oxygen (100%) that the chemostat would approach in the absence of any yeast respiration. The general solution to eq. 2.5 is:

$$pO_2(t) = pO_2(0) \cdot e^{-kt} + \left[pO_2^* - \frac{OUR}{k} \right] \cdot (1 - e^{-kt}) \quad (2.6)$$

The bioreactor oxygen mass-transfer coefficient k determines the timescale of how quickly an initial pO_2 reaches its new steady state after a change in yeast OUR. Our calibration measurements show that steady state is reached quickly: at $k \approx 1.2 \text{ min}^{-1}$, the chamber is halfway to the new steady state within 0.6 min and 90% equilibrated within 2 minutes. Observed pO_2 shifts during the yeast metabolic cycle occur on timescales much slower than this - the fastest shift from very high to very low oxygen consumption observed requires approximately 15 minutes. When yeast OUR changes on a timescale slower than k , eq. 2.6 is well-approximated by the steady state solution:

$$pO_2(t) = 100\% - \frac{OUR(t)}{k} \quad (2.7)$$

This indicates that the oxygen uptake rate of the yeast in a chemostat chamber controls the dissolved oxygen level, with a higher OUR leading directly and promptly to a lower pO_2 . Therefore, pO_2 is an excellent measurement of oxygen consumption rate rather than pO_2' , and descriptions of the phase of the yeast metabolic cycle based on absolute pO_2 are valid.

2.1.6 YMC Sampling and Data Collection

During chemostat culture, sensors were operated automatically by the Multifors control computer. We recorded temperature, pO_2 , pH, the cumulative volume of 1M NaOH added, the cumulative volume of 1M H_2PO_4 added, and the cumulative media volume added. Measurements of pO_2 served as a readout of yeast oxygen uptake rate (OUR).

Each chemostat run lasted from 1 to 3 weeks. During each run, the dilution rate

was varied systematically so as to acquire pO_2 traces at as many growth conditions per strain as possible. The timing of every change in culture conditions was recorded. Dilution rate was varied between 0.035 and 0.13, for a doubling time τ_{cdc} of between 1184 and 320 min.

Oak isolate YPS670 exhibited a very slow initial growth to saturation in synthetic chemostat media and a tendency for the YMC to spontaneously collapse before reestablishing itself after several hours. Clinical isolate YJM128 exhibited vigorous growth in synthetic media, but was highly flocculent and rapidly built biofilms on metal surfaces in the chemostat chambers. After approximately 10 days of oscillating chemostat growth its metabolic cycle would permanently collapse, possibly due to excessive biofilm growth. This led to less data being collected for YPS670 and YJM128 than the laboratory strains CEN.PK and DBY12007. There were 16, 12, 9, and 10 total chemostat chamber runs for CEN.PK, DBY12007, YJM128, and YPS670 respectively. This represented 52, 50, 16, and 30 usable time series, each representing a contiguous period of time at a given dilution rate.

In order to determine the timing of DNA replication during the YMC, time courses of samples were taken from cycling chambers every fifteen minutes or every ten minutes for a total of eight hours each sampling run. The frequency of sampling was held constant over an individual sampling run. Samples were fixed in ethanol with a final concentration of 70% and stored in 96 well plates at 4° C. Before DNA content measurement, cells were treated with a RNase and pepsin protocol (modified from [Haase and Reed, 2002]) to eliminate all RNA and cellular protein, and reduce background. Cells were sonicated to break up any flocculent clumps and stained with Sytox green before measurement of total DNA content via flow cytometry - see Materials and Methods.

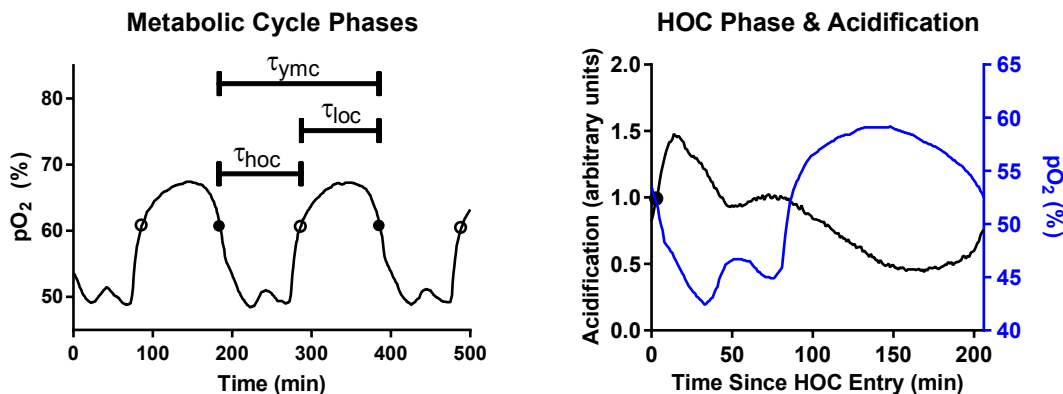


FIGURE 2.3: (A) Separation of the phases of the yeast metabolic cycle. Entry into HOC phase (solid points) is defined using a 35% drop from maximum to minimum pO_2 during an oscillation, and exit from HOC (empty points) is defined using a 65% rise from minimum to maximum pO_2 . The length of the YMC τ_{YMC} , and length of each phase τ_{HOC} and τ_{LOC} are defined. (B) Half maximum (black point) of the acidification of growth media (black line) corresponds with entry into HOC ($t=0$ min).

2.1.7 Data Analysis

A custom Matlab script was used to segment the YMC into phases using the pO_2 data trace. A peak detection algorithm first identified local maxima and local minima in the pO_2 trace. We included a minimum peak-size filter to exclude small pO_2 fluctuations and identify the global maximum and minimum pO_2 point of each oscillation. Filter parameters had to be manually adjusted for each experiment to ensure that exactly one global maximum and minimum were identified per cycle.

Previous work on the YMC defined three phases based on gene expression data: oxidative, reductive building, and reductive charging [Tu et al., 2005]. The boundary between two of these - ‘oxidative’ and ‘reductive building’ phase - is generally not apparent from pO_2 levels - see Fig. 1.2 in Chapter 1. In this work, we followed the procedure of the Botstein laboratory [Slavov and Botstein, 2011] and empirically separated the YMC into *two* phases based on the pO_2 data: high oxygen consumption

(HOC) and low oxygen consumption (LOC) - see Fig. 2.3a.

Entry and exit from YMC phases were defined relative to the maximum and minimum pO_2 values observed during each individual oscillation, in order to minimize the effect of slow drifts in oxygen probe calibration. Every oscillation contains a maximum and minimum pO_2 level, with HOC entry occurring after a maximum and before a minimum and HOC exit/LOC entry occurring after a minimum and before a maximum. Entry into HOC was defined as the time after a global pO_2 maximum of an oscillation that pO_2 falls by 35% of the difference between this global maximum and the upcoming global minimum. Entry into LOC was then defined as the first time after this global pO_2 minimum that oxygen level rises by 65% of the difference between this global minimum to the next global maximum.

These boundaries were chosen for several reasons. First, when overlaying pO_2 traces from multiple oscillations, use of these boundaries as landmarks leads to the most consistent overlap. Second, this definition of entry into HOC coincides with the rise in aerobic fermentation as measured by acidification of the growth media. See Fig. 2.3b for an overlay of metabolic cycle phase and acidification rate.

The length of the YMC, τ_{ymc} , was defined as the time between two successive entries into HOC phase. The length of HOC phase, τ_{loc} , was defined as the time between entry into and exit from HOC. The length of LOC phase, τ_{hoc} , was defined as the time between entry into and exit from LOC. A time series of oscillations at a particular dilution rate was discarded if the coefficient of variation of τ_{ymc} , τ_{hoc} , or τ_{loc} exceeded 0.1, which removed a total of 19 unstable or noisy YMC time series from a total of 148.

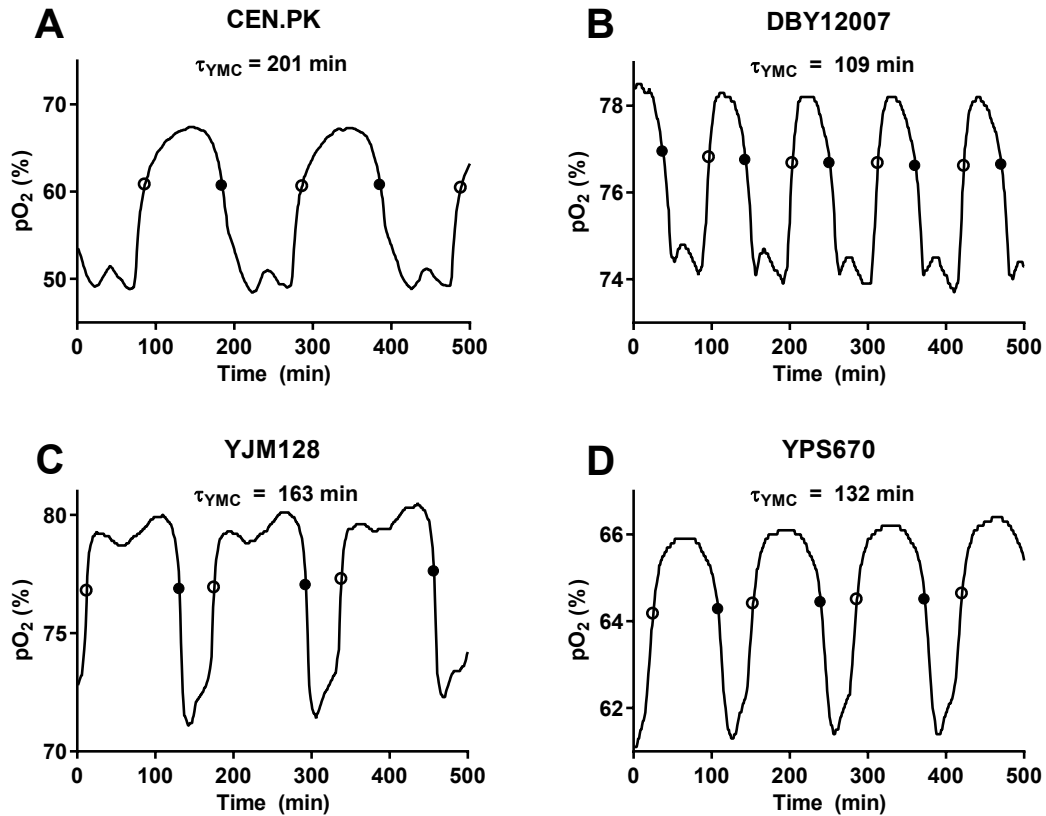


FIGURE 2.4: Typical YMC phenotypes. Strains (A) CEN.PK, (B) DBY12007, (C) YJM128, and (D) YPS670 have distinctive pO_2 waveforms with different τ_{ymc} periods. All are shorter than τ_{cdc} , 416 minutes at $D=0.1 \text{ hr}^{-1}$.

2.2 Results

2.2.1 Effects of Growth Rate on the Yeast Metabolic Cycle

All tested strains were capable of synchronous metabolic cycles, including the wild isolates. The presence of the YMC appears to be robust to genetic variation present across our samples. They did however show strong strain-specific YMC phenotypes. As seen in Fig. 2.4, all four strains have unique and distinctive pO_2 waveforms and different values for τ_{ymc} , τ_{hoc} , and τ_{loc} at a given dilution rate.

In order to determine the effects of varying growth rates on the behavior of the

yeast metabolic cycle τ_{ymc} , τ_{hoc} , and τ_{loc} were compared for each strain across multiple dilution rates. As visualized in Fig. 2.5 for strain CEN.PK, as dilution rate falls and τ_{cdc} increases τ_{ymc} increases monotonically while remaining significantly shorter than the population doubling time.

LOC and HOC phase of the YMC do not maintain a fixed relationship as the YMC gets longer. As τ_{ymc} increases, τ_{hoc} remains low or even decreases while maintaining roughly the same pO₂ waveform. Large increases in τ_{loc} almost entirely account for the lengthening of the HOC at slow growth rates, such that at the lowest growth rates the YMC consists almost entirely of a very long LOC phase. These broad relationships were consistent for all strains tested.

To better quantify the relationship between growth rate and YMC variables, we plotted τ_{ymc} , τ_{hoc} , and τ_{loc} as a function of τ_{cdc} (Fig. 2.6). All strains exhibited a monotonic increase in YMC length and LOC length with increasing τ_{cdc} . This monotonic increase was not consistently linear, instead exhibiting a leveling-off towards a maximum value for τ_{ymc} for some strains, and was best fit with a hyperbolic relationship between τ_{ymc} and τ_{cdc} .

Not all phase relationships were best fit with hyperbolic relationships. A linear relationship between τ_{hoc} and τ_{cdc} universally produced the best fits. A mixed model in which τ_{ymc} is a hyperbolic function of τ_{cdc} , τ_{hoc} is a linear function of τ_{cdc} , and τ_{loc} , represents the difference between these two values, described below, produces the lowest total fitting residuals. See Fig. 2.7 for a comparison of residuals between fully hyperbolic models, fully linear models, and this mixed model of YMC/CDC period relationships.

The following hyperbolic equation was fit to all τ_{ymc} data for the mixed model, in which T_{max} represents the strain-specific maximum YMC or phase period reached at slow growth rates and k represents the τ_{cdc} at which τ_{ymc} reaches half of T_{max} :

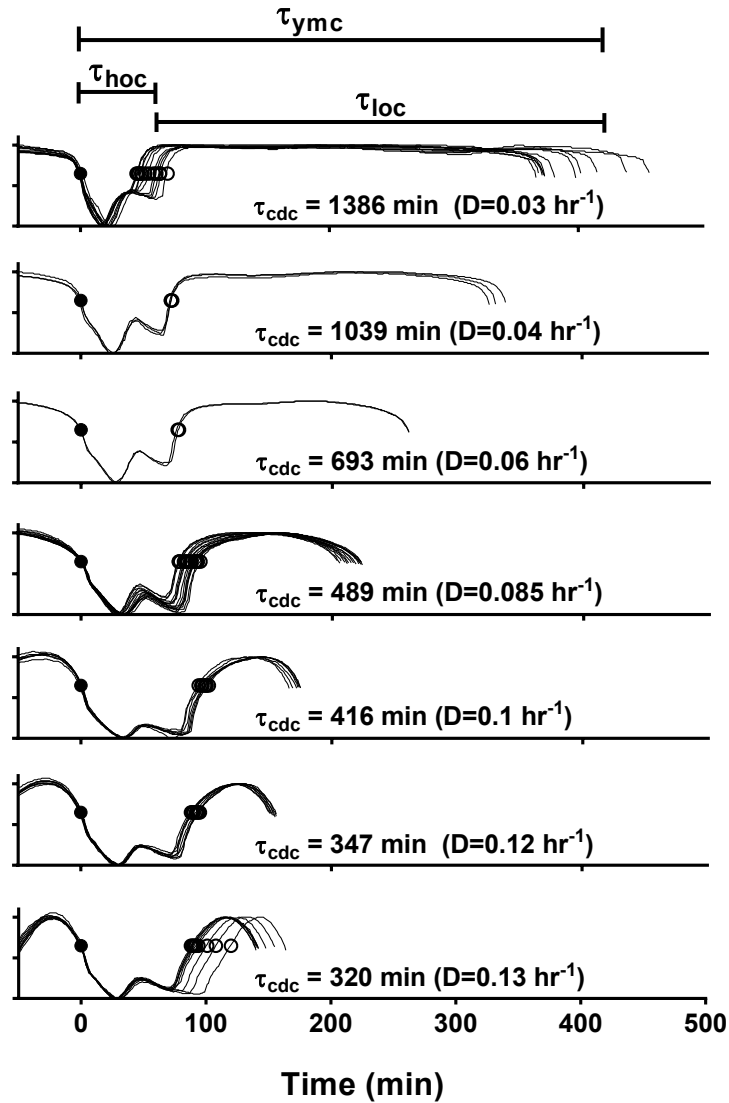


FIGURE 2.5: Increase in YMC period at slower dilution rates occurs by lengthening LOC phase. All pO_2 traces from a single chemostat run are pictured, normalized in amplitude and stacked to overlay HOC entry (solid points) at $t=0$. HOC exit (open circles) occurs a consistent length of time after HOC entry. As dilution rate falls, the HOC waveform stays fairly consistent. τ_{hoc} shrinks slightly at slower dilution rates, while τ_{ymc} and τ_{loc} increase.

$$\tau_{ymc} = \frac{T_{max} \cdot \tau_{cdc}}{k + \tau_{cdc}} \quad (2.8)$$

A linear relationship best fits the relationship between τ_{hoc} and τ_{cdc} . A simple linear equation of the form:

$$\tau_{hoc} = m \cdot \tau_{cdc} + b \quad (2.9)$$

was fit to all τ_{hoc} data, in which m represents the slope of the relationship between τ_{hoc} and τ_{cdc} and b represents the inferred Y-intercept.

As $\tau_{ymc} = \tau_{hoc} + \tau_{loc}$, in this mixed model the length of LOC is given by the following equation:

$$\tau_{loc} = \tau_{ymc} - \tau_{hoc} = \frac{T_{max} \cdot \tau_{cdc}}{k + \tau_{cdc}} - m \cdot \tau_{cdc} + b \quad (2.10)$$

These equations were fit to the data for all four strains - see Fig. 2.6 for fits. For CEN.PK and DBY12007, all parameters could be robustly fit and the mixed model resulted in much smaller residuals than a fully linear model or fully hyperbolic model. For YJM128 and YPS670, a mixed model fit was indistinguishable from a fully linear fit - see total residuals of each in Fig. 2.7. For these strains very small perturbations to the data could cause very large changes to T_{max} and k while preserving their ratio, and the hyperbolic model was indistinguishable from a linear model in which $\tau_{ymc} = T_{max}/k \cdot \tau_{cdc}$. All mixed-model parameters can be found in Table 2.1.

This quantitative data can be replotted in units of frequency. In this form, the YMC frequency $f_{ymc} = 1/\tau_{ymc}$ and the average cell division frequency $f_{cdc} = 1/\tau_{cdc}$ is proportional to the average growth rate set by the dilution rate D . The data show a linear relationship between frequency of division and the frequency of division space with a unique slope and y-intercept for each strain, regardless of the linear or

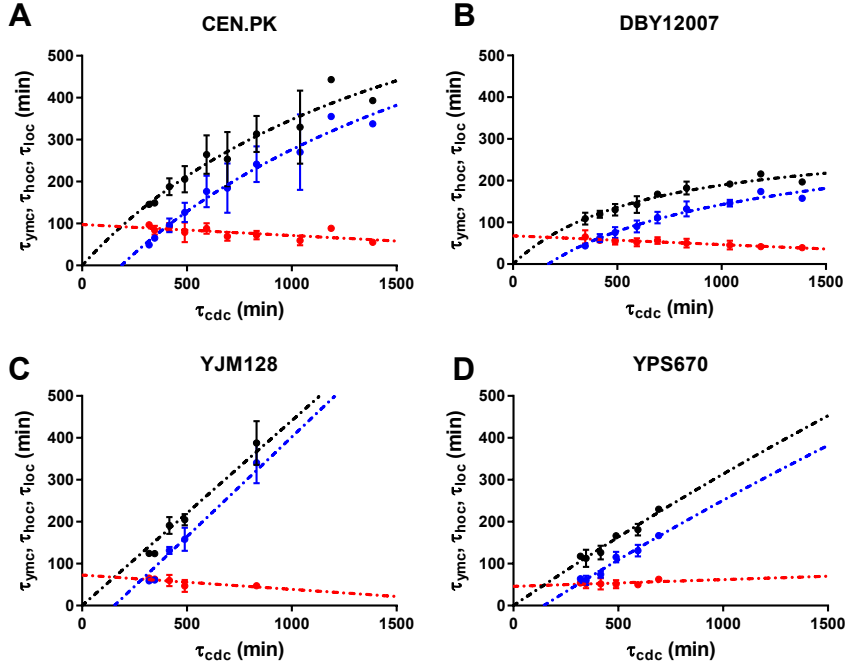


FIGURE 2.6: Quantitative relationship between the YMC and CDC for all strains examined - (A) CEN.PK, (B) DBY12007, (C) YJM128, (D) YPS670. Length of the YMC, separated into τ_{ymc} in black, τ_{hoc} in red, and τ_{loc} in blue, versus τ_{cdc} . The mixed hyperbolic/linear model fit in which τ_{ymc} is an increasing hyperbolic function of τ_{cdc} and τ_{hoc} is a decreasing linear function of τ_{hoc} is pictured for each strain.

Table 2.1: Best-fit parameters of the mixed model to YMC and HOC across strains. The mixed model is a hyperbolic model (T_{max} , k) fit to τ_{ymc} [left] and a linear model (b , m) fit to τ_{hoc} [right] where $\tau_{loc} = \tau_{ymc} - \tau_{hoc}$. For wild isolates YJM128 and YPS670, the best mixed model fit was indistinguishable from a best linear fit, where $b=0$ and $m = T_{max}/k$. This best linear fit is used above for these strains because while T_{max} and k were not robust to small perturbations in the data their ratio was.

Strains	T_{max} (min)	k (min)	b (min)	m
CEN.PK	$9.45 \pm 4.84 \times 10^2$	$1.72 \pm 1.33 \times 10^3$	$9.75 \pm 0.79 \times 10^1$	$-2.61 \pm 0.97 \times 10^{-2}$
DBY12007	$3.12 \pm 0.61 \times 10^2$	$6.49 \pm 2.83 \times 10^3$	$16.78 \pm 0.23 \times 10^1$	$-2.10 \pm 0.28 \times 10^{-2}$
Strains	T_{max}/k	b (min)	m	
YPS670 (oak)	$5.18 \pm 0.32 \times 10^{-1}$	$7.28 \pm 0.76 \times 10^1$	$-3.41 \pm 1.48 \times 10^{-2}$	
YJM128 (lung)	$3.06 \pm 0.33 \times 10^{-1}$	$4.59 \pm 0.69 \times 10^1$	$1.61 \pm 1.40 \times 10^{-2}$	

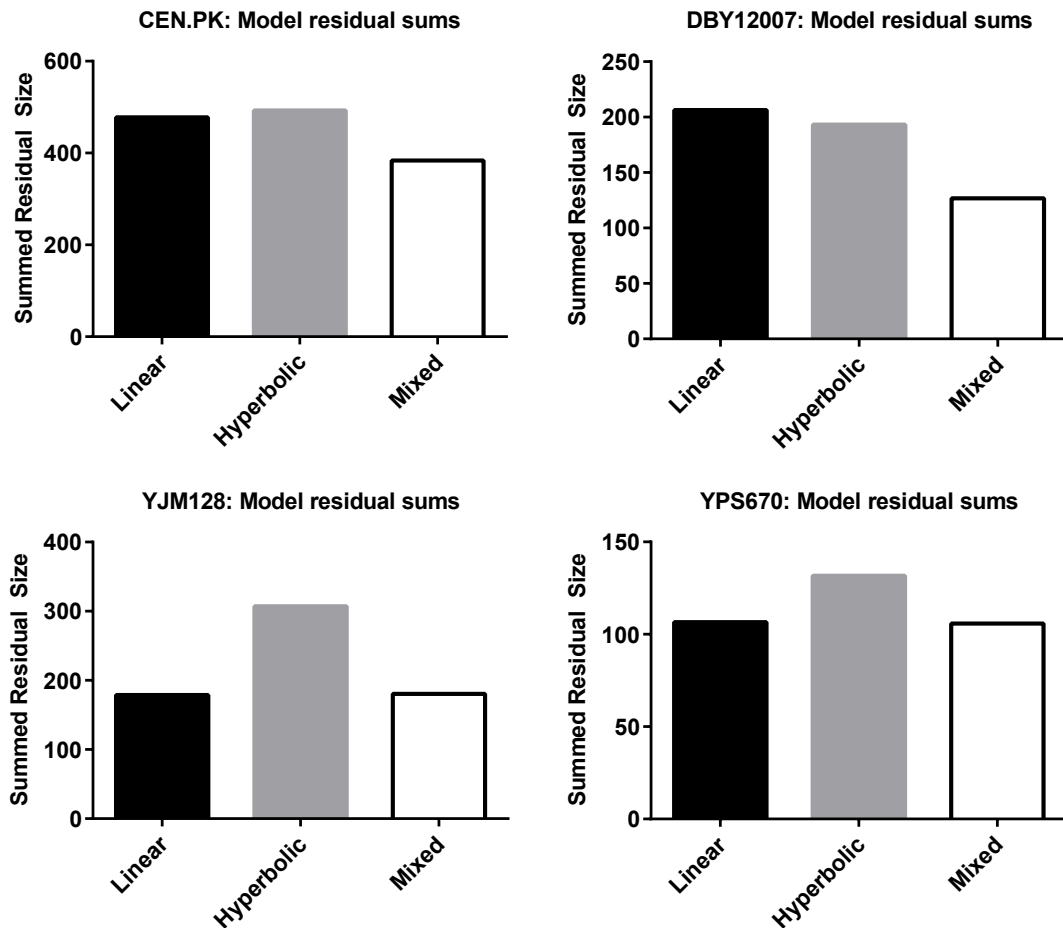


FIGURE 2.7: Residuals of best-fit linear, hyperbolic, and mixed models. Residual sums for each strain and model indicate that the mixed model is optimal for laboratory strains CEN.PK and DBY12007. Linear and mixed models were similar to each other and significantly better fits than hyperbolic models for YJM128 and YPS670. We thus use the mixed model to fit the relationship between the YMC and CDC for all strains.

hyperbolic nature of the fit - see Fig. 2.8. This indicates that the speed of progression of the yeast metabolic cycle and cell division cycle are tightly linked.

A regularity was observed in the relationship between the duration of phases of the YMC and growth rate when the fraction of time that a culture spends in HOC phase (ϕ_{hoc}) was plotted against growth rate (f_{cdc} or D). Despite the differences

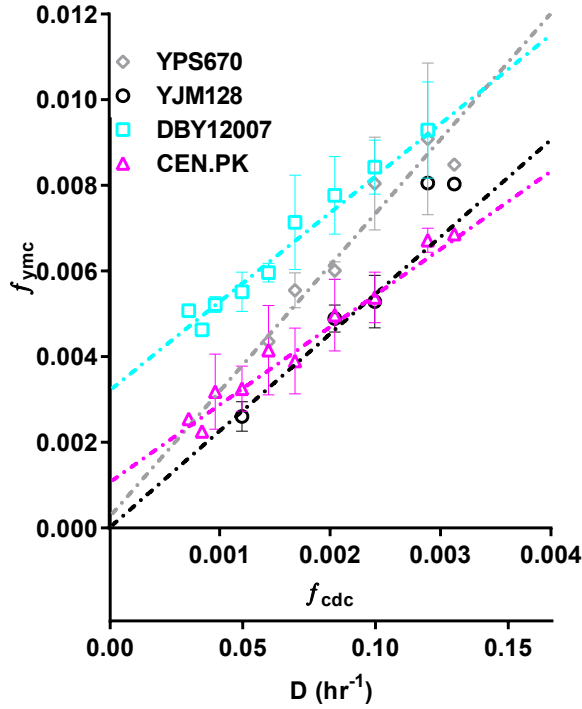


FIGURE 2.8: Quantitative relationship between the YMC and HOC for all strains examined: f_{ymc} versus f_{cdc} and D . The frequency of the YMC is a linear function of the average division frequency for all strains examined.

in average period of the YMC, all strains spend similar fractions of time in HOC at a given growth rate - see Fig. 2.9. Furthermore, all four strains have a linear relationship between ϕ_{hoc} and growth rate that roughly passes through the origin - at zero growth cells would spend no time in HOC, and at a finite growth rate cells would spend all time in HOC with the fraction increasing linearly with growth rate. This suggests underlying regulation of the *relative* length of the phases of yeast metabolic cycle, such that yeast strains spend a similar fraction of time in HOC and LOC at a given growth rate despite their differences in other YMC behaviors and genetic background.

We used the mixed model of YMC phase lengths (see Table 2.1 for parameters)

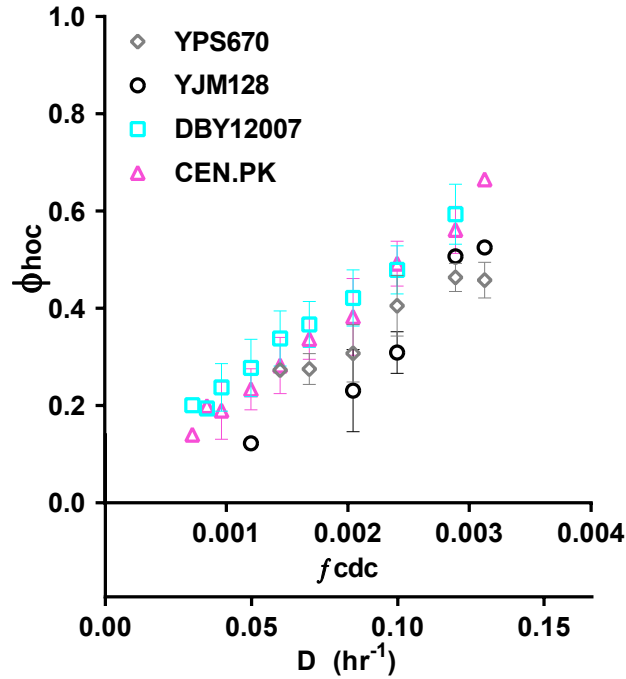


FIGURE 2.9: Fraction of time spent in HOC phase by yeast (ϕ_{hoc}) versus growth rate for all strains examined. There is a linear relationship between ϕ_{hoc} and growth rate that roughly passes through the origin.

to extrapolate the growth rates at which $\tau_{hoc} = \tau_{ymc}$ and $\phi_{hoc} = 1$. This represents the growth rate at which low oxygen consumption phase does not exist, and a yeast spends all its time in high oxygen consumption phase. This value varied by less than 30% for all four strains examined with an average of $f_{cdc} \approx 0.006\text{min}^{-1}$. When these critical growth rates were compared to physiological data from previous chemostat studies of yeast, it was discovered that $\phi_{hoc} = 1$ corresponds closely to the critical dilution rate at which yeast switch from fully aerobic growth to aerobic fermentation at high growth rates [Kaspar von Meyenburg, 1969; Van Maris et al., 2001] - see Fig. 2.10.

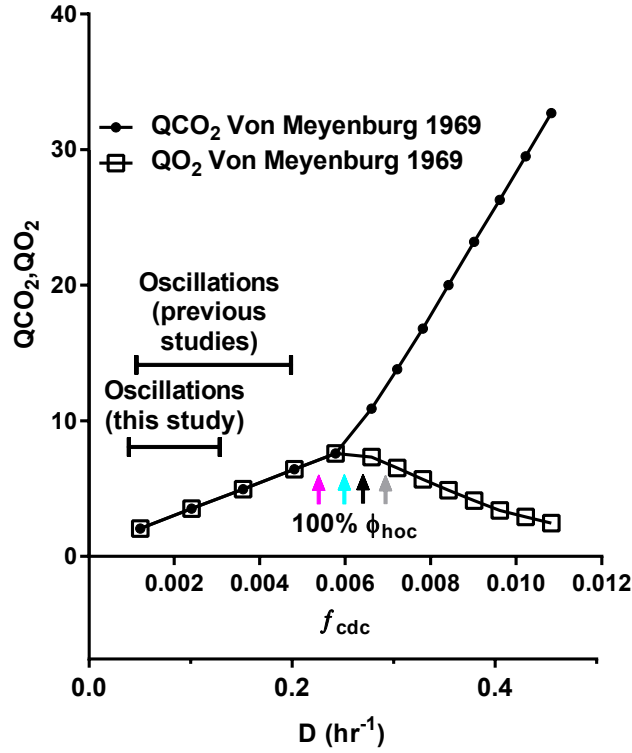


FIGURE 2.10: Rate of CO₂ production Q_{CO_2} and rate of O₂ consumption Q_{O_2} at different growth rates according to Von Meyenburg, 1969 [Kaspar von Meyenburg, 1969]. The growth rates at which CEN.PK (magenta), DBY12007 (blue), YJM128 (black), and YPS670 (grey) yeast reach 100% HOC occupancy are indicated by arrows. These growth rates cluster around the critical growth rate at which cells switch from fully aerobic respiration ($Q_{CO_2}=Q_{O_2}$) to aerobic fermentation ($Q_{CO_2} > Q_{O_2}$). Oscillations are only observed at growth rates consistent with fully aerobic respiration.

2.2.2 Timing of DNA Replication

The timing of DNA replication during the YMC has dominated discussion of the significance of YMC/CDC coupling. In order to understand their true relationship, an examination of the behavior of multiple strains in the same growth medium at multiple growth rates was required. We were able to determine the timing of DNA replication during the YMC for all four strains we examined, and obtained timing

data at multiple growth rates for three of them.

In agreement with previous studies, our flow cytometry results showed a single pulse of yeast initiating DNA replication each metabolic cycle for all strains, as seen in Fig. 2.11. Each pulse consists of $\leq 1/3$ of the population, and every pulse observed from a given strain at a given growth rate represents a consistent fraction of the population. The low fraction of cells dividing each metabolic cycle means that multiple oscillations are required for a complete population doubling, consistent with the YMC period τ_{ymc} being significantly shorter than the population doubling time τ_{cdc} at all growth rates observed.

The metabolic state of cells during DNA replication showed considerable strain-to-strain variability. While strains CEN.PK and YJM128 replicate their DNA in the middle of HOC in our chemostat conditions (Fig. 2.11a,c), DBY12007 and YPS670 replicate their DNA approximately during the transition from HOC into LOC (Fig. 2.11b,d) - there is *no strict separation* between DNA replication and any HOC phase.

In order to search for relationships between the timing of YMC and CDC events that were invariant across strains, we analyzed DNA replication at a number of different growth rates. As dilution rate was dropped and τ_{cdc} was increased, the length of LOC increased and the length of HOC decreased - see Fig. 2.12 for an example of the behavior of CEN.PK across four different growth rates. See Fig. 2.13 for the same analysis of DBY12007 and Fig. 2.14 for YPS670. The fraction of cells going through DNA replication during a given metabolic cycle is approximately equal regardless of growth rate for a given strain. Additionally, the timing variables Δ (minutes after HOC entry at which half of cells that will enter S/G2/M phase) and Δ_S (minutes after HOC entry at which the maximum fraction of cells are in S phase) were *approximately constant* and approximately equal to each other for all strains with multiple examined growth rates - see Table 2.2.

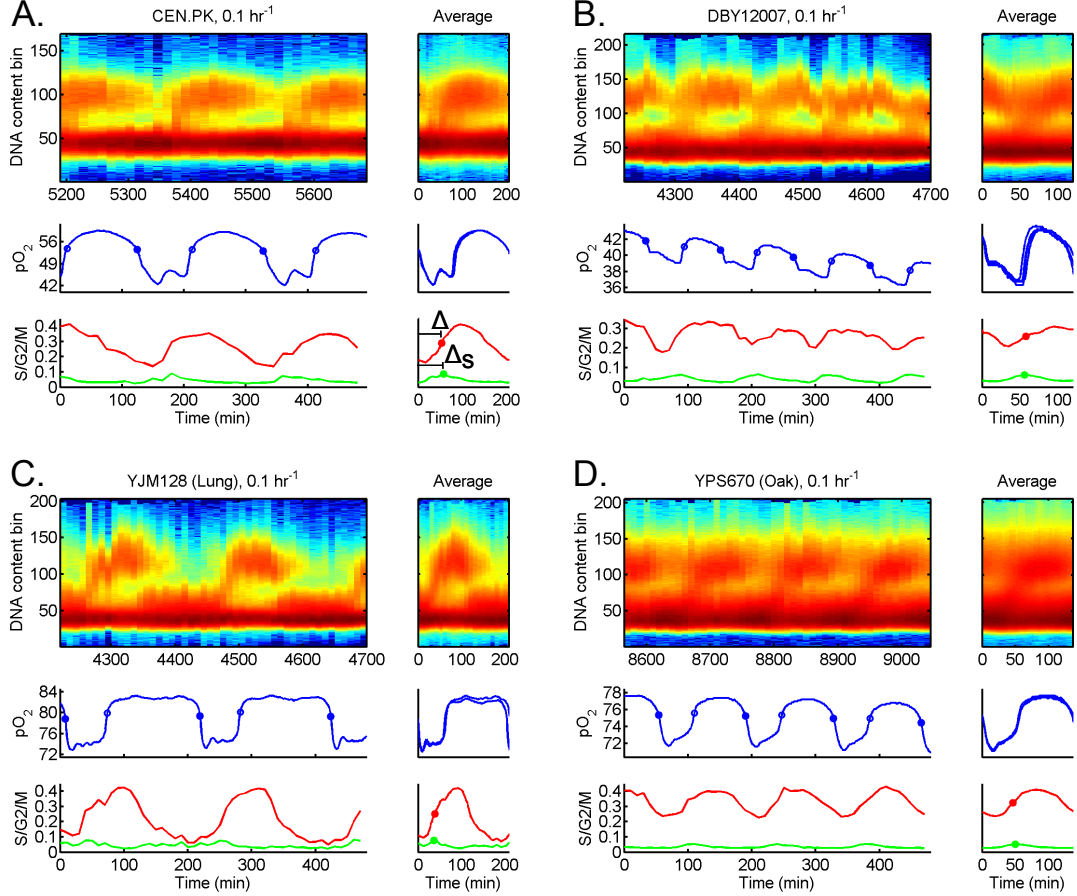


FIGURE 2.11: Timing of DNA replication relative to HOC varies across strains. (A) CEN.PK, (B) DBY12007, (C) YJM128, (D) YPS670 were cultured in chemostat conditions at the same growth rate ($D=0.1 \text{ h}^{-1}$). Samples were extracted every 10-15 minutes while pO_2 was recorded every minute. Normalized DNA content plotted as heat maps, pO_2 as blue lines, S/G2/M fraction as red lines, and S fraction as green lines. The average over a single YMC plotted to the right of each full dataset, where $t = 0$ corresponds to HOC entry. The time of the midpoint of the S/G2/M fraction (red circle) is defined as Δ and is nearly identical to the time of maximum S fraction (solid green circle) is defined as Δ_s .

When the length of HOC τ_{hoc} is compared to the timing of DNA replication Δ_S , an interesting pattern is revealed. While Δ_S is constant for any given strain, as growth rate decreases τ_{hoc} decreases or is roughly constant. This is most apparent for strain CEN.PK - see Fig. 2.15. This is consistent with the pattern observed by the Botstein laboratory [Slavov and Botstein, 2011] in which depending on the growth rate, DNA

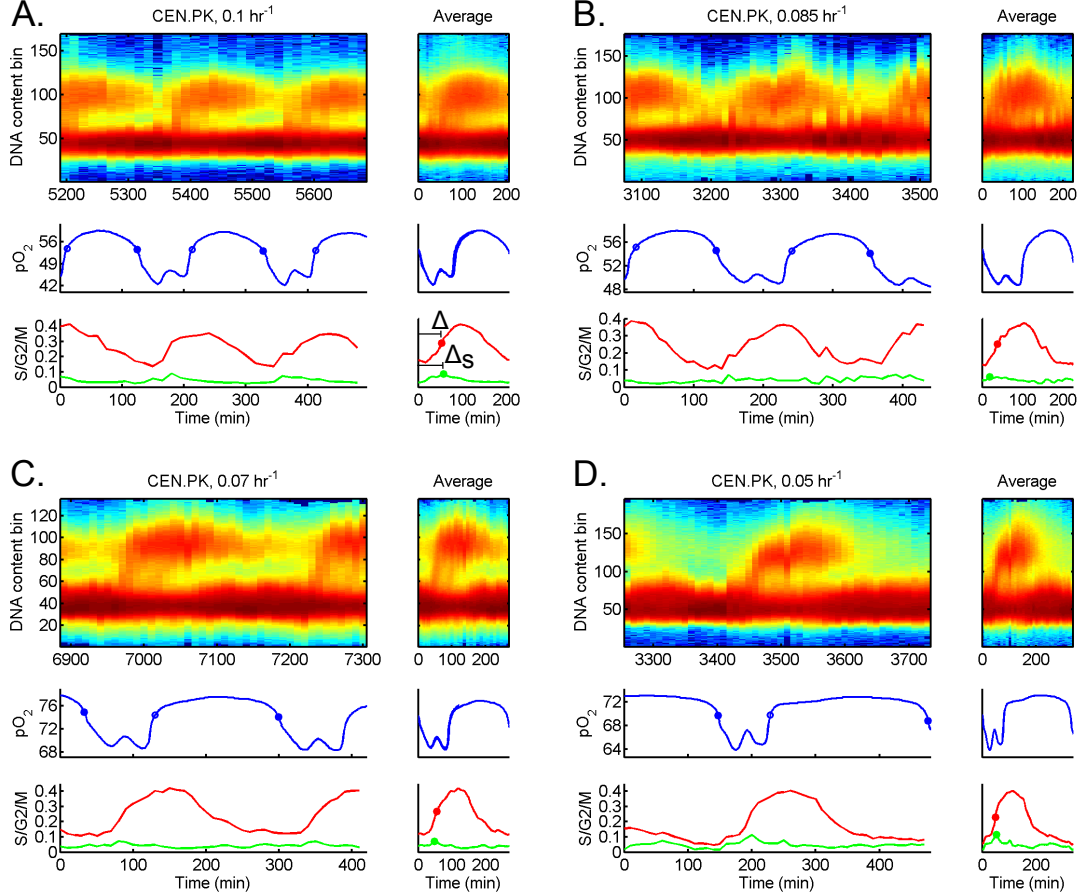


FIGURE 2.12: Additional analysis of the timing of DNA replication relative to HOC in strain CEN.PK at dilution rates of (A) $D=0.1h^{-1}$, (B) $D=0.085h^{-1}$, (C) $D=0.07h^{-1}$, and (E) $D=0.05h^{-1}$. Normalized DNA content plotted as heat maps, pO_2 as blue lines, S/G2/M fraction as red lines, and S fraction as green lines. The average over a single YMC plotted to the right of each full dataset, where $t = 0$ corresponds to HOC entry. The time of the midpoint of the S/G2/M fraction (red circle) is defined as Δ and is nearly identical to the time of maximum S fraction (solid green circle) is defined as Δ_s .

replication was observed at both high and low oxygen consumption levels. When their data is examined in terms of time after HOC entry, the same delay between HOC entry and DNA replication is observed as in our data while HOC length varies considerably over their dataset. Thus, while the length of the phases of the yeast metabolic cycle can vary according to growth rate, the δ_S between entry into HOC

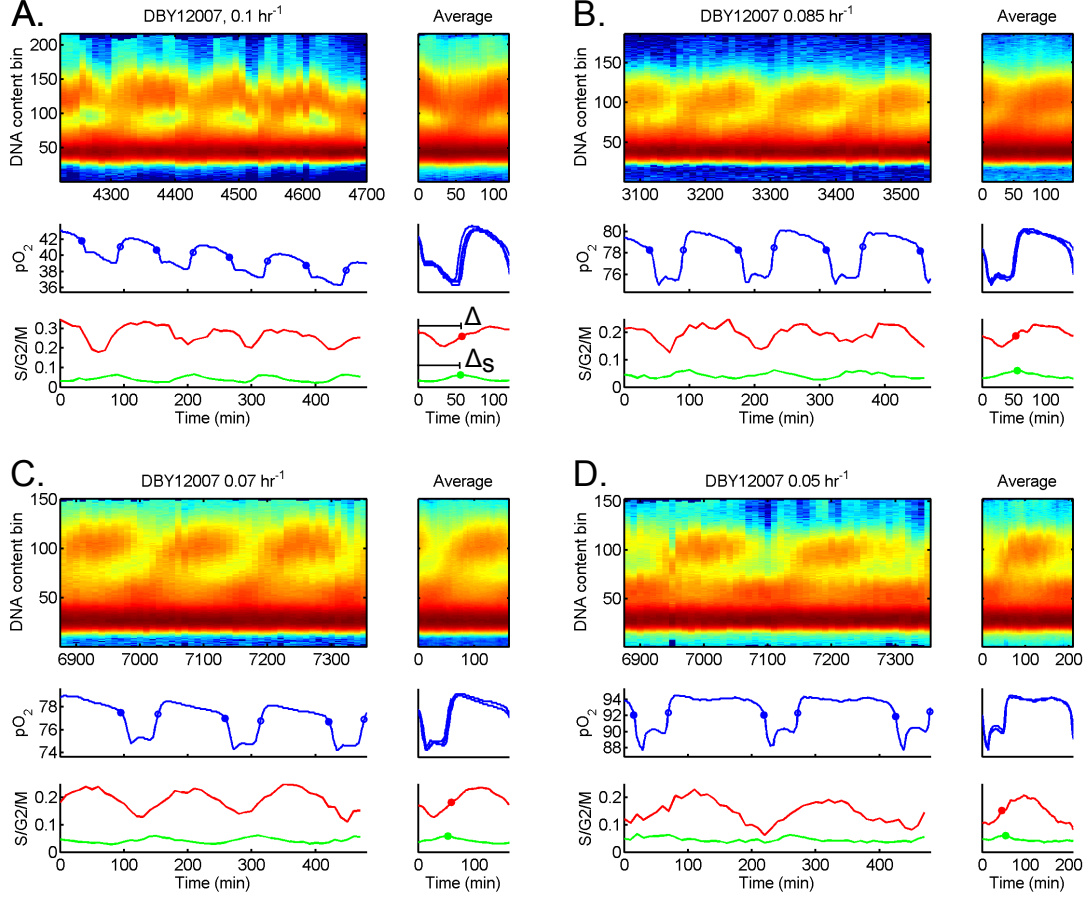


FIGURE 2.13: Additional analysis of the timing of DNA replication relative to HOC in strain DBY12007 at dilution rates of (A) $D=0.1h^{-1}$, (B) $D=0.085h^{-1}$, (C) $D=0.07h^{-1}$, and (D) $D=0.05h^{-1}$. Normalized DNA content plotted as heat maps, pO_2 as blue lines, S/G2/M fraction as red lines, and S fraction as green lines. The average over a single YMC plotted to the right of each full dataset, where $t = 0$ corresponds to HOC entry. The time of the midpoint of the S/G2/M fraction (red circle) is defined as Δ and is nearly identical to the time of maximum S fraction (solid green circle) is defined as Δ_s .

and DNA replication is an invariant for a particular strain.

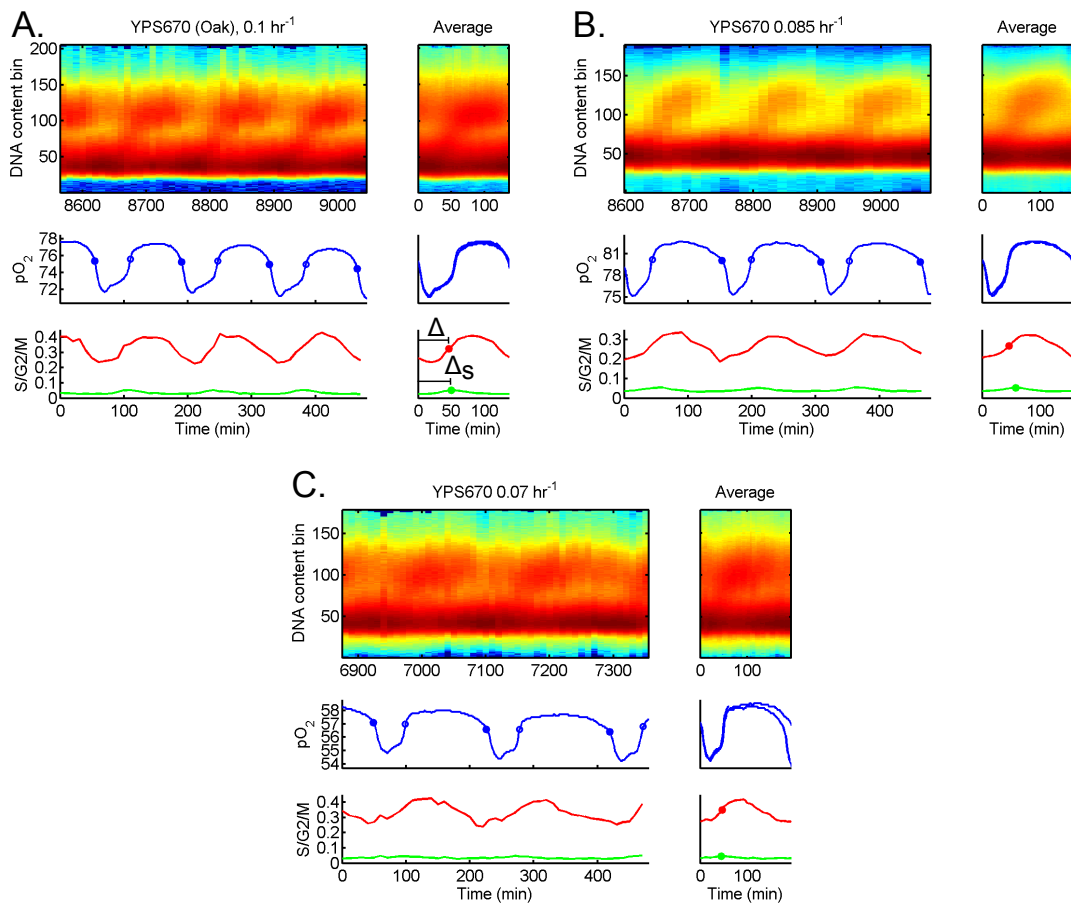


FIGURE 2.14: Additional analysis of the timing of DNA replication relative to HOC in strain YPS670 at dilution rates of (A) $D=0.1h^{-1}$, (B) $D=0.085h^{-1}$, and (C) $D=0.07h^{-1}$. Oscillations were unstable in YPS670 at $D=0.05h^{-1}$. Normalized DNA content plotted as heat maps, pO_2 as blue lines, S/G2/M fraction as red lines, and S fraction as green lines. The average over a single YMC plotted to the right of each full dataset, where $t = 0$ corresponds to HOC entry. The time of the midpoint of the S/G2/M fraction (red circle) is defined as Δ and is nearly identical to the time of maximum S fraction (solid green circle) is defined as Δ_s .

2.3 Discussion

2.3.1 Biological Significance of the Yeast Metabolic Cycle

While every strain examined exhibited unique YMC dynamics, systematic comparison of their behavior revealed regularities that suggest the biological significance of the metabolic cycle. In all strains, the length of HOC phase was roughly constant or

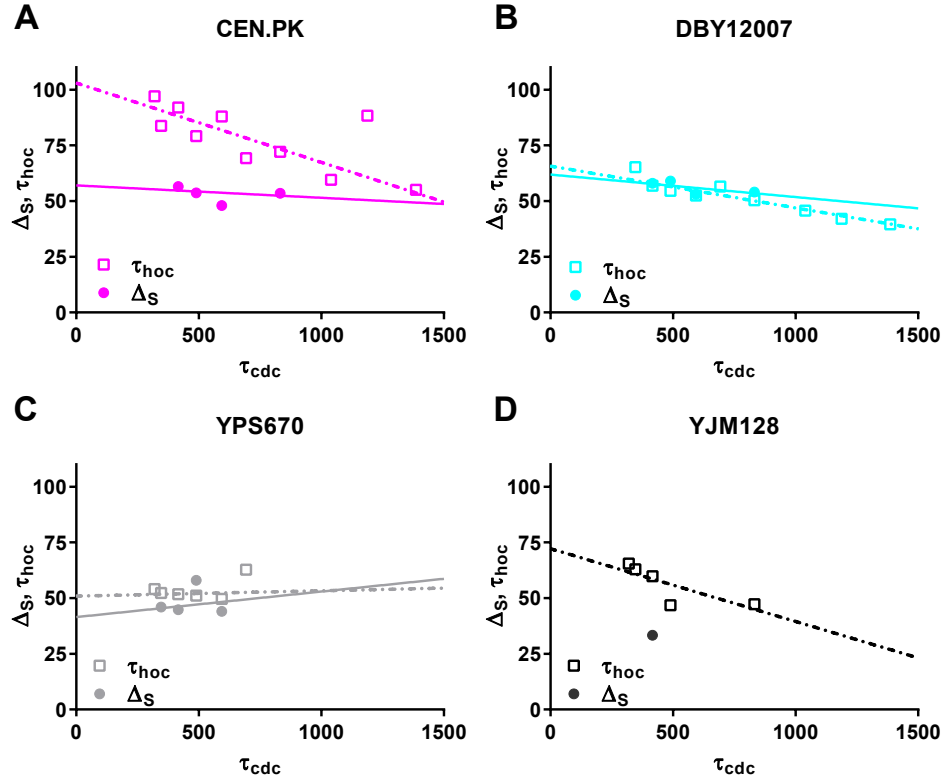


FIGURE 2.15: Timing of DNA replication Δ_S during HOC phase for (A) CEN.PK, (B) DBY12007, (C) YPS670, (D) YJM128. Solid symbols represent Δ_S , and open symbols represent τ_{hoc} . Lines represent linear regressions. Each strain with multiple data points for Δ_S has a characteristic time from HOC entry that has very low variation as τ_{hoc} changes.

slowly decreased with decreasing growth rate while LOC phase became significantly longer at low growth rates. Regardless of the exact form this relationship takes, f_{ymc} is a linear function of f_{cdc} suggesting that the progression of the two cycles is tightly linked. More interestingly, the HOC occupancy fraction ϕ_{HOC} increases linearly with growth rate (Fig. 2.9) and when the growth rate at which $\phi_{HOC} = 1$ is extrapolated, it corresponds to the critical growth rate at which yeast switch from fully aerobic growth to aerobic fermentation (Fig. 2.10). This growth rate represents the rate of glucose addition above which yeast mitochondria performing aerobic respiration

Table 2.2: Timing of maximal DNA replication (Δ_S) for all strains examined at dilution rates of $D=0.1$, $D=0.085$, $D=0.07$, and $D=0.05$. CEN.PK and DBY12007 showed robust oscillations at all growth rates, while YJM128 and YPS670 were difficult to sample at higher growth rates. Δ_S remains similar at different growth rates for any given strain.

D (h^{-1})	0.1	0.085	0.07	0.05
CEN.PK	56.5 \pm 0.7	53.7 \pm 32.6	48.0	53.5 \pm 0.7
DBY12007	58.0 \pm 2.0	59.0 \pm 5.7	59.0	54.0
YPS670 (oak)	44.8 \pm 8.5	58.0	44.0	
YJM128 (lung)	33.3 \pm 3.8			

at full capacity cannot metabolize all incoming glucose, and glucose buildup triggers fermentation due to glucose repression [Van Maris et al., 2001; Gancedo, 1998; Rolland et al., 2002; Kaspar von Meyenburg, 1969]. Therefore, it appears that the YMC represents a pattern of regulation of respiratory rate in yeast in which rather than smoothly ramping it with the rate of carbon assimilation, *pulses* of aerobic respiration in which mitochondria are activated at $\approx 100\%$ capacity are frequency modulated.

2.3.2 Response of the YMC to Growth Rate

The observed pattern of gene expression during the YMC may suggest additional significance of the relationship between growth rate and ϕ_{hoc} . According to studies of transcription and chromatin structure in oscillating yeast populations [Tu et al., 2005; Machné and Murray, 2012; Kuang et al., 2014], there are multiple periods of gene expression and chromatin modification patterns over the course of a single oscillation. These have been broadly labeled oxidative, reductive building, and reductive charging by the McKnight and Tu groups (Fig. 1.2). These occur during what we label as early HOC, late HOC, and LOC respectively. The oxidative gene cluster is enriched for genes involved in ribosome biosynthesis, translation factors, RNA metabolism, and amino acid synthesis with many extremely short-lived transcripts restricting their

expression to a very short period during the YMC [Tu et al., 2005]. The reductive building cluster is enriched in mitochondrial ribosome biosynthesis genes as well as genes involved in DNA replication and mitosis. The reductive charging cluster is enriched in genes involved in protein degradation, fatty acid metabolism, and other catabolic processes.

Work done in the Botstein laboratory has shown that there is a reproducible cluster of genes with a universal ‘growth rate response’ regardless of growth conditions or carbon source [Slavov and Botstein, 2011]. Growth rate can even be robustly inferred from gene expression data alone [Brauer et al., 2005]. Positive rate response genes increase in expression with growth rate in asynchronous chemostat or during batch culture, and negative response genes decrease with growth rate. Universal growth rate response genes represent a full 25% of the yeast genome and all of these genes are periodically expressed during the YMC [Slavov and Botstein, 2011]. Positive growth rate response genes (including ribosome biogenesis and biosynthetic genes) are expressed during oxidative/reductive building phases (HOC) and negative growth rate response genes (such as autophagy and vacuolar catabolic enzyme genes) expressed during reductive charging phase (LOC).

Given these data the Botstein laboratory proposed that the yeast metabolic cycle is always occurring in individual cells even outside synchronous chemostat cultures, with slow-growing cells spending more time in longer LOC phases. Under this interpretation the universal growth rate response is due to the change in the relative length of YMC phases averaged over an asynchronous population. These dynamics would only become visible in bulk culture when the entire population synchronizes under the proper chemostat conditions. The YMC does appear to continue in a cell-autonomous fashion in asynchronous populations of yeast according to single-molecule FISH data on the expression of YMC-regulated genes in single cells from the Botstein laboratory [Silverman et al., 2010] and live-cell microscopy of metabolic

probes by the Heinemann laboratory [Papagiannakis et al., 2016].

The relationship between growth rate and ϕ_{hoc} we have observed is consistent with this hypothesis. As the growth rate of our aerobic cultures increases, they spend a larger and larger fraction of time in HOC phase with a linear relationship between growth rate and ϕ_{hoc} . The expression of growth genes and production of biomass during HOC, taking up larger and larger shares of time at faster growth rates, would account for much of the observed dynamics of the YMC.

2.3.3 Similarity of YMC Dynamics to Bacterial Growth Laws

It has long been observed that in bacteria, both size and the fractional rRNA content of cells increase as a simple linear function of growth rate [Schaechter et al., 1958] due to the necessity for new protein biomass to be produced by active ribosomes. The Hwa laboratory and colleagues have extended this analysis of bacterial 'growth laws', identifying relationships between growth rate and 'sectors' of the transcriptome and proteome responsible for different cellular processes. [Klumpp et al., 2009; Scott et al., 2010; Scott and Hwa, 2011; You et al., 2013; Scott et al., 2014; Hui et al., 2015]. They propose that a simple model of efficient partitioning of limited transcription and translation resources between these sectors to maximize growth rate by adjusting the share allocated to each sector can account for much of the observed variation in transcription rate of different genes in *E. coli* under carbon limitation [Scott and Hwa, 2011; You et al., 2013]. According to this model, to a first approximation the transcriptome and proteome of a bacterium is composed of three sectors - fixed expression level genes, ribosome-associated and biomass production genes, and catabolic genes. The faster *E. coli* grows under the influence of environmental and nutritional factors, the larger the fraction of transcription/translation taken up by ribosome biogenesis and other anabolic processes. The slower the growth rate, the larger the fraction of transcription/translation taken up by catabolic and metabolic

genes [You et al., 2013; Scott et al., 2014; Hui et al., 2015].

Together with our results and previous research on transcription during the YMC, we suggest that the yeast metabolic cycle represents an expression of similar growth laws on the transcription and synthesis of different gene products in *Saccharomyces cerevisiae*. As growth rate increases, HOC occupancy fraction ϕ_{hoc} increases linearly. Oxidative and reductive building genes known from previous data [Tu et al., 2005; Machné and Murray, 2012; Kuang et al., 2014] to be expressed during HOC phase include cytosolic ribosome biogenesis genes, mitochondrial ribosome biogenesis genes, and genes associated with DNA replication and cell division (which only occurs in actively growing cells). Reductive charging genes expressed during LOC, with a decreasing fraction of time spent in this phase as growth rate increases, include a number of catabolic genes. Broadly speaking, the group of genes expressed during HOC is similar to those which increase in expression with growth rate in bacteria. The group expressed during LOC is similar to those which decrease with growth rate. Thus, rather than smoothly ramping their metabolic rate, growth rate, and transcription of anabolic genes with average growth rate like bacteria, yeast smoothly ramp the *fraction of time spent* in pulses of maximal transcription of anabolic genes, carbon metabolism, and cell growth/division when growing aerobically. This modulation of the pulse rate of “productive” periods in between “quiescent” periods during which enough carbon is assimilated to fuel biosynthesis and energy production would serve the same purpose as modulation of the steady-state transcription level of these genes and of the steady rate of carbon metabolism.

2.3.4 Potential Reasons for Metabolic Cycling in Yeast

Biological reasons for yeast to temporally separate growth and quiescence or the expression of different suites of genes are uncertain. The classic explanation is that it represents temporal segregation of incompatible cellular processes like oxidative

and reductive metabolism [Klevecz et al., 2004; Tu and McKnight, 2007; Lloyd and Murray, 2005]. Alternately, it could represent a bet-hedging strategy. Cells taken from a cycling population in HOC are significantly more sensitive to heat-shock than those taken during LOC [Slavov et al., 2012], and in slow-growing asynchronous populations heat-shock resistance is bimodal, with populations of heat-sensitive and heat-resistant cells coexisting [Lu et al., 2009; Slavov et al., 2012].

A bet-hedging strategy could ensure that slow-growing yeast are quiescent and stress-resistant for most of their lives before going through brief vulnerable productive periods in which they grow and reproduce but are less resistant to environmental insult, and allow larger numbers of cells to survive in a hostile and fluctuating environment. It has also been noted that genes with the greatest amplitude in expression oscillations during the YMC have the highest metabolic costs of expression due to RNA transcript and protein mass and are primarily expressed during oxidative/reductive building phase [Wang et al., 2015]. By coordinating the expression of these genes into a short period of time, the total cost of maintenance of protein levels in the face of protein/mRNA degradation and turnover is minimized and a ‘just-in-time’ supply chain is established [Kuang et al., 2014]. This would increase the metabolic efficiency of gene expression, although why yeast might do this when other microbes have not been observed to do so is unclear.

2.3.5 Timing of DNA Replication

The observed timing of DNA replication has important implications. In our growth conditions, strains CEN.PK and YJM128 showed DNA replication occurring in the middle of HOC phase while DBY12007 and YPS670 showed DNA replication occurring at approximately the HOC-to-LOC transition (Fig. 2.11, 2.12). The hypothesis that DNA replication is consistently prevented from occurring during periods of high oxygen consumption can be excluded. DNA replication is not timed to occur dur-

ing periods of minimal production of reactive oxygen species or coordinated with maximum cellular energy production.

For any given strain with multiple examined growth rates (CEN.PK, DBY12007, and YPS670), we measured a consistent delay Δ_S between HOC entry and the time of maximal DNA replication - see Fig. 2.15. While the length of HOC τ_{hoc} varies considerably over the range of growth rates examined for CEN.PK and DBY12007, Δ_S varies considerably less. YPS670 showed both a consistent HOC length and Δ_S over a range of growth rates. This constant delay may explain the variable relationship between metabolic state and DNA replication observed for strain DBY12007 by the Botstein laboratory, which was seen to replicate DNA in the middle of HOC phase at $D=0.1$ and in early HOC at $D=0.133$ [Slavov and Botstein, 2011].

While DNA replication is not explicitly coordinated with *or* excluded from any particular phase of the YMC, it is closely coordinated with the *shift* from LOC to HOC. The constant delay at least in part represents the delay that exists between a cell's commitment to progress through the cell division cycle (Start) and firing of origins of DNA replication upon entry into S phase. The relationship between cell cycle Start commitment and HOC entry is not clear from these data. For example, a CDC-synchronized cohort of cells entering Start could trigger HOC entry, or cell cycle Start could push a cohort of cells to enter HOC. In either case, the association of cell cycle commitment and HOC entry can explain the variety of coupling patterns between the YMC and HOC observed in the literature and may help unify the relationships observed across many strains and growth conditions.

2.4 Contributions and Publications

Work done in this chapter was done by Anthony Burnetti with some assistance from Mert Aydin (laboratory technician) who helped perform experiments. This work was funded by Defense Advanced Research Projects Agency Biochronicity Grant

DARPA-BAA-11-66, National Institutes of Health Director's New Innovator Award DP2 OD008654-01, and Burroughs Wellcome Fund CASI Award BWF 1005769.01.

Data from this chapter has been published as: Burnetti, A. J., Aydin, M., and Buchler, N. E. (2016), "Cell cycle Start is coupled to entry into the yeast metabolic cycle across diverse strains and growth rates," *Molecular Biology of the Cell* 27, 64-74.

Timing of Cell Cycle Start During the YMC at Single Cell Resolution

3.1 Introduction

Our results described in Chapter 2 suggest that cell cycle progression is closely tied to entry into HOC during the yeast metabolic cycle. However, this conclusion was based on observations of DNA replication. In *Saccharomyces cerevisiae*, DNA replication occurs some time after the primary restriction point in cell cycle progression, known as Start. Start represents a binary decision in the life of a cell at which it irreversibly commits to a round of division. Start is controlled by a number of checkpoints and environmental signals to ensure it is not prematurely initiated. As such, we hypothesized that cell cycle Start was the cell cycle event closely coupled to HOC entry during the yeast metabolic cycle. We designed a set of experiments to observe Start timing relative to HOC entry.

The Futcher and Skotheim labs have recently demonstrated that progression of the cell division cycle past Start triggers the breakdown of storage carbohydrates via the phosphorylation and activation of trehalose-consuming enzyme Nth1 and

the glycogen-consuming enzyme Gph1 by the cyclin-dependent kinase complexed with S-phase cyclins [Ewald et al., 2016; Zhao et al., 2016]. In contrast, the Tu lab has demonstrated that a pulse of acetyl-coA produced during breakdown of storage carbohydrates during the YMC causes the acetylation of large swaths of chromatin which upregulates many genes expressed during HOC, including the G1 cyclin *CLN3*, which is involved in pushing the cell cycle through Start [Shi and Tu, 2013a]. These models have opposite predictions regarding the relative timing of cell cycle Start and entry into HOC. If Start precedes the sharp metabolic shifts at the onset of HOC, then it would indicate that metabolism was shifting in response to commitment to the cell cycle, as described by Futcher and Skotheim. If Start occurs after the onset of HOC, then it would indicate that the metabolic cycle forces cell division forward, as described by the Tu group. My goal is to determine the precise timing of cell cycle Start relative to HOC entry in order to clarify whether the YMC or CDC is the driving oscillator in the coupled system.

By using a fluorescent reporter of cell cycle Start that can be observed and quantified via microscopy, we determined that Start occurs *after* the shift into HOC during the yeast metabolic cycle. The average delay is 14 minutes with nearly all commitment occurring during HOC when chromatin acetylation is presumably occurring. This supports a model in which metabolism drives commitment to cell division in yeast in a cycling chemostat population. The ability to image individual cells and determine their cell cycle status also allowed us to determine the properties of those cells (size, replicative age) which did or did not commit to cell cycle at a given time. With this data, we were able to determine that cell size is significantly more predictive than replicative age at determining cell cycle behavior during the yeast metabolic cycle. These data suggest a combined model of yeast cell size control and the Tu laboratory's model of YMC/CDC coupling, where the YMC triggers commitment to cell division by lowering the threshold size at which Start is triggered.

3.1.1 Measuring Cell Cycle Start in Single Cells

We used a fusion of the Start network protein Whi5 with the red fluorescent protein tdTomato as a probe to observe cell cycle Start via fluorescence microscopy. The localization of Whi5 is one of the most precise and binary markers of cell cycle Start [Ball et al., 2011; Skotheim et al., 2008]. When Whi5 is localized to the nucleus, its activity inhibiting the transcription factor SBF holds cells in G1 phase. During G1 phase of the cell cycle, increasing activity of the G1 cyclin Cln3 Starts to phosphorylate nuclear Whi5 and causes its export from the nucleus. As the activity of nuclear Whi5 decreases below a critical Start threshold, the transcription factor SBF activates the transcription of CLN1 and CLN2, which together with the cyclin dependent kinase Cdk1p further phosphorylate Whi5p in a positive feedback loop until it is entirely cytoplasmic [De Bruin et al., 2004; Costanzo et al., 2004] - See Fig. 1.4 in Chapter 1. This indicator of cell cycle status can be preserved in sampled cells by formaldehyde fixation and is stable in refrigerated storage in PBS for weeks, allowing the analysis of cell cycle state during YMC time-courses via fluorescence microscopy.

3.1.2 Cell Size and Replicative Age

Budding yeast divide asymmetrically, where small ‘daughter’ cells bud from large ‘mother’ cells - see Fig. 3.1. Mother cells rapidly pass Start again after completing cell division, while daughter cells require an initial growth period before reaching a minimum cell size and passing Start. Upon completing this first division they become a mother cell and will continue regularly passing through the cell cycle. Thus, mothers divide more rapidly than the population average and daughters more slowly. For example, in a culture with a population doubling time of 250 minutes, daughter cells take approximately 450 minutes to divide while mother cells require less than 200 [Hatzis and Porro, 2006]. The mother/daughter difference in average

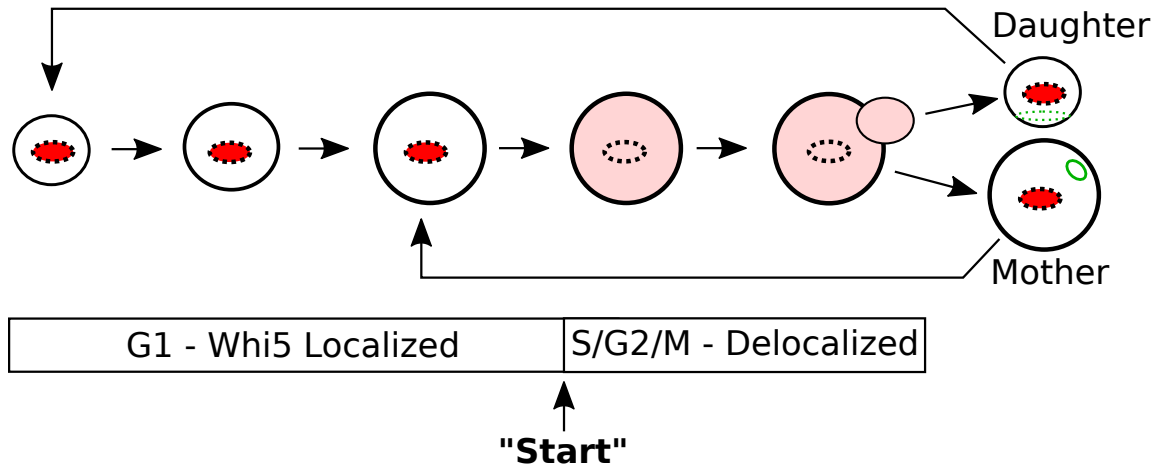


FIGURE 3.1: Growth and cell cycle Start in mother and daughter cells. All cells in G1 have Whi5 localized to the nucleus. At cell cycle Start, Whi5 (visualized in red) rapidly delocalizes to the cytoplasm and remains delocalized through S phase, and G2/M. Whi5 relocalizes upon completion of mitosis, at which point the budded cell undergoes cytokinesis and splits. The budded cell becomes a mother cell if it was not already a mother, and gains a permanent bud scar (visualized in green) with each bud it produces. A small daughter cell is produced which may transiently have a dim birth scar. Large mothers are able to re-divide rapidly after a small amount of growth, while daughters must grow significantly before reaching the critical size threshold required for division.

cell cycle time increases at slower growth rates. Under chemostat conditions with a dilution rate of $D = 0.05hr^{-1}$, the average population doubling time is 831 minutes and the mother-daughter differences are expected to be large.

The more rapid division of mother cells than daughter cells at slow growth rates raised the possibility that the period of the YMC could be similar to the mother CDC period, and that these two oscillators coupled 1:1 in this subpopulation. If these periods were equal it could indicate that the intrinsic period of the mother cell division cycle was the driving force determining the period of the YMC. This would support a model of YMC/CDC coupling in which cell cycle events drove and dominated metabolism, at least in mothers. The population-level YMC period would then be determined by the cell cycle period of this frequently dividing cohort who

then act as a pacemaker for the remainder of the population via cell-to-cell metabolic coupling.

In order to test this hypothesis, the fraction of mother and daughter cells that divide during a given YMC had to be measured. Formaldehyde-fixed fixed Whi5-tdTomato yeast were stained with wheat germ agglutinin (WGA) conjugated with AlexaFluor488. WGA binds tightly to chitin which is present at high levels at the bud scars left behind on mother cells when a daughter buds off. Upon exposure to WGA a bud scar becomes a brightly stained ring. Mother cells possess one or more bright bud scars, while daughter cells either have no visibly stained rings or possess a ‘birth scar’ - a dimmer-staining ring that is much larger than a bud scar, stretching as the cell grows. A typical image of fixed Whi5-tdTomato yeast stained with fluorescent WGA to reveal bud scars can be seen in Fig. 3.2. This allowed us to easily distinguish the fraction of mother and daughter cells which had committed to the cell division cycle in any chemostat sample.

3.1.3 *Strains and Genotypes*

Cell cycle Start was primarily examined in the diploid prototroph GZ240/GZ241 strain. This strain was constructed by mating two haploid strains generously provided by Bruce Futcher (created from strains described in [Zhao et al., 2016]). Its genetic background is similar to DBY12007, having been created from the S288C standard laboratory strain and having all auxotrophies repaired. GZ240/241 also contains the same repaired *HAP1* allele, restoring the wild type function of this metabolically significant oxygen and heme sensing transcription factor which is interrupted by a transposon in S288C. However, the GZ240/241 strain goes on to also restore wild-type alleles of four additional genes (*MKT1*, *SAL1*, *CAT5*, *MIP1*) known to be mutated in S288C, which are important for mitochondrial genome stability and respiratory regulation [Dimitrov et al., 2009]. This background is therefore

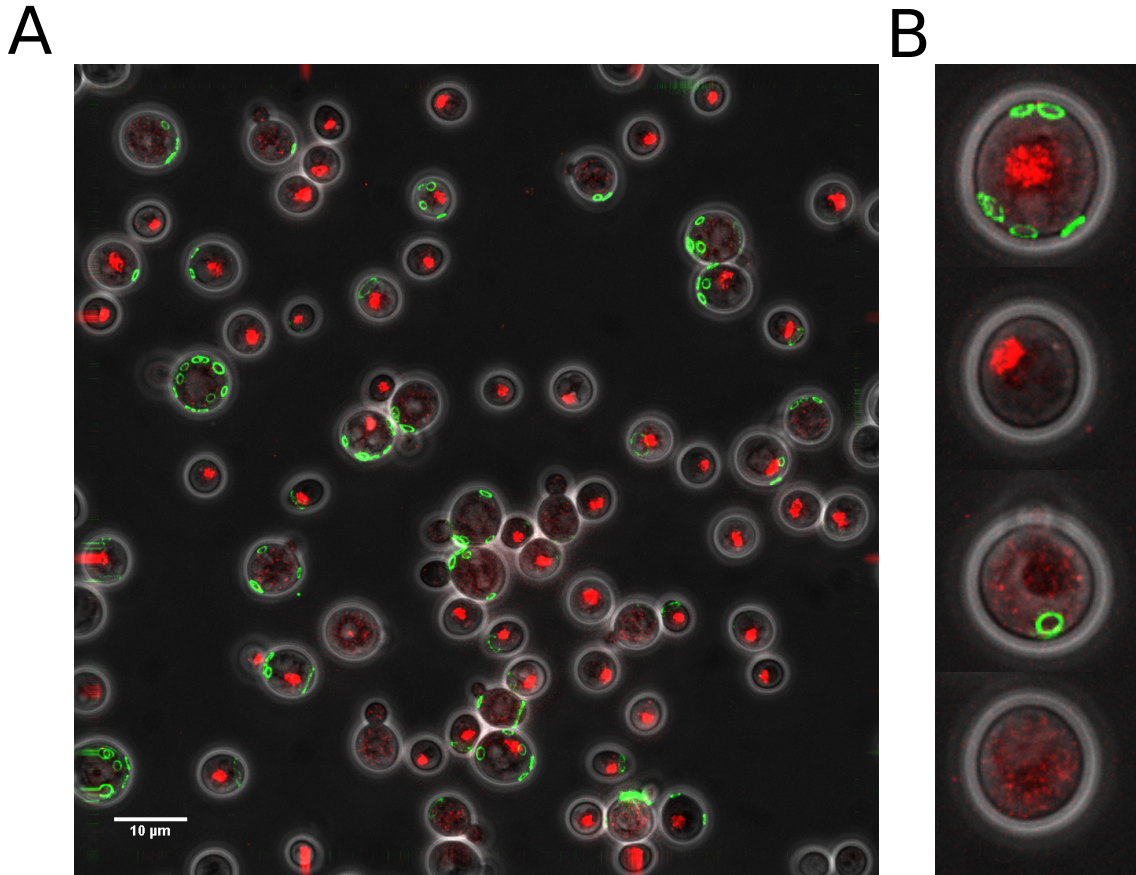


FIGURE 3.2: (A) A typical microscope image frame, scale bar 10 micrometers. Phase contrast image in grey, Whi5-tdTomato visible in red, bud scars stained by wheat germ agglutinin visible in green. Occasional ‘birth scars’ are visible and distinguished from bud scars by dim color and large size relative to cell diameter. (B) individual cells of the four classes identified - from top to bottom, G1 mother, G1 daughter, committed mother in S/G2/M, committed daughter in S/G2/M.

closer to wild-type in terms of mitochondrial function than DBY12007, but nearly isogenic with it. GZ240/241 is also useful for ongoing work on the yeast metabolic cycle and its relationship with the cell cycle because the Futcher laboratory has generated a number of strains in this background bearing mutations in storage carbohydrate synthesis and breakdown genes.

One endogenous chromosomal copy of Whi5 was fused with the red fluorescent protein tdTomato to produce the GZ240/241 strain used in this analysis (simply

referred to as GZ240/241 after this point) - see Materials and Methods. A copy of the pH-sensitive green fluorescent protein pHluorin [Miesenböck et al., 1998; Isom et al., 2013] was also introduced at the HO locus. This pH biosensor was integrated to allow flow cytometry analysis of the metabolic state of yeast cells, enabling a second indirect readout of cellular metabolic state besides pO_2 . The cytosolic pH of yeast grown in acidic media becomes closer to neutral when high levels of ATP are available as proton pumps run faster to acidify vacuoles.

The Whi5-tdTomato fusion was also introduced into the endogenous Whi5 locus in the DBY12007 background, to produce a second strain in which cell cycle Start was visible. This strain was used to test the reproducibility of results across strains.

3.1.4 Chemostat Sampling and Microscopy

Yeast were cultured in chemostat conditions and oscillations were established as previously described in Chapter 2, and the dilution rate set to $D=0.05 \text{ hr}^{-1}$ for a τ_{cdc} of 831 minutes. Chemostat chambers were allowed to reach a steady state oscillation before sampling. Samples were taken regularly via a sterile syringe port, at intervals of 5 minutes during natural HOC phase and varied slower cadences during LOC and induced HOC phase - see Fig. 3.3. Periods of rapid sampling cadence corresponding to HOC phase were chosen based on preliminary experiments in which live cells were extracted from the cycling chemostat and examined microscopically to determine periods of rapid change in cell cycle status. Two usable GZ240/241 time courses were gathered, one representing a single natural oscillation and one representing two back-to-back oscillations followed by an artificially induced HOC triggered by introducing ethanol into the chemostat chamber to a final concentration of 1mM. Two confirmatory DBY12007 time courses were gathered, each constituting a single natural oscillation.

Extracted 0.5 mL samples were immediately fixed in 4% formaldehyde for 10

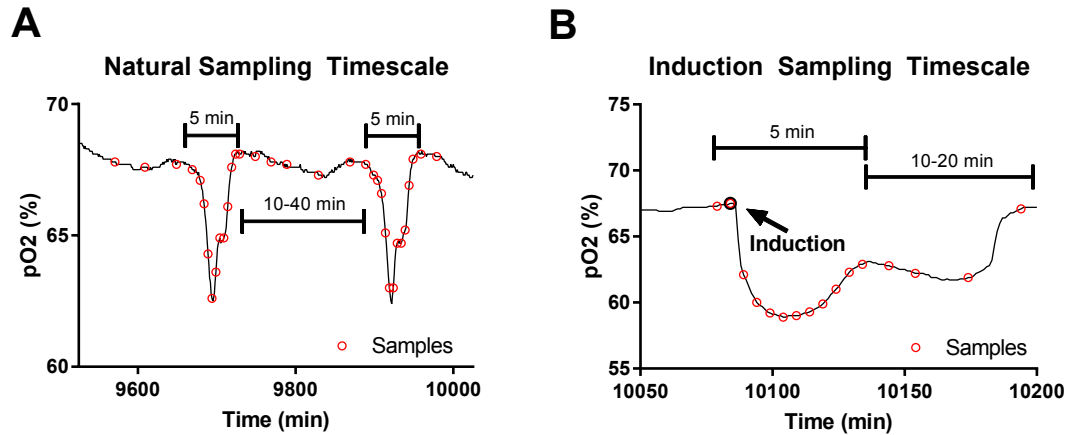


FIGURE 3.3: (A) One GZ240/241 natural oscillation dataset spanning two YMC periods. Samples (red circles) were extracted, fixed, and stored every five minutes during HOC and whenever pO₂ was changing rapidly, and every 10-40 minutes during LOC when pO₂ was changing slowly. (B) Samples (red circles) taken during an artificially induced HOC phase. The first sample was taken 5 minutes before ethanol induction (black circle), and sampling continued on a 5 minute timescale until midway through the artificially lengthened HOC phase. Sampling was gradually lengthened to every 10 and every 20 minutes in late artificial HOC phase, as preliminary data indicated that the cell division cycle was less dynamic in late HOC under these conditions.

minutes before one PBS wash and storage in PBS. These cells were imaged via fluorescence microscopy within three weeks of collection. All cells from a given time course were imaged within 4 days of each other. This was done because fluorescent proteins in fixed cells degrade over time, and it avoided the possibility of excessive Whi5-tdTomato degradation between imaging of multiple timepoints in the same time course. All cells imaged during a given day were stained at the start of the day with AlexaFluor488-tagged wheat-germ agglutinin at a concentration of 33 $\mu\text{g}/\text{mL}$ in PBS for 10 minutes, then washed four times in PBS, just before imaging began.

For each timepoint, approximately 400 cells were imaged using a DeltaVision Elite (GE) microscope with up to ≈ 50 cells per microscope stage position. At every stage position a phase contrast reference image was recorded, as well as a 10 micron,

25 image z-stack of Whi5-tdtomato and WGA-AlexaFluor488 stained bud scar images. This z-stack was deconvolved on the DeltaVision microscope workstation in parallel with image acquisition and then projected into a single two dimensional image using a maximum-intensity projection, to maximize the difference between cells with localized and delocalized Whi5 [Ball et al., 2011]. See Materials and Methods for details of image processing.

3.1.5 Microscopy Image Analysis

Stacked phase contrast, Whi5-tdTomato, and bud scar images were segmented using image analysis software CellStat in Matlab [Kvarnström et al., 2008], as seen in Fig. 3.4. When cells were budding, buds were not segmented to speed and simplify image segmentation. Buds were distinguished from small cells adjacent to large cells by both the bud and its parent cell having delocalized whi5-tdTomato and very low contrast between the parent cell and bud. While this leads to underestimation of the volume of budding cells in S/G2/M, this does not affect measurements of the unbudded cells in which cell cycle Start actually *occurs*. Conclusions about the relationship between cell size and Start are therefore unaffected. CellStat was used to record the area (in pixels), eccentricity (major axis over minor axis), Whi5-tdTomato average intensity, and Whi5-tdTomato standard deviation for each segmented cell. Mother/daughter status was annotated manually for all GZ240/241 cells and for a subset of DBY12007 cells.

Cell size affects microbial physiology and size homeostasis is a critical component of the control of Start in yeast. The volume of all imaged cells was calculated in order to distinguish between behavior based on replicative age and behavior based on size. Cell volume in femtoliters was calculated from the two dimensional surface area in pixels (A) and eccentricity (e) statistics provided by cellStat image analysis software, and the scale of the image in pixels per micron (s). Calculations were

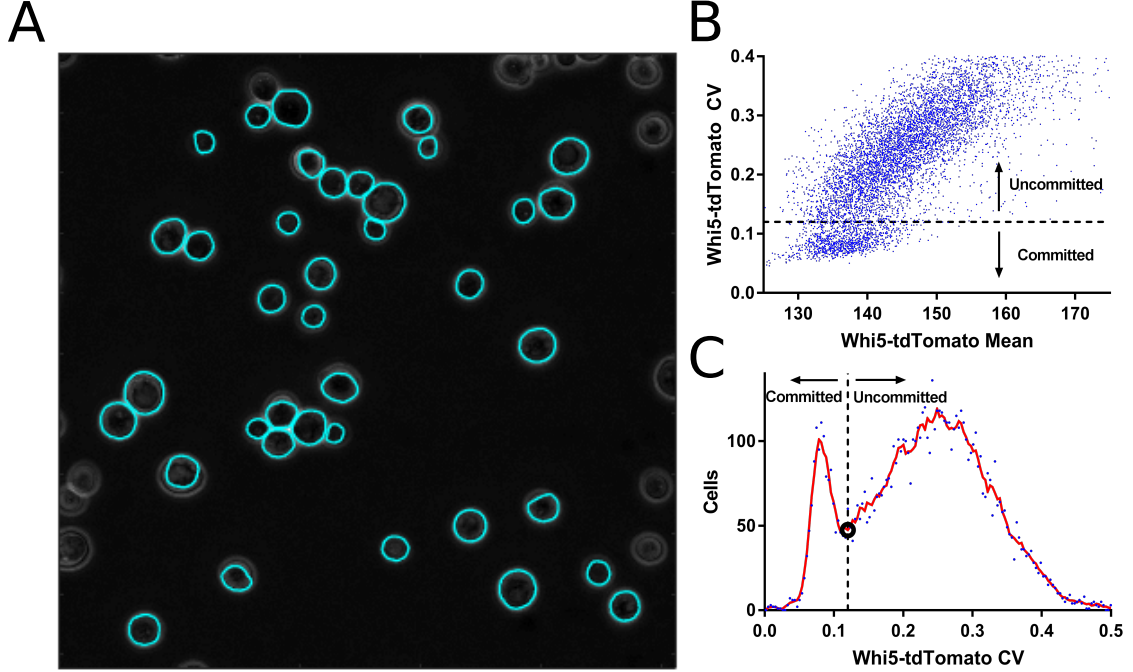


FIGURE 3.4: (A) Segmentation of images. Cell boundaries were identified semi-automatically using cellStat. All pictured cells are unbudded. Growing buds were not segmented. (B) Representative plot of mean Whi5-tdTomato fluorescence versus the coefficient of variation (CV) of pixel intensity within each cell for a dataset spanning a full oscillation. Two populations are clearly visible, separated by CV. Cells manually annotated as budding universally fall into the low-CV population, indicating that it represents cells with delocalized Whi5-tdTomato which have committed to division. (C) Distribution of Whi5-tdTomato CV in the same dataset. Local minimum of CV frequency is indicated (black circle), and used as the dividing line between cells annotated as delocalized/committed (low CV) and localized/uncommitted (high CV).

performed assuming all cells have the three-dimensional figure of a prolate spheroid, extracting the major axis a in microns, minor axis b in microns, and volume V in femtoliters as follows:

$$a = \sqrt{\frac{A}{s^2} e / \pi} \quad (3.1a)$$

$$b = \sqrt{\frac{A}{s^2} / e \pi} \quad (3.1b)$$

$$V = \frac{4}{3}\pi b^2 a \quad (3.1c)$$

Cells were automatically classified as committed (S/G2/M phase) or not committed (G1 phase) based on the coefficient of variation (CV) of pixel intensity in the Whi5-tdTomato channel. A CV cutoff was chosen for each time course based on the distribution of CV values at a local minimum of CV frequency between two distinguishable populations - see Fig. 3.4b and Fig. 3.4c. All cells with CVs below this threshold were annotated as committed to division because this indicated a cytoplasmic Whi5p distribution rather than localization to the nucleus. All analysis was performed using custom Matlab scripts.

Up to 22,000 individual cells were imaged in a given time series, with many variables (timepoint, size, replicative age, and Whi5-localization) available to sort and distinguish them. In order to investigate the CDC behavior of subpopulations of cells during the YMC, these variables could be used to bin cells into categories. These categories include mother/daughter, cell volume ranges, and committed versus noncommitted to the cell division cycle.

3.1.6 *pHluorin Flow Cytometry*

The medium in which yeast were grown for our chemostat experiments is maintained at a pH of 4 ± 0.1 , while cellular cytoplasm is maintained close to neutral. In *Saccharomyces cerevisiae*, the level of ATP available is a primary determinant of the exact cytosolic pH [Miesenböck et al., 1998; Isom et al., 2013]. When more ATP is available, vacuolar ATPases pump protons out of the cytoplasm more rapidly and the pH is maintained further from equilibrium with the surroundings (i.e. closer to neutral). Cytosolic pH is therefore an indirect marker of metabolic state in yeast, which could be measured at single-cell resolution by flow cytometry using pHluorin. pHluorin is potentially a more useful metabolic marker than pO_2 because it could be

used to distinguish between two populations of yeast which change metabolic rates at different times, while pO_2 dynamics are the result in shifts in the average oxygen uptake rate of a yeast culture with no possibility of distinguishing subpopulations.

The absorption spectrum of pHluorin shifts with pH: it increases absorption at short wavelengths near 400 nm at alkaline pH and increases absorption at longer wavelengths near 480 nm at acidic pH [Miesenböck et al., 1998]. In order to observe the cytosolic pH of GZ240/241 yeast with pHluorin, samples were extracted from a cycling chemostat at five minute intervals during HOC phase and at longer intervals during LOC phase and measured via flow cytometry within 20 seconds of extraction. This rapid measurement prevented fluctuations in metabolic state due to depletion of carbon sources in the media or temperature shifts. The ratio of fluorescence when excited at 405 nm and 488 nm was measured. This fluorescence ratio was calibrated to cytosolic pH using yeast which had been permeabilized with the detergent digitonin and resuspended in known pH buffers. See Materials and Methods for details of flow cytometry setup and calibration of pH measurements.

3.2 Results

3.2.1 Measurement of Metabolic State With pHluorin

The pH-sensitive ratiometric pHluorin protein was successfully used as a metabolic probe of the YMC. As seen in Fig. 3.5, calibration samples of permeabilized yeast in known pH buffers show distinct patterns of fluorescence with increased fluorescence when excited 488 nm at alkaline pH and when excited at 405 nm at acidic pH.

Unfortunately, there was a great deal of cell-to-cell variability in fluorescence even in control cells with their cytoplasm artificially brought to a known pH. This leads to significant overlap between the distribution of the 405 nm : 488 nm excitation ratios for all practically useful pH ranges (Fig. 3.5a). However, ratiometric pHluorin can still be used as a probe of the average energy state of a yeast culture, much

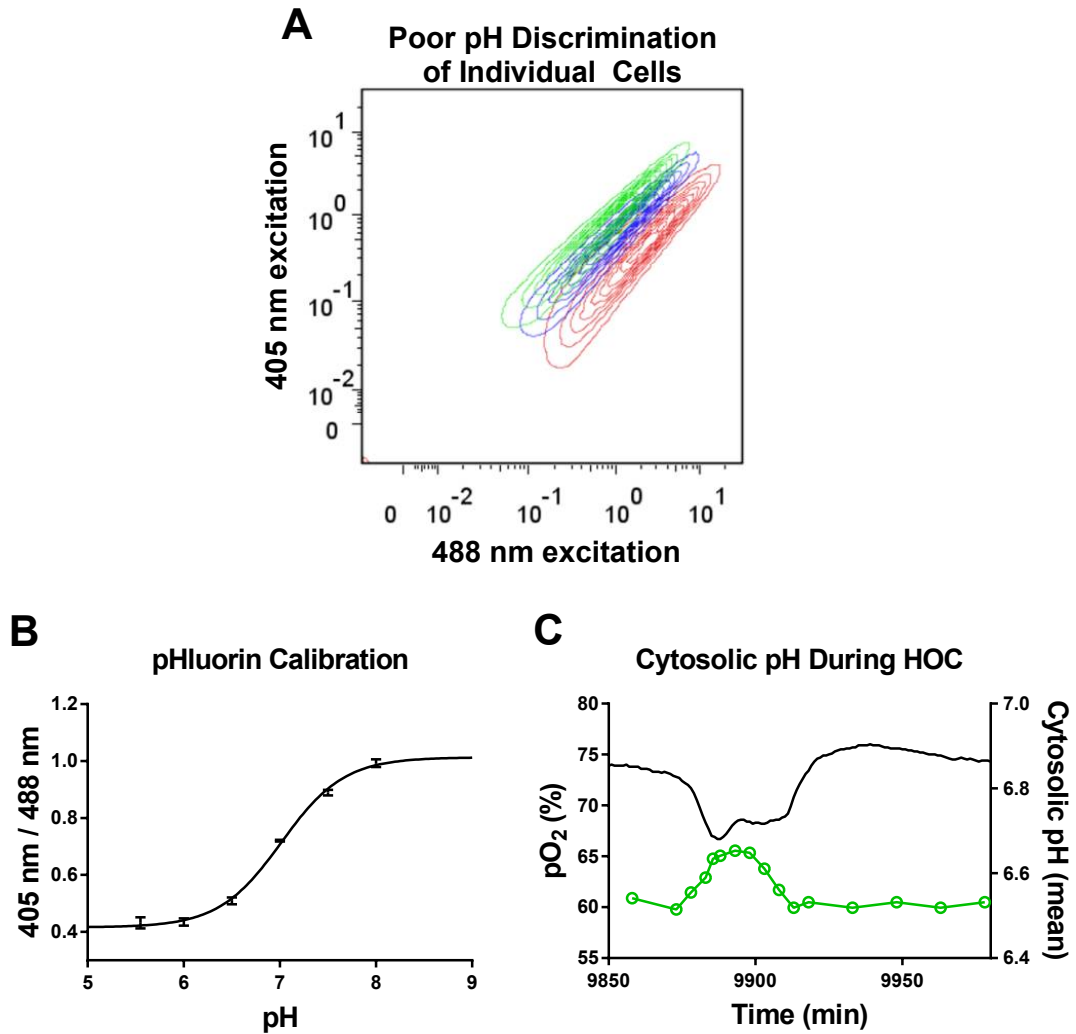


FIGURE 3.5: (A) pHluorin was unable to reliably distinguish the internal pH of individual cells. Red contours represent the fluorescence values of permeabilized control cells at pH 5.5, blue represents pH 7.0, green represents pH 8. While each population forms a tight distribution with a reproducible mean ratio, there is significant overlap. (B) Calibration of *average* pH measurements to fluorescence ratios illustrates that measurement of the population-average pH is extremely robust and reproducible. Permeabilized yeast extracted from chemostat culture were resuspended in buffers of known pH. A calibration curve for cytosolic pH versus the average ratio of fluorescence of GFP at 405 and 488 nm is pictured. (C) Average cytosolic pH from yeast taken from a cycling chemostat at $D=0.1 \text{ hr}^{-1}$. Cytosolic pH rises during HOC phase, indicating an increase in available cellular energy.

like pO_2 when the *average* 405:488 nm ratio is used. See Fig. 3.5b for a sample calibration curve - the noise present when considering individual cells cancels out when considering the population average and the *average* 405:488 nm ratio at a given pH is extremely reproducible.

When this was used to impute the dynamics of cytosolic pH over the course of the YMC, a consistent relationship was visible. Average cytosolic pH was low and constant during LOC phase, and rose by ≈ 0.2 pH units during HOC phase (Fig. 3.5c). The dynamics of cytosolic pH closely mirror those of pO_2 , further establishing the validity of pO_2 as a marker of population level metabolic state.

3.2.2 Cell Size and Replicative Age

Analysis of mother/daughter status is confounded with analysis of cell volume. These two attributes are related, with daughter cells growing to a minimum viable size before undergoing their first division and becoming mothers, and mothers being on average much larger than daughters. In order to understand what factors are driving heterogeneity in a cycling population, the relationship between these two attributes must be understood.

The populations of GZ240/241 mothers and daughters have quite different size distributions. As seen in Fig. 3.6a, daughter cells cluster strongly at small sizes below ≈ 90 fL with a small tail of larger cells, while mother cells have a wide distribution of sizes. This is expected because mother cells continue to grow through multiple cell cycles and reach larger sizes, while daughters are born small and require growth and time to reach sufficient size to undergo their first division (Fig. 3.1). Daughters grow after birth but upon reaching a critical size enter the cell cycle and leave the daughter subpopulation to become mothers. As shown in Fig. 3.6b, mothers dominate the population of large cells while the smallest cells are almost exclusively daughters. As such, any difference between the behavior of mother cells and daughter cells must be

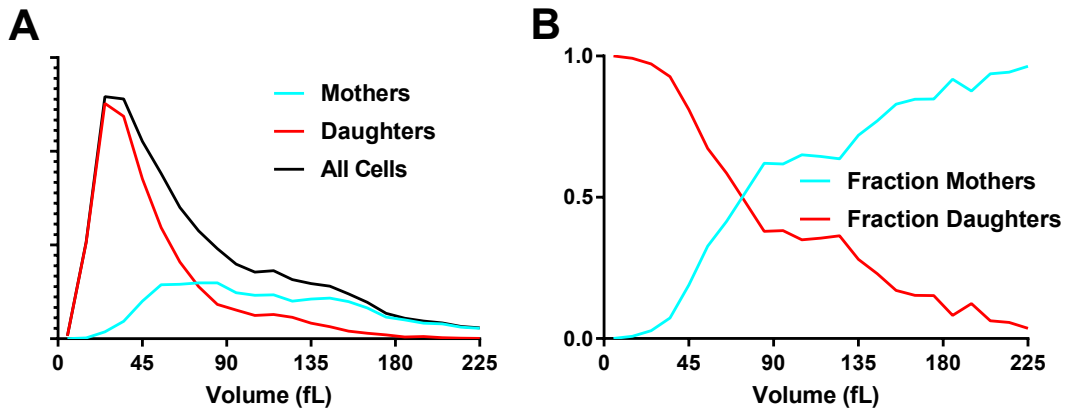


FIGURE 3.6: (A) Volume distribution (in fL) from one representative dataset of all cells in black, mother cells in blue, and daughter cells in red. Mothers are on average much larger than daughters. (B) Fraction of cells of different volumes that are mothers in blue, and daughters in red. The larger a cell, the more likely it is to be a mother.

carefully considered because it could simply represent a difference in average size.

3.2.3 Timing of Cell Cycle Start Relative to HOC entry

In all natural oscillations observed, cell cycle Start was confined to high oxygen consumption phase. As can be seen in Fig. 3.7, during natural oscillations yeast only begin committing to the cell division cycle at entry to HOC phase, reach their highest level of cell cycle commitment at the very end of HOC, and slowly slip back into G1 phase over the course of LOC as budding is completed. It is clear from this data that during natural oscillations, cell cycle Start is delayed until *after* the metabolic shift into HOC begins, with few to no cells passing through Start before the shift.

The continuous decrease in cells committed to division during LOC phase suggests that all commitment to the cell cycle is confined to HOC phase. Assuming a constant growth and division rate, over the course of a single YMC (which is a fraction of τ_{cdc} , the population doubling time) the expected growth in cell number is $\approx 2^{\tau^{YMC}/\tau^{CDC}}$.

Start Occurs During HOC

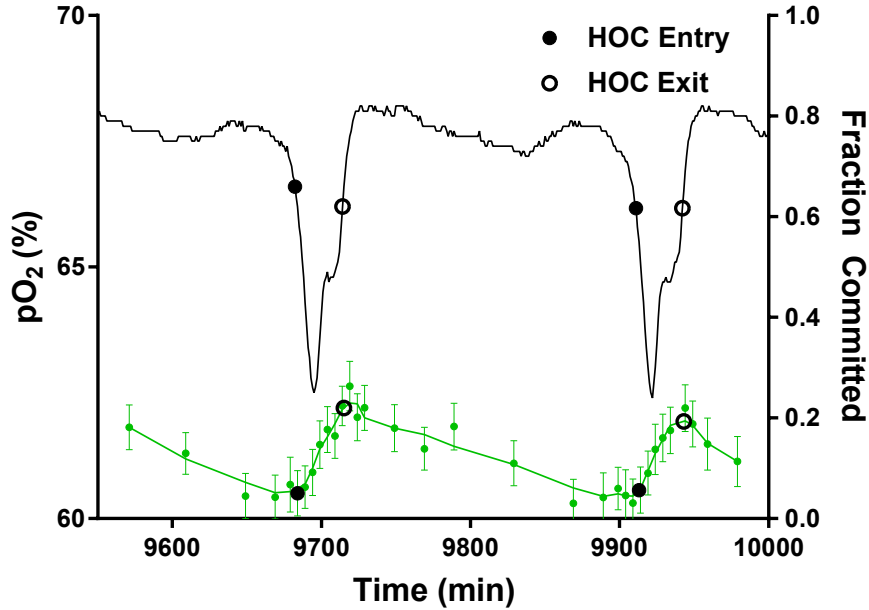


FIGURE 3.7: Timing of cell cycle Start in all cells. Two consecutive natural oscillations of GZ240/241 yeast are visualized. Entry into HOC is indicated by solid black points on the pO_2 curve, exit with black circles. Entry and exit do not occur at the same pO_2 level for the first HOC due to a long-term trend in pO_2 probe calibration. Fraction of cells committed to cell cycle progression are visualized in green with 95% margin of error, and smoothed data as a continuous line. HOC entry and exit are indicated on the smoothed data as on pO_2 . Error bars indicate 95% margins of error of the fraction committed. Cells begin entering Start at the time of HOC entry and end at the time of HOC exit.

For every new cell that is produced a previously existing cell must divide; therefore the fraction of existing cells that are expected to divide once per metabolic cycle is $\approx 2^{\tau_{YMC}/\tau_{CDC}} - 1$. At $D=0.05 \text{ hr}^{-1}$, τ_{cdc} is 831 minutes, and the observed τ_{ymc} for GZ240/241 at this growth rate is 229 minutes. Therefore, the fraction of cells expected to divide during a single oscillation is $2^{231/831} - 1 = 0.21$. This is precisely what is observed, supporting the idea that all cell cycle commitment during the YMC occurs during HOC phase.

The population of cells can be subdivided according to both replicative age and

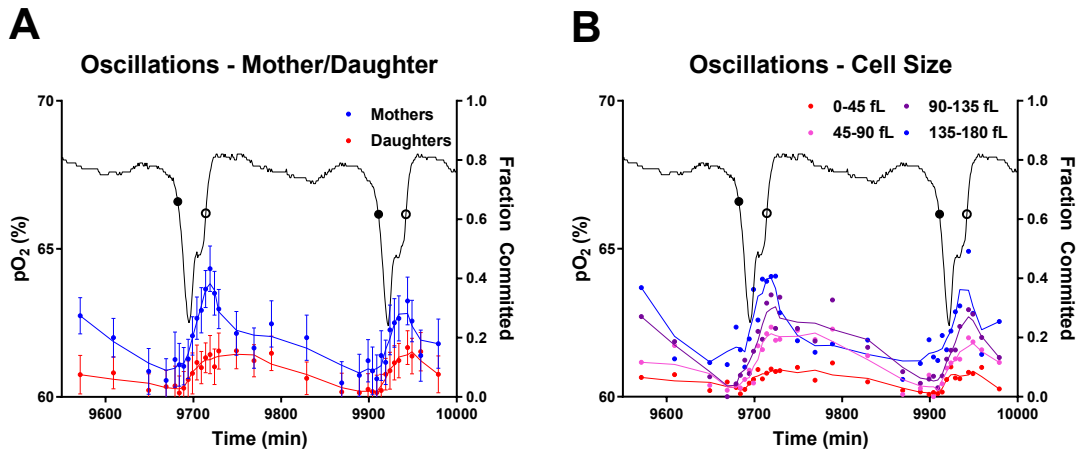


FIGURE 3.8: Timing of cell cycle Start, with cells separated according to replicative age and cell volume. (A) Two consecutive natural oscillations of GZ240/241 yeast are visualized. Entry into HOC is indicated by solid black points. Fraction of cells committed to cell cycle progression are visualized, with mother cells in blue and daughter cells in red and smoothed data as a continuous line. Error bars indicate 95% confidence intervals for the margin of error of the fraction. The timing of mother and daughter cells are similar, with commitment occurring after HOC entry but more mother cells committing to division than daughters. (B) Cells from the same dataset separated into four volume bins, with the smallest cells in red and the largest cells in blue. Error bars omitted for clarity. Larger cells commit to division more frequently than smaller cells.

volume. As seen in Fig. 3.8a, during natural oscillations both mothers and daughters begin commitment to division *after* entry into HOC. Mothers commit more frequently, with over 40% of mothers the cell division cycle during a single HOC at $D=0.05$ while less than 20% of daughters commit. When segregating cells by volume, larger cells commit to cell cycle progression more frequently - less than 10% of cells below 45 fL in volume pass Start during a given HOC while over 40% of cells between 135 and 180 fL commit (see Fig. 3.8b). In all cases, commitment to the CDC begins during entry into HOC and continues until approximately the time of exit from HOC. The fraction of cells committed to the cell cycle falls rapidly from its maximum during LOC for mothers and large cells, but remains high for longer in

small cells and daughters. One possible explanation for this could be that S/G2/M phase lasts longer for daughters and small cells.

There is no subpopulation in which large numbers of cells pass Start before entry into HOC and, furthermore, cells appear to pass Start throughout HOC phase of the YMC. This indicates that cell cycle Start is triggered by entry into HOC and during HOC itself, and supports the hypothesis that the YMC drives the CDC under chemostat growth conditions.

3.2.4 Artificial Induction of HOC

HOC phase can be artificially induced by adding ethanol, acetate, or acetaldehyde to a cycling chemostat [Robertson et al., 2008; Cai et al., 2011; Shi and Tu, 2013b]. These metabolites are produced spontaneously during early HOC phase [Murray et al., 2003; Porro et al., 1988; Martegani et al., 1990] and likely constitute diffusible signals by which metabolic synchrony is maintained during the YMC. By adding one of these metabolites at concentrations in excess of what is observed during natural oscillations one can phase-shift the YMC and induce entry into HOC. Thus, the effect of the metabolic shift into HOC on cell cycle Start can be directly observed without the confounding factors of different cell populations entering HOC at different times during a single population-scale metabolic cycle.

We added ethanol to a cycling chemostat chamber in late LOC phase to a final concentration of 1mM, which is several times the concentration observed during natural oscillations. This induced a very strong HOC phase (Fig. 3.9). This artificial induction immediately triggered an HOC phase with significantly higher oxygen consumption than natural HOC, and which disrupted the natural YMC rhythm for ≈ 650 minutes. It lasted approximately 100 minutes compared to the natural oscillation's 30 minute duration.

Samples taken during this artificial induction reveal that cells begin to pass Start

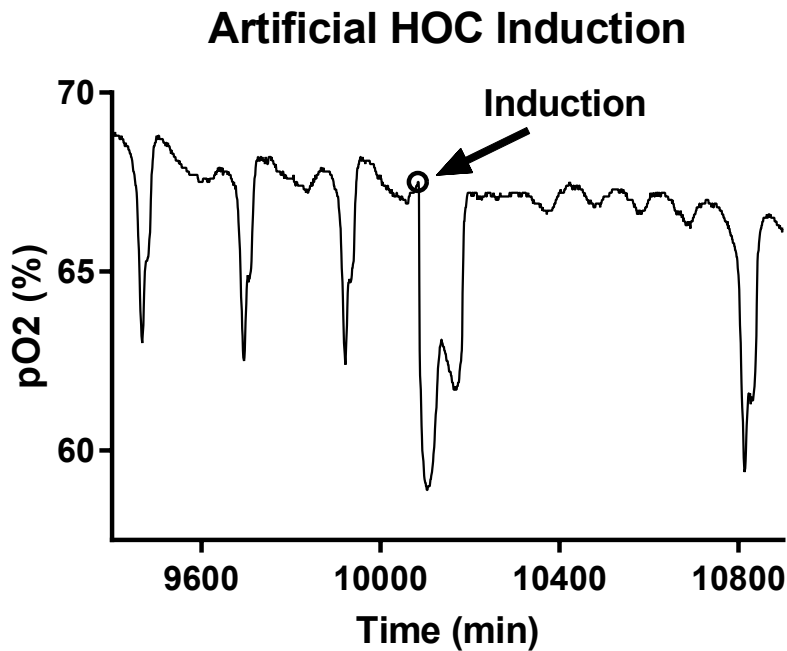


FIGURE 3.9: Artificial induction of HOC in GZ240/241 by 1 mM ethanol. At the time of induction (open circle), a strong HOC was observed lasting 3x as long as normal with much higher rates of oxygen consumption. The YMC is disrupted for several normal oscillation periods afterwards.

shortly after induction. As seen in Fig. 3.10, cells begin committing to cell cycle progression roughly simultaneously with entry into HOC as previously defined by a drop of pO_2 by 35% of the full range of pO_2 values during this oscillation. The fraction of cells committed to cell cycle progression continues to increase over the entire artificially induced HOC, although commitment is more rapid during the first third of this period. LOC phase after artificial induction was not examined, as the metabolic cycle was highly disrupted and somewhat irregular for several days after artificial induction, making timing of samples difficult.

Cells responding to this artificial HOC induction can be separated into subpopulations according to replicative age and cell volume, identically to cells from natural oscillations. As seen in Fig. 3.11a, a much larger fraction of mother cells divide than

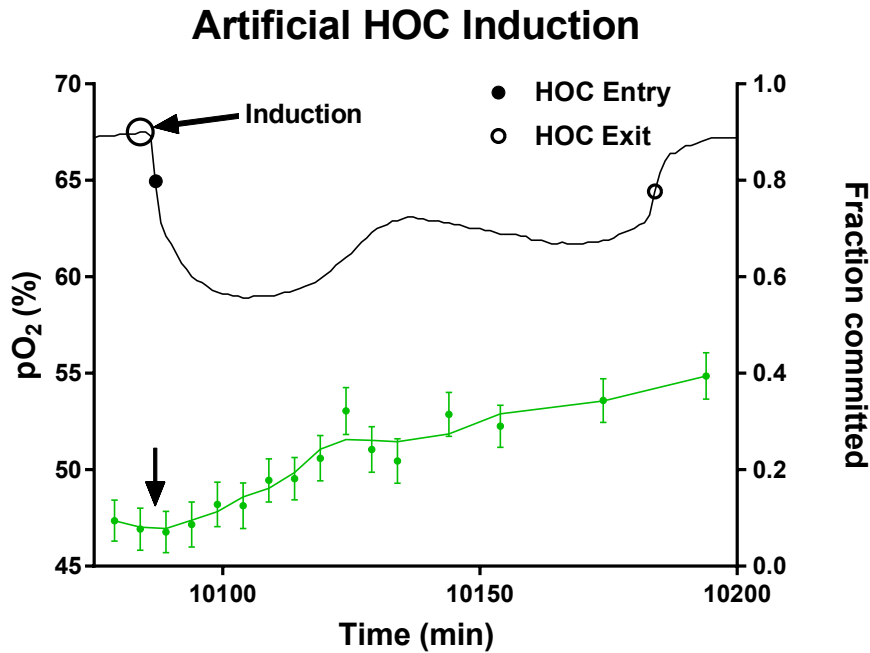


FIGURE 3.10: Timing of cell cycle Start in all cells during artificial induction of HOC in GZ240/241 by 1 mM ethanol. Fraction of all cells committed to the cell division cycle in green, with the margin of error based on the number of sampled cells and line derived by smoothing the dataset. Committed cells begin rising immediately upon entry into HOC (black circle, arrow), with commitment continuing throughout the induced HOC.

daughter cells as in natural oscillations, although both fractions are significantly higher than during natural oscillations. Unlike natural oscillations, the timing of commitment differs between mothers and daughters. Mother cells begin committing to cell cycle progression immediately upon HOC entry and saturate at 50% committed by halfway through HOC, while daughters do not begin to commit until 25 minutes after HOC entry and continue to commit over the entirety of HOC.

Separating cells according to size bins reveals another difference between artificial HOC inductions and natural oscillations. Separating cells into four bins as in Fig. 3.8, it can be seen in Fig. 3.11b that as in natural oscillations larger cells commit to division at a higher rate than smaller cells. However during an artificially induced

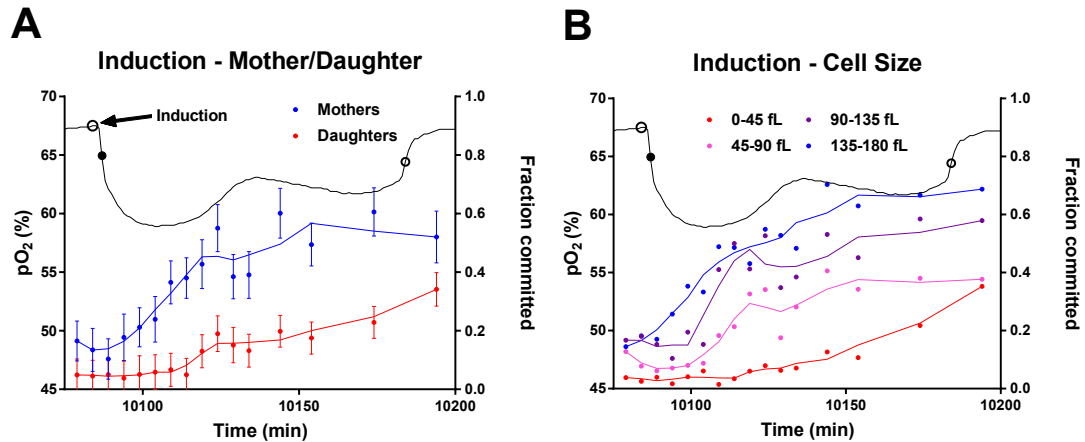


FIGURE 3.11: Timing of cell cycle Start after an artificial induction of HOC by introduction of 1mM ethanol, with cells separated according to replicative age and cell volume. (A) Fraction of cells committed to cell cycle progression are visualized, with mother cells in blue and daughter cells in red and smoothed data as a continuous line. Error bars indicate the margin of error of individual measurements. Mothers begin passing Start 5-10 minutes after HOC entry, while daughters are delayed by 25 minutes. (B) Artificial induction of HOC with cells separated into four volume bins as in Fig. 3.8b. The largest cells immediately begin committing to cell cycle progression upon HOC entry, with smaller cells experiencing longer delays. Error bars omitted for clarity.

HOC, the largest cells (135-180 fL) begin passing Start immediately after entry into HOC while smaller cells commit later. The smallest cells delay commitment the most.

3.2.5 Numerical Analysis of Cell Cycle Start Timing in Subpopulations of Cells

These data show qualitative differences between subpopulations of cells, separated according to replicative age and cell size. During natural oscillations much higher fractions of mother cells and large cells commit to division, and during an artificially induced HOC phase mothers and large cells commit both in larger numbers and at earlier times after induction than daughters and small cells. However, the correlation between mother/daughter status and cell size makes it difficult to determine

which of these attributes is a more important determinant of cell cycle behavior. By *quantifying* the relationship between these factors and cell cycle commitment, we can determine which attribute of a cell dictates its behavior during metabolic oscillations.

In order to robustly quantify the fractions of cells committing to cell division during both natural and artificially induced oscillations, a cubic smoothing spline was fit to the data using the Matlab ‘smoothingspline’ function. For datasets with a single oscillation, the spline was fit to the unprocessed data. For datasets with multiple oscillations in series, they were overlaid according to the time of entry into HOC (as in Chapter 2). The time of cell cycle commitment T_c was defined as the first time at which the value of the smoothing spline reaches the midpoint between its minimum and maximum and has a positive slope. This measure was highly robust to the use of different fitting parameters; see Fig. 3.12 and Materials and Methods.

Additional data was extracted from these spline fits. The fraction of cells which have passed Start F_c and the maximum *rate* of commitment R_{max} (maximum first derivative of the spline fit) was also recorded, as was the maximum fraction of committed cells F_{max} . These parameters can be extracted from any subset of cells defined by replicative age, cellular volume, or both. Parameters were calculated for all cells, mothers, and daughters, during both natural oscillations and artificial induction. Parameters were also calculated for all cells separated into size bins of 0-45 fL, 45-90 fL, 90-135 fL, and 135-180 fL, as well as mother cells and daughter cells separated into the same bins.

Representative data can be seen in Fig. 3.13. In this stacked pair of HOC phases, splines have been fit to mother cells, daughter cells, and cells in four size bins. T_c is universally observed during the first half of HOC phase, with a variation of less than five minutes from subpopulation to subpopulation. The maximum fraction of cells committed F_{max} universally occurs at the end of HOC phase or slightly

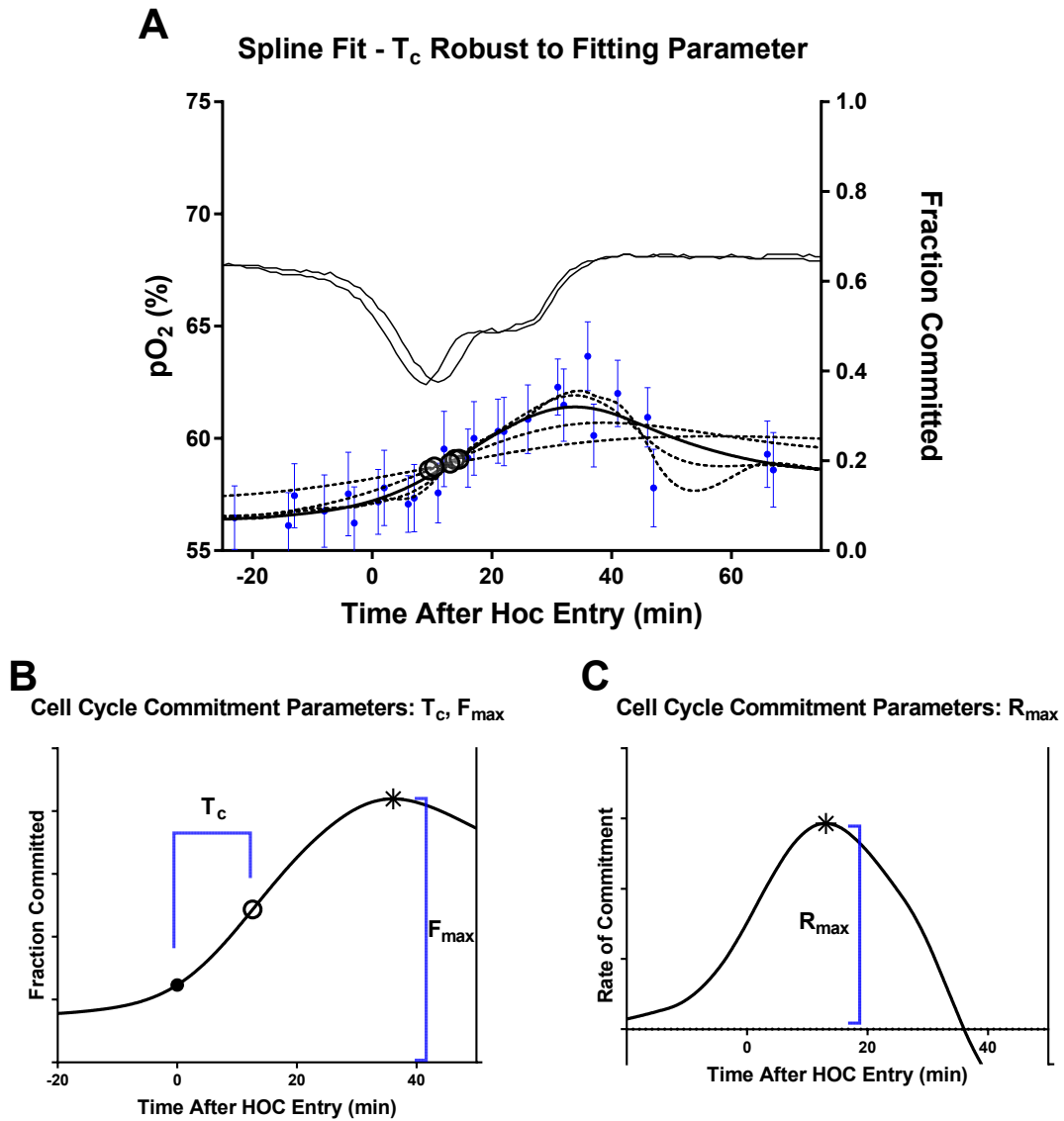


FIGURE 3.12: A) Fraction of committed mothers during HOC in blue points, fit to a cubic smoothing spline with fitting parameter p set to 0.1, 0.01, 0.001, 0.0001, and 0.00001. Bold line is the fit at $p = 0.001$, used in all numerical analyses. Open circles represent the timing of half-maximum of commitment (T_c) from minimum to maximum, and is robust to within 8 minutes with variation in p over four orders of magnitude. (B) Cell cycle commitment parameters extracted from spline fits. Commitment time T_c after HOC entry, and the maximum fraction of committed cells F_{max} are indicated. (C) Additional cell cycle commitment parameter R_{max} , the maximum rate of commitment.

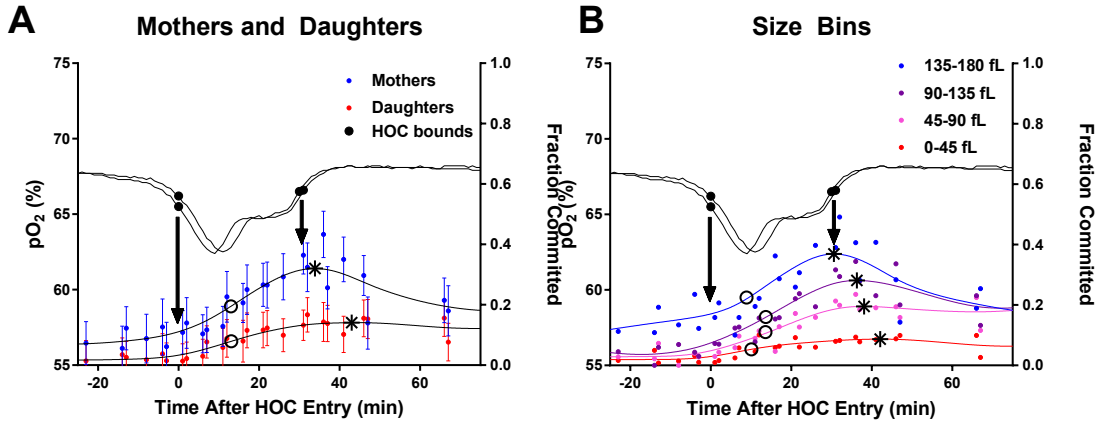


FIGURE 3.13: (A) Spline fit of the commitment to cell division cycle of mothers and daughters during two stacked oscillations of GZ240/241 yeast. Spline fit quantifies the commitment to cell cycle Start occurring during HOC. T_c (open circles) occurs for mothers and daughters at 13.0 and 13.1 minutes after HOC, and F_{max} (asterisks) is 0.32 and 0.14 respectively. F_{max} occurs almost exactly at HOC exit for mothers and shortly after HOC exit for daughters. (B) The same dataset segregated into four size bins. T_c always occurs in early to mid HOC and F_{max} always occurs at the end of HOC or shortly thereafter.

afterwards, although when it occurs during early LOC the smoothing spline is nearly flat and $>0.9 \times F_{max}$ at the end of HOC phase. This continues to demonstrate the tight connection between HOC phase and commitment to Start and indicates that commitment ends either at the end of HOC or very shortly thereafter. See Appendix A for tabulated T_c , R_{max} , and F_{max} values for all natural and artificially induced oscillations for GZ240/241, and additional data from strain DBY12007 which exhibits similar relationships.

3.2.6 Timing Analysis

When T_c is compiled for mothers, daughters, and all cells during natural oscillations it reveals that neither size nor mother/daughter status has a strong effect on the timing of cell cycle Start during the YMC. As seen in Fig. 3.14a, regardless of replicative age, GZ240/241 yeast reach T_c about 14 minutes after HOC entry. When these cells

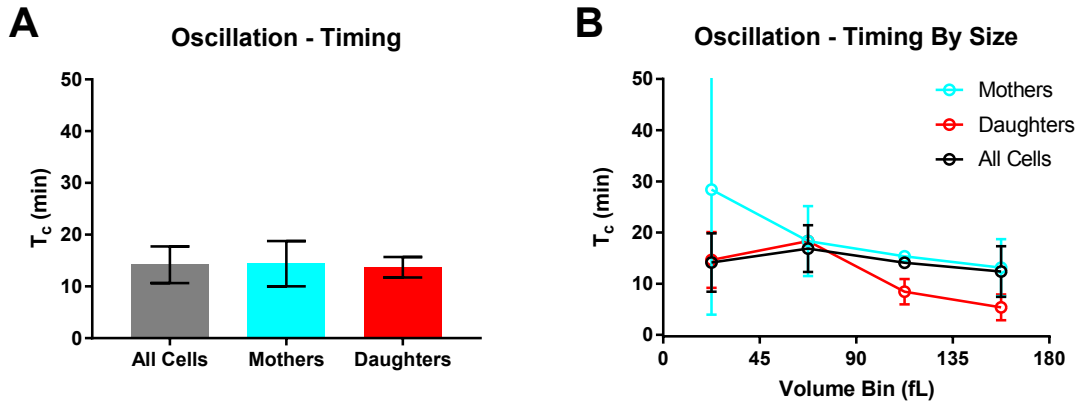


FIGURE 3.14: (A) Time of commitment (T_c) for mothers, daughters, and all cells during a natural oscillation of strain GZ240/241. Mothers and daughters commit at approximately the same time. (B) Mothers, daughters, and all cells divided into four size bins. Mothers commit at approximately the same time regardless of size, while the very rare largest daughters appear to commit earlier. Large standard deviation of smallest mothers is due to the near absence of mothers in this size bin.

are divided into four size bins (Fig. 3.14b), the only cells that deviate from this consistent timing are rare large daughters whose numbers are too small to affect the aggregate behavior of the population as a whole. These patterns in commitment time appear reliably in multiple runs of both GZ240/241. The significance of an earlier commitment time in rare larger daughters is unknown.

In contrast, the commitment time T_c is not consistent across subpopulations during an artificially induced HOC phase. As seen in Fig. 3.15a, after adding ethanol, mothers reach T_c within 24 minutes while daughters appear to require 66 minutes. Upon decomposing cells into size bins, this large difference proves to be an artifact of the fact that daughters are much smaller than mothers. T_c is not significantly different between mothers and daughters of a particular size range (Fig. 3.15b).

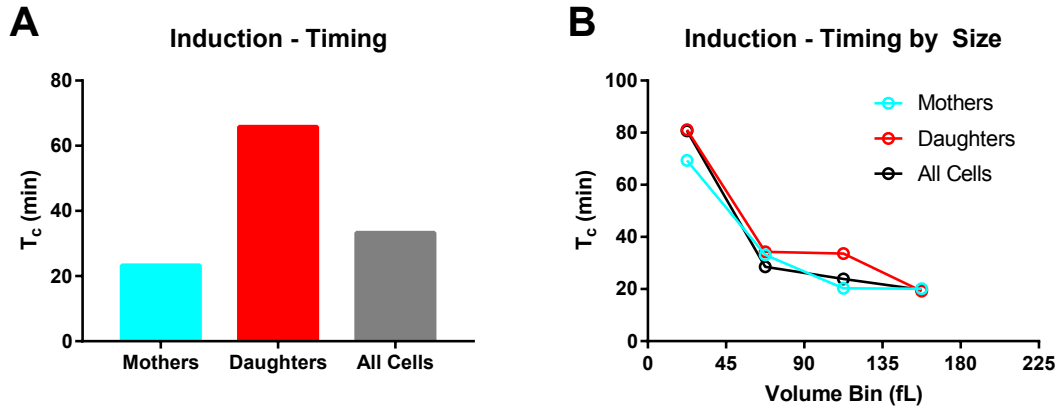


FIGURE 3.15: (A) Maximum fraction of committed cells (T_c) for mothers, daughters, and all cells during an artificial HOC induction of strain GZ240/241. Daughters commit significantly later than mothers. (B) Mothers, daughters, and all cells divided into four size bins. For both both mothers and daughters, the larger the cells are the earlier they commit with very little difference between the two. This indicates that size is the determining factor in timing of commitment during artificially induced HOC phase, not replicative age.

3.2.7 Rate of Commitment and Fraction of Cells Committing

Both R_{max} and F_{max} are indications of the rate of commitment of cells to the CDC. R_{max} directly measures the rate of cells passing through Start per minute. F_{max} is indirectly related to R_{max} - the higher the average rate of cells passing Start, the more cells will have committed to cell cycle progression in a given period of time.

When examined in a natural oscillation, both of these variables were significantly higher for mothers than daughters (Fig. 3.16a, Fig. 3.17a). Upon decomposition into size bins, F_{max} monotonically increases for all cell types as cell volume increases (Fig. 3.16b). A significant part of the difference between mother and daughter cells is due to larger cells committing at a higher rate, though not all - a slightly higher fraction of mothers commit than daughters of a similar size. R_{max} shows an almost identical pattern when separating mothers and daughters (Fig. 3.17a). R_{max} generally increases with cell size, but the relationship with size is less consistent than that

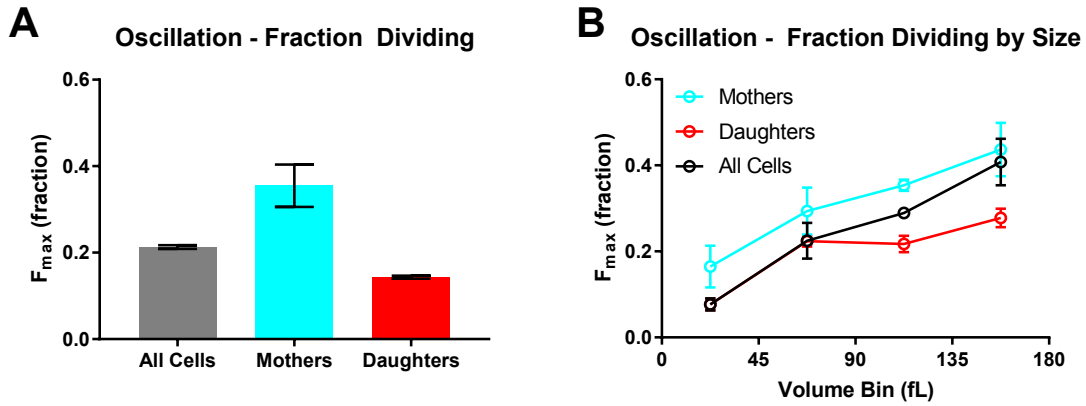


FIGURE 3.16: (A) Maximum fraction of committed cells (F_{max}) for mothers, daughters, and all cells during a natural oscillation of strain GZ240/241. Significantly more mothers commit to division during a metabolic cycle than daughters. (B) Mothers, daughters, and all cells divided into four size bins. For both mothers and daughters, the larger the cells are the more likely they are to commit to division.

of F_{max} especially for small mother cells (Fig. 3.17b).

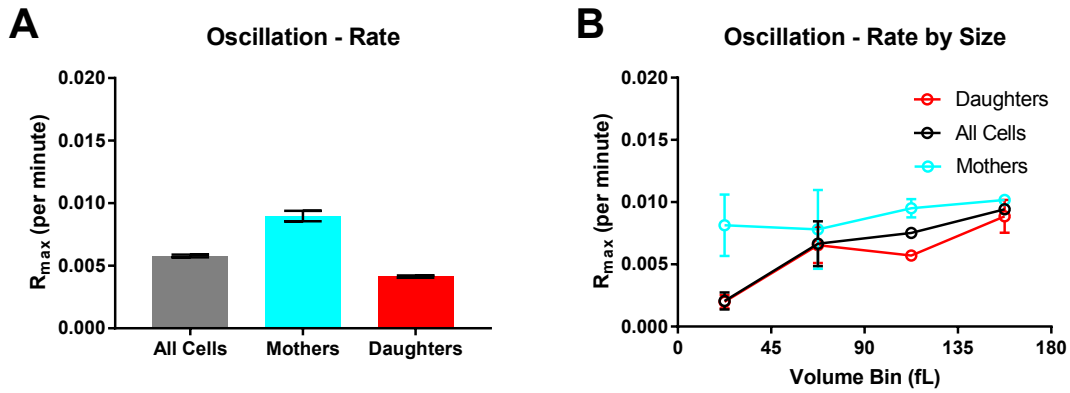


FIGURE 3.17: (A) Rate of commitment (R_{max}) for mothers, daughters, and all cells during a natural oscillation of strain GZ240/241. Mothers commit at approximately double the rate of daughters. (B) Mothers, daughters, and all cells divided into four size bins. Generally, large cells commit more rapidly than small cells.

During an artificial induction of HOC variation in F_{max} is observed to be qualitatively similar to during a natural oscillation. While the total fraction of cells commit-

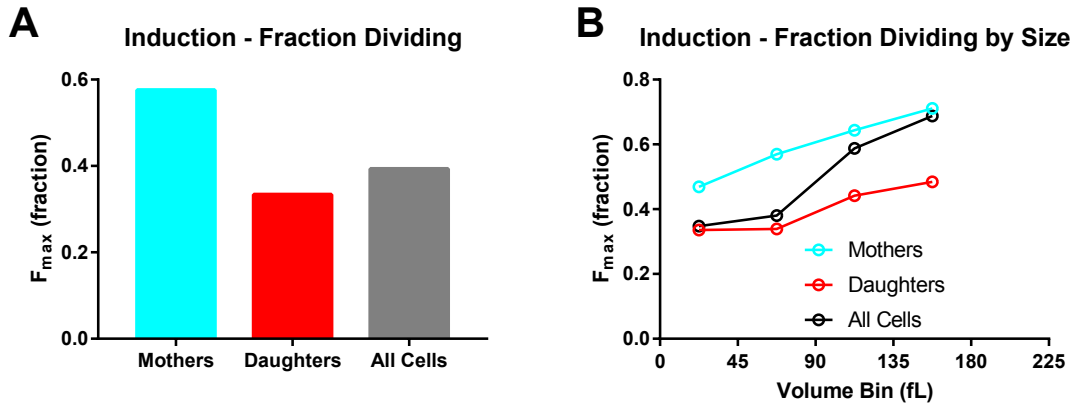


FIGURE 3.18: (A) Maximum fraction of committed cells (F_{max}) for mothers, daughters, and all cells during an artificial HOC induction of strain GZ240/241. Significantly more mothers commit to division during a metabolic cycle than daughters, and more cells commit to division during an induced HOC than a natural HOC. (B) Mothers, daughters, and all cells divided into four size bins. For both mothers and daughters, the larger the cells are the more likely they are to commit to division.

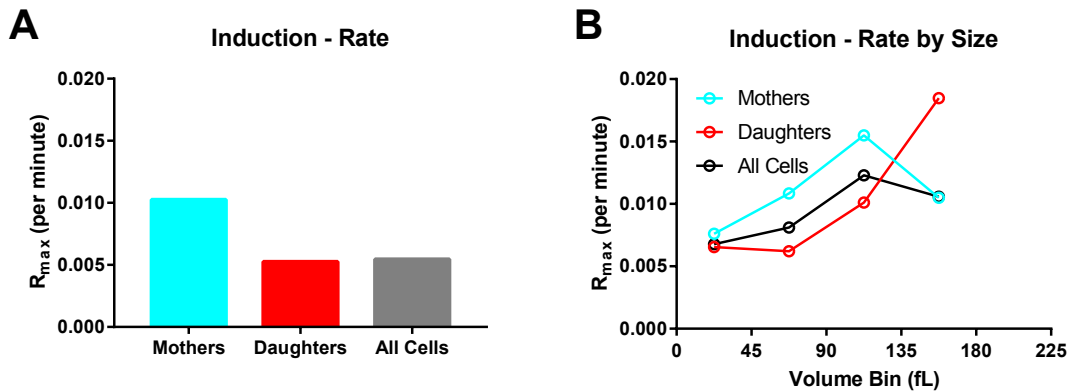


FIGURE 3.19: (A) Rate of commitment (R_{max}) for mothers, daughters, and all cells during an artificial induction of HOC for strain GZ240/241. Mothers commit much more rapidly than small cells. Low R_{max} values indicate that the time of maximum commitment rate does not correspond to T_c . (B) Mothers, daughters, and all cells divided into four size bins. Large cells generally commit more rapidly than small cells.

ting to division is larger in every subpopulation, more mothers commit to cell cycle progression than daughters and larger fractions of larger cells commit (Fig. 3.18). Variation in R_{max} again recapitulates this pattern, although the relationship between cell size and commitment rate is much less robust than that of F_{max} (Fig. 3.19), and the largest daughters actually have the fastest maximum commitment rate. This is likely due to a highly uneven course of cell cycle commitment in daughter cells, since T_c is highly variable over the range of sizes that most daughters exhibit during an artificially induced HOC phase (Fig. 3.15). Thus, the late burst of division that large daughters undergo appears to result in a very fast rate of commitment even though it only goes on for a short time.

3.3 Discussion

3.3.1 Cell cycle Start Occurs After Entry into HOC

The onset of Start after HOC entry supports the Tu laboratory model (Fig. 3.20) where increased metabolic carbon flux triggers Cln3 production and gates cell cycle Start. Entry into HOC phase of the yeast metabolic cycle involves the catabolism of glycogen and trehalose to glucose which is rapidly metabolized to ethanol, acetate, and acetyl-coA which rises to high levels. In the presence of high levels of acetyl-coA, the SAGA chromatin modification complex autoacetylates itself to become more active and acetylates chromatin at a number of genes, including CLN3. Cln3 is a G1 cyclin, involved in the transition into cell cycle Start and an increase in the production of this protein should push cells through Start. A large number of other genes (e.g enzymes) are activated by chromatin acetylation during the YMC, providing a potential mechanism by which diffusible two-carbon metabolites can synchronize YMC oscillations [Kuang et al., 2014].

An alternate model that encapsulates recent Futcher and Skotheim laboratory results [Ewald et al., 2016; Zhao et al., 2016] posits that cell cycle progression triggers

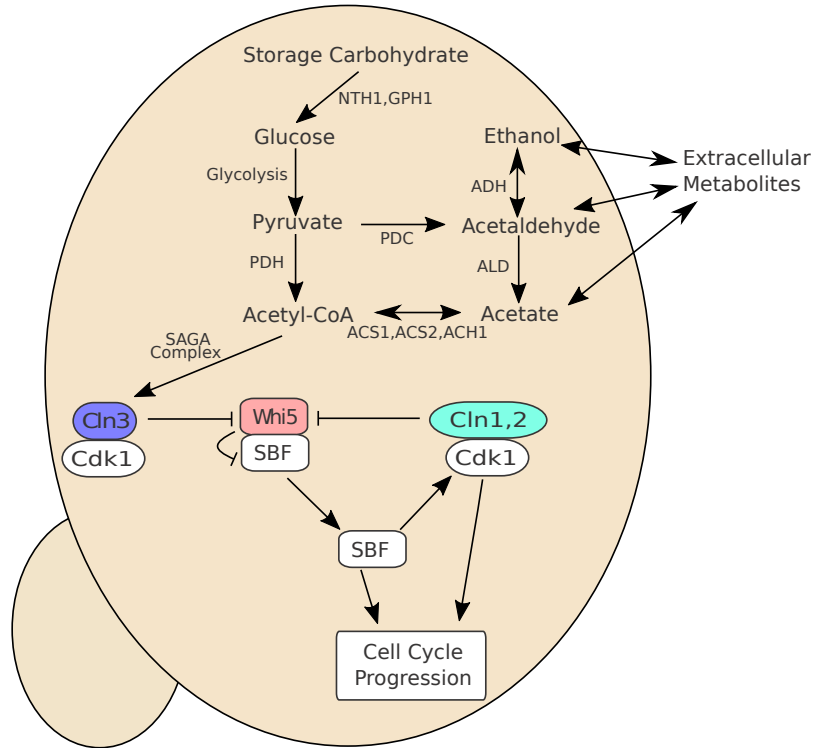


FIGURE 3.20: Model of control of cell cycle Start by metabolic carbon flux as described by the Tu laboratory [Shi and Tu, 2013b; Cai et al., 2011]. Production of acetyl-coA by glycolysis or by the assimilation of extracellular two-carbon metabolites triggers the activity of the SAGA chromatin acetyltransferase complex, activating the expression of CLN3 which proceeds to deactivate Whi5 and push cells through Start.

the phosphorylation and activation of trehalose and glycogen degradation enzymes Nth1 and Gsy1 by B-type cyclin-Cdk1 complexes. Our metabolic cycle data do not support this model. If cell cycle progression were required to activate enzymes to increase metabolic carbon flux and advance the YMC, one would expect to see cells passing cell cycle Start before the metabolic shift from LOC to HOC phase of the metabolic cycle. Instead, we observe entry into HOC phase preceding cell cycle Start, and only observe cells committing to cell cycle progression during HOC phase.

3.3.2 Standard Models of Cell Size Control May Explain Observed YMC/CDC Coupling

Yeast of different sizes display different behavior during both natural oscillations and ethanol-induced HOC phases. Larger cells exhibit higher rates of commitment to cell cycle progression during natural oscillations for both mother and daughter cells (Fig. 3.16b, Fig. 3.18b). While mother and daughter cells of the same size do not behave identically, size is an important determinant of their rate of cell cycle progression.

The fact that larger cells pass through Start more rapidly during HOC phase may be due to the interaction between YMC/CDC coupling in the form of acetyl-coA driven production of Cln3 and mechanisms of cell size control in yeast. A recent study of the behavior of single yeast cells by the Skotheim laboratory [Schmoller et al., 2015] integrates a molecular model of the cell cycle Start network and cell size homeostasis [Johnston et al., 1977; Carter and Jagadish, 1978; Tyson and Lord, 1979], where smaller yeasts cells experience a significantly longer G1 phase of the cell division cycle (Fig. 3.21a). The Skotheim lab observed hundreds of cells bearing fluorescently tagged Cln3 and Whi5 over time during growth and division in a microfluidic device. They found that the average Cln3 concentration [Cln3] in yeast cells was approximately constant for a given strain regardless of cell size or age, while the average Whi5 concentration [Whi5] was inversely proportional to cell size. This means that the total quantity of Whi5 is constant regardless of cell size whereas Cln3 quantity scales with cell size (Fig. 3.21b).

As cell size increases, the effective dilution of the cell cycle inhibitor Whi5 relative to its own inhibitor Cln3 ensures that a size threshold is reached at which Start is triggered and cell division is assured. Schmoller et al. noted significant spread in the observed division size threshold due to molecular noise, but when they control for observable protein quantities a clear threshold appears with division occurring

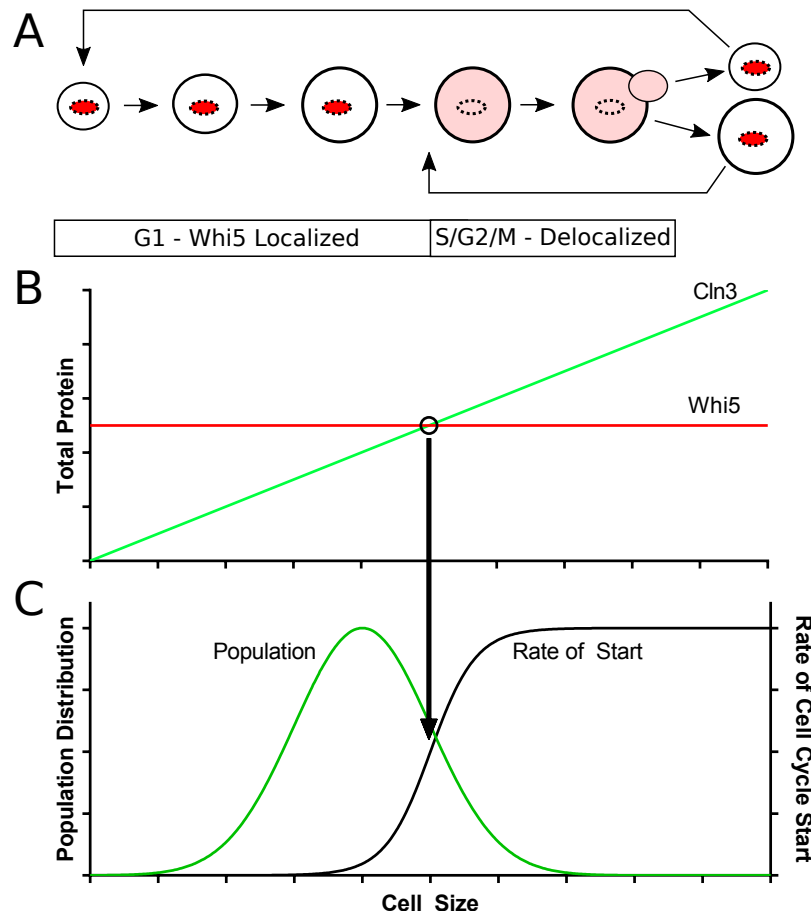


FIGURE 3.21: Skotheim laboratory model [Schmoller et al., 2015] of size regulation of cell cycle Start in yeast. (A) Yeast life cycle. A daughter cell grows throughout G1 phase, eventually reaching threshold size at which it passes Start as Whi5 delocalizes from the nucleus. After passing through S/G2/M and budding it is now a mother, able to re-enter the cell division cycle quickly. It buds off a daughter, which must grow to critical size again. (B) As cell size increases, total cellular Whi5 remains constant while total cellular Cln3 increases. When the Cln3 to Whi5 ratio reaches a critical value at the critical size, Whi5 is inhibited and can no longer suppress commitment to cell division. (C) In practice, due to molecular noise the critical size is not a sharp threshold and represents a range of sizes at which the *rate* of commitment to cell cycle progression increases with increasing size. The largest cells in a yeast population will pass through Start at a high rate, while the smallest will pass through at a very low rate or not at all until they grow.

reliably at a given cellular [Cln3]:[Whi5] ratio. The molecular noise in the expression of both of these proteins manifests as an increasing *rate* of cells passing Start at higher cell size and thus higher *average* [Cln3]:[Whi5] ratios (Fig. 3.21c).

According to the Tu et al. model of YMC/CDC coupling, chromatin-acytlation-driven CLN3 expression should increase the [Cln3]:[Whi5] ratio and lead to the size threshold for division being depressed (Fig. 3.22a). As acetyl-coA is produced during HOC, CLN3 expression will rise triggering a wave of division. This division will occur at a faster rate in the largest cells, as they are closer to the critical size threshold, and thus mother cells which are on average larger will commit to CDC progression at a higher rate (Fig. 3.22b). This is qualitatively consistent with our observations. The fraction of cells of varied size and replicative age subpopulations rises approximately linearly over the course of HOC phase of the YMC (see Fig. 3.7, Fig. 3.8), and the fraction of cells ultimately committing to cell cycle progression rises monotonically with cell size (Fig. 3.16). Further research is required to test this model of the role of size control of cell cycle Start in YMC/CDC coupling quantitatively.

The behavior of yeast during an ethanol-induced HOC phase is not completely accounted for by this model. The fraction of cells passing through Start does monotonically increase with cell size but the timing of cell cycle Start is now also affected by size. The smallest cells do not reach T_c until 80 minutes after induction while the largest cells require only 20 minutes regardless of mother/daughter status (Fig. 3.14). This could be consistent with our model if during artificially-induced HOC phase the level of acetyl-coA and subsequent CLN3 expression rises slowly but continuously as ethanol is assimilated from the growth medium. This could be tested via the measurement of acetyl-coA and CLN3 mRNA levels during natural and ethanol-induced HOC phases.

A complicating factor in this model is the size growth of individual cells over the course of a single metabolic cycle. The biomass doubling time at $D=0.05hr^{-1}$ is 832

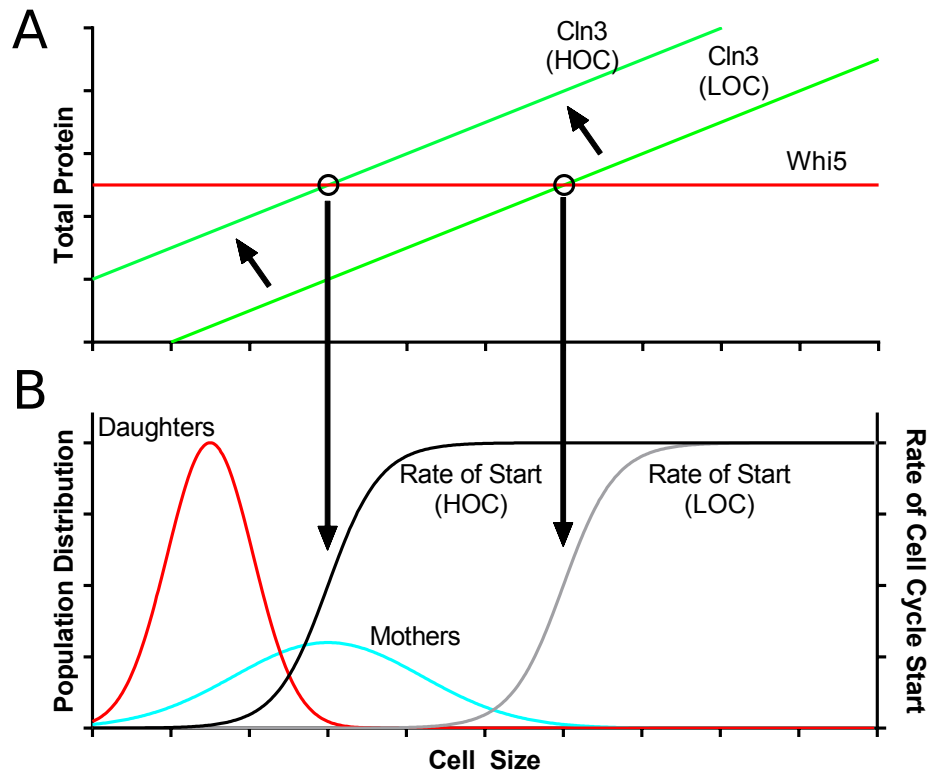


FIGURE 3.22: Proposed model of size control based coupling of the YMC and CDC. (A) During LOC phase, Cln3 levels are low and the critical size for cell cycle Start is large. Upon the increase in acetyl-coA flux during HOC phase, Cln3 levels rise and the critical size drops. (B) During LOC phase, the rate of cells committing is low or zero for all but the largest cells. During HOC phase, the sudden decrease in the critical size threshold brings it close to the sizes of cells in the population. The larger cells, especially mother cells, now pass through Start at a high rate for the duration of HOC phase.

minutes, and the observed metabolic cycle period for GZ240/241 at this growth rate was 229 minutes (0.275x as long). Assuming a constant growth rate per unit biomass, over the course of a single metabolic cycle the average biomass of an individual cell would be expected to increase by a factor of $2^{229/831} = 1.21x$. While individual cells were only ever measured at a single timepoint in our data, *distributions* of cell sizes are available for all phases of the YMC. We fit smoothing splines as previously described to the average volumes of mothers, daughters, and all cells over the course of the YMC. The observed ratios of the maxima and minima of these fits were 1.33x

Cell Size Over the YMC

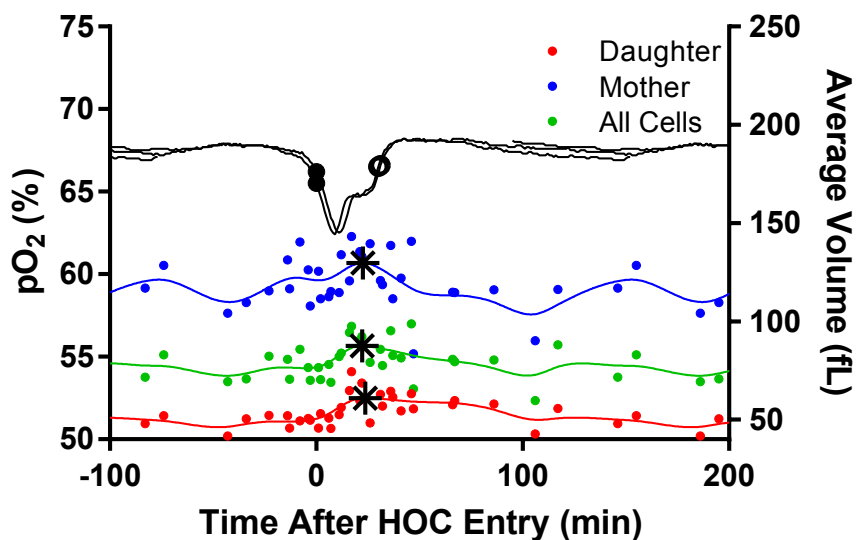


FIGURE 3.23: Measured average volumes and fitted splines for mother cells (blue), daughter cells (red), and all cells (green) during two stacked HOC phases, excluding buds. Maximum size indicated by asterisks. Maximum size is universally achieved in late HOC phase, at $\approx 1.3x$ minimum LOC phase sizes.

for mothers, 1.21x for daughters, and 1.26x for all cells, in close agreement with the expected value.

The maxima of average cell size fits over time were universally reached in late HOC phase of the yeast metabolic cycle (see Fig. 3.23) indicating that growth of cell volume occurs during HOC phase as carbon stores are consumed and converted into cell wall polysaccharides and cytoplasmic biomolecules. Cell size then decreases over the course of LOC phase as new, small cells are produced and bud off. This increase in cell volume during HOC is not large enough to account for the increase in cell division rate during HOC, however. The maximum average volume of a daughter cell during HOC is much lower (61 fL) than the minimum average volume of a mother cell during LOC (103 fL). Nevertheless, a daughter has a much higher rate of passing Start during HOC than a mother does during LOC. The critical size for cell cycle

progression is likely extremely large during LOC, only falling close to the size of the largest cells during HOC.

3.3.3 Short-Period Oscillators Dominate Long-Period Oscillators in Coupled Systems

As seen in Chapter 2, the CDC period of a cycling chemostat culture is always longer than the YMC period at a given set of growth conditions. Our analysis of Start at single cell resolution demonstrated that less than half of cells divide during a given HOC phase. There is no one cohort of cells whose rate of division could be driving the YMC. Rather, our data suggest that the shorter yeast metabolic cycle *gates* the longer cell division cycle by controlling the timing of Start.

The phenomenon of a short biological oscillator gating a longer oscillator has been observed elsewhere in the coupling between the mammalian circadian rhythm and cell division cycle. It was first discovered in the 1970s that the circadian rhythm appears to gate cell division in mouse tissues [Scheving et al., 1978; Matsuo et al., 2003], with a pulse of division occurring in skin, respiratory epithelium, and bone marrow once per day at a particular circadian time. Study of the molecular mechanisms of the mammalian circadian clock have revealed it to share protein components with the cell division cycle [Gérard and Goldbeter, 2012] and provided a mechanistic basis for this coupling. Experiments in tissue culture at single cell resolution have also revealed that the CDC is phase-locked to the circadian rhythm with a preferred circadian time during which the G1/S transition occurs [Nagoshi et al., 2004; Feillet et al., 2014]. Crucially, these experiments involved cells in samples taken from living animals in which the CDC period of a cell is generally at least several days long, or from tissue cultures with an average CDC period of greater than or equal to 24 hours.

More recently, experiments in rapidly dividing mammalian tissue cultures in

which the period of the cell cycle approaches or is less than 24 hours have revealed that multiple coupling patterns between these oscillations are possible [Feillet et al., 2014, 2015; Bieler et al., 2014]. Bieler et al. observe that in rapidly dividing cultured cells in which the interval between divisions approaches 24 hours, cell division cycles lock into a 1:1 phase-locked relationship with circadian cycles. They also observe a subset of cells in which two back to back cell cycles occur in less than one circadian period, and the circadian rhythm is advanced by the cell division cycle rather than the cell division cycle being regulated by circadian rhythms. In these cells, the cell cycle dominates the circadian rhythm and can push the period of the circadian rhythm to as short as 18 hours. Feillet et al. similarly observed that in cells in which the natural cell division cycle varies between 24 and 36 hours, 1:1 and 3:2 resonances appear in which the circadian rhythm is forced to a ‘compromise’ frequency different from its free-running frequency. They concluded that describing one cycle as rigidly gating the other is misleading and that, “the cell cycle is capable of impacting on the circadian clock and vice versa, the dominant influence being dependent on the environment of the cell.” [Feillet et al., 2015]

This supports a generalized principle of coupling between oscillators with different periods, under which it is always the faster cycle which can gate or advance the longer cycle. When one cycle runs faster than another, and is capable of advancing or delaying another cycle, this point of coupling will be reached more frequently and earlier than any points of coupling in the longer cycle. Thus, the shorter oscillator will tend to advance or delay the longer oscillator and phase lock its progression to the shorter autonomous oscillator.

Work by the Heinemann laboratory [Papagiannakis et al., 2016] examined the relationship between single-cell NAD(P)H/ATP oscillations (likely connected to the YMC) and the timing of the cell cycle in individual cells. They showed 1:1 phase locking between single-cell yeast metabolic oscillations and the cell division cycle in

a microfluidic device. This coupling was observed at rapid division rates in which the CDC period was short, and slowed the natural metabolic cycle that occurred when the CDC was blocked to a common ‘compromise frequency’ about 16% longer than the uncoupled oscillations. This slowdown of the metabolic cycle in response to the cell division cycle occurs in a narrow range of frequencies at which the two periods are similar. This is the opposite relationship than what we observed during the chemostat-hosted YMC, in which the YMC gates and advances the CDC. This demonstrates that in the coupled yeast metabolism/CDC system, regulation can pass from metabolic shifts to cell cycle progression or vice versa depending on the relative period of the oscillators.

3.3.4 YMC/CDC Crosstalk May Lead to Mutual Coupling

Based on the above research, we hypothesize that the yeast metabolic cycle and cell division cycle may be *mutually coupled* rather than the metabolic cycle simply gating cell cycle Start at HOC phase under all circumstances. While the triggering of cell cycle Start by acetyl-coA production may be dominant during YMC oscillations, the feedback from cell cycle progression to carbohydrate degradation observed by the Futcher and Skotheim laboratories likely operates simultaneously. This would create a positive feedback loop between cell cycle Start and storage carbohydrate degradation - see Fig. 3.24.

Positive feedback between HOC entry and cell cycle Start would ensure their temporal coordination, no matter which cycle ran faster. If a cell commits to Start unusually quickly it would immediately trigger HOC phase, increasing metabolic carbon flux, converting it into biomass required for S phase and mitosis, and triggering the activation of growth-related genes via chromatin acetylation. This is consistent with the apparent biological significance of the yeast metabolic cycle observed in Chapter 2. The fraction of time spent in HOC phase increases linearly with growth

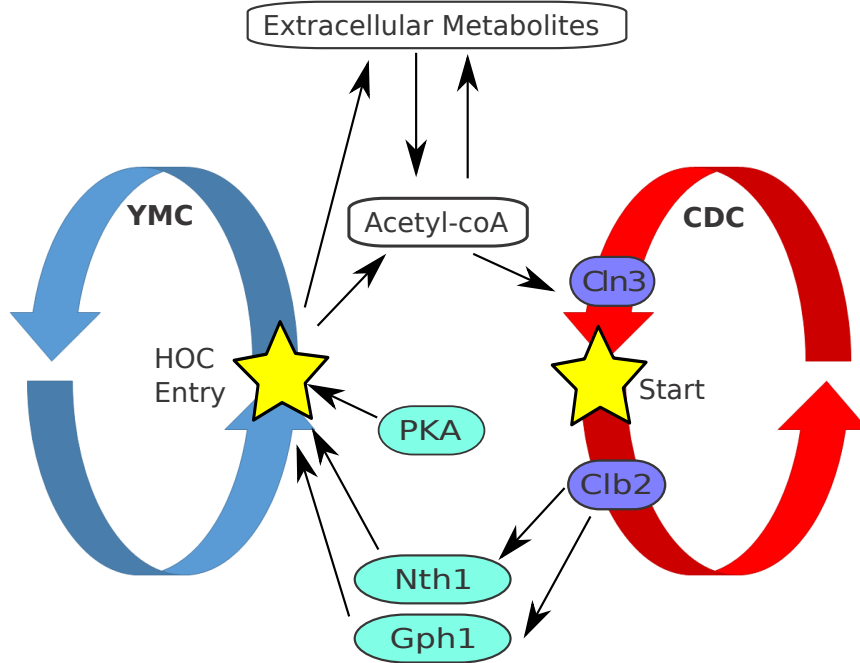


FIGURE 3.24: Proposed model of YMC/CDC feedback loop. Cell cycle Start and entry into HOC entry are mutually reinforcing. Start is triggered by CLN3 expression caused by acetyl-coA production during HOC, and HOC entry is triggered by phosphorylation and activation of the trehalose and glycogen breakdown enzymes Nth1 and Gph1 by Clb2-Cdk1 and PKA. Cells are synchronized by the interconversion of extracellular metabolites and acetyl-coA, and progression of the YMC in response to metabolite induction would require signals to pass through the CDC to advance the YMC.

rate, indicating that HOC represents most cellular growth and division being segregated into brief pulses with LOC phase dedicated to the accumulation of resources. This coordination of the production of biomolecules from stored carbon and high rates of energy production with cell cycle Start is likely adaptive due to the prevention of cell cycle commitment when there is insufficient material available for DNA replication and budding. It could also act as a feed-forward reinforcement mechanism ensuring that onset of HOC phase, high rates of energy metabolism, and the expression of anabolic genes are reinforced and proceed at especially high levels in cells that pass Start as a result of metabolic shifts.

Feedback ensuring that an early commitment to Start triggers HOC phase is unlikely to be the trigger for HOC entry for most cells during synchronous oscillations in a chemostat, because $\tau_{ymc} < \tau_{cdc}$. The coupling between cells by small molecule metabolites that maintains synchrony represents a positive feedback loop by which the fastest cells to advance through the YMC set the frequency for all other cells. However, individual cells likely still pass through the metabolic cycle in the absence of synchrony [Silverman et al., 2010; Papagiannakis et al., 2016] and in an asynchronous population without positive feedback from other cells the periods of both the YMC and CDC will vary substantially due to molecular noise. In such a system, a positive feedback loop between events in two oscillators which must occur together could ensure their coordination even when both oscillators have different periods.

There is some evidence from our artificial HOC induction experiments that the cell division cycle could drive the yeast metabolic cycle. After artificial induction of HOC phase with 1 mM ethanol, the ≈ 209 minute long normal YMC is disrupted and takes several days to recover (Fig. 3.25). A much longer complex pattern of superimposed oscillations of different frequencies is observed during this time period, with an overall period of ≈ 650 minutes. This period is closer to the 831 minute biomass doubling time of the culture at $D=0.05hr^{-1}$ than to the previous oscillation period, but not identical, and slowly decays back into the normal YMC.

HOC induction triggers the commitment to cell cycle progression of $\approx 40\%$ of all cells and 60% of mothers, compared to $\approx 21\%$ of all cells and $\approx 32\%$ of mothers during a natural HOC phase. We hypothesize that this artificially high cell cycle commitment rate during artificial HOC could synchronize the cell division cycles of some large cohort of cells which would ordinarily have divided over several discrete HOC phases. These cells would pass through Start together for several cycles. If their CDC progression triggers YMC progression, this could cause a long-period oscillation with the same period as their cell division cycle. This model is admittedly

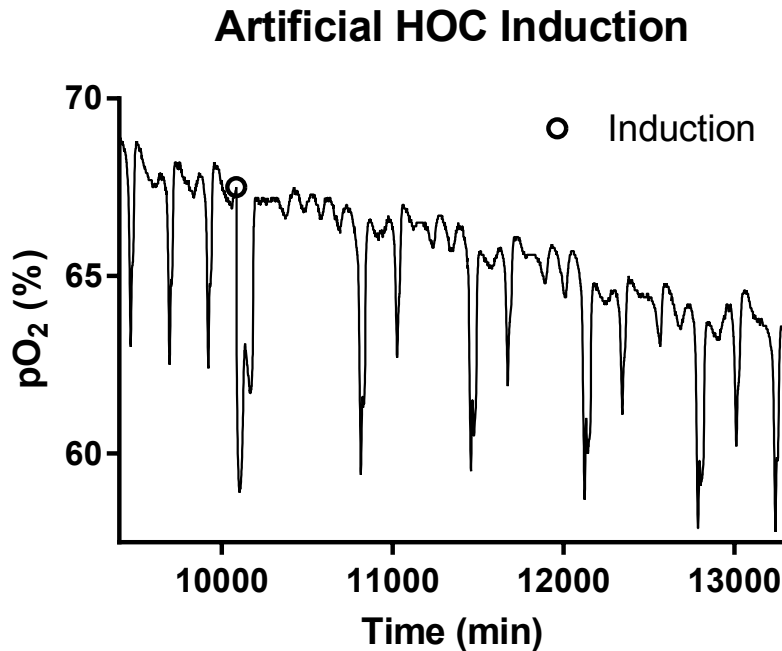


FIGURE 3.25: Artificial induction of HOC in GZ240/241 by 1 mM ethanol. After the long HOC caused by ethanol injection (open circle), the metabolic cycle is disrupted for over a day. The normal 229 minute YMC is replaced by a complex rhythm with a period of ≈ 650 minutes which is eventually supplanted by the normal YMC again.

speculative, but given the variable cell cycle length between mothers and daughters it is possible that the ≈ 650 minute period could represent the cell cycle period of some subdemographic of the yeast population in the chemostat. An experimental protocol based on TrackScar [Maxwell and Magwene, 2017] tagging cells which divide during a given timeframe may be able to test this hypothesis.

3.4 Contributions

Work described in this chapter was done by Anthony Burnetti with assistance from Mert Aydin (laboratory technician) who helped build strains, and Shiyu Liu (graduate student), who helped build plasmids and strains and segment cells. This work was funded by National Institutes of Health Directors New Innovator Award DP2

OD008654-01 and Burroughs Wellcome Fund CASI Award BWF 1005769.01.

Conclusions

4.1 The Yeast Metabolic Cycle Segregates Cell Growth/Division Into Pulses

The high oxygen consumption phase of the yeast metabolic cycle consists of pulses of maximal aerobic respiration, separated by LOC phases which increase in length at low growth rate in order to accumulate additional carbon to fuel these pulses. The fraction of time spent in HOC increases linearly with growth rate, and extrapolating this relationship shows that cells would spend 100% of their time in HOC phase at the growth rate corresponding to the switch from aerobic respiration to constitutive aerobic fermentation. The YMC thus represents yeast altering the frequency of pulses of maximal carbon flux in between periods of carbon buildup, rather than smoothly ramping carbon flux with growth rate. HOC phase is associated with the expression of growth-associated anabolic genes while LOC phase is associated with the expression of catabolic and stress-response genes. These gene clusters are qualitatively similar to gene clusters observed to vary in expression with growth rate in bacteria, with the expression of anabolic genes increasing in a similar linear relationship with growth rate. This indicates that the yeast metabolic cycle serves a similar

function to bacterial gene expression growth laws by segregating the expression of anabolic and growth genes and high metabolic carbon flux into pulses and regulating their frequency. Why yeast should segregate the expression of growth genes into discrete pulses is unclear.

4.2 The YMC Drives Cell Cycle Commitment

As described in Chapter 2, DNA replication is consistently delayed by a fixed time period after the onset of high oxygen consumption phase in the YMC. This suggested that cell cycle Start was associated with the entry into HOC phase. By directly observing the onset of cell cycle Start in chapter 3, we demonstrate that cell cycle Start occurs *after* entry into HOC and is confined to HOC phase. Thus the yeast metabolic cycle drives progression of the cell division during the YMC, consistent with a model of YMC/CDC coupling proposed by the Tu laboratory, in which increased metabolic carbon flux during HOC phase triggers chromatin acetylation and the expression of the G1/S cyclin Cln3 which pushes cells through the commitment to cell cycle progression.

Larger yeast cells pass through cell cycle Start at a higher rate than smaller cells. This is the result of an interaction between yeast cell size homeostasis and the expression of Cln3 in response to increased carbon flux during HOC phase. Increased Cln3:Whi5 ratio leads to a decrease in the critical size threshold for cell cycle Start during HOC, leading to a higher rate of cell division cycle progression in larger cells.

4.3 Potential Mutual Coupling of the YMC and CDC

There are known pathways by which cell cycle progression can activate carbohydrate degradation enzymes and increase the metabolic carbon flux associated with the YMC, although during synchronous metabolic oscillations they do not appear to be the primary means of coupling between the YMC and CDC. This may indicate that

the YMC and CDC are mutually coupled, with a positive feedback loop between cell cycle Start and entry into high oxygen consumption phase. This positive feedback loop may help ensure that these events are coordinated to occur together despite the fact that the YMC and CDC have different intrinsic periods in many circumstances, increasing fitness. Additional research is required to confirm this hypothesis.

Additional Materials and Methods

5.1 Strains

GZ240 and GZ241 yeast bearing significant repairs to respiratory genes in the S288C background were generously provide by the Futcher laboratory. GZ240 and GZ241 were used as the base for additional investigation into the timing of cell cycle Start and the behavior of individual cells.

Whi5-tdTomato was introduced into diploid GZ240/241 and DBY12007 yeast via standard PCR-based transformation techniques [Longtine et al., 1998]. DBY12007 was transformed via PCR of plasmid DLB 3640 generously provided by the Lew laboratory carrying tdTomato and hygromycin-resistance gene HygR to create the fusion gene with HygR present in the chromosome downstream. After unacceptably low transformation efficiency with this technique, GZ240/241 was transformed via PCR of genomic DNA of DBY12007 + Whi5-tdTomato cells which created a PCR product with 500 base pairs of homology rather than the standard 50 base pairs, which proved successful. The pH-sensitive GFP pHluorin was then introduced to the HO locus of GZ240/241 + Whi5-tdTomato by transformation with plasmid pNB 1161 digested in a region of HO homology using AfeI. This plasmid contains the

Table 5.1: Primary yeast strains used for analysis of the timing of cell cycle Start in Chapter 3, obtained from other laboratories or constructed for these experiments.

Strain	Genotype	Background	Notes
GZ240	<i>MATα MKT1-30G SAL1 CAT5-91M MIP1-661T HAP1</i>	S288C	from Futcher lab
GZ241	<i>MATα MKT1-30G SAL1 CAT5-91M MIP1-661T HAP1</i>	S288C	from Futcher lab
GZ240/241 + Whi5 + pfluorin	<i>MATα/α MKT1-30G SAL1 CAT5-91M MIP1-661T HAP1 WHI5 / WHI5-tdTomato:HYG HO / HO:pfluorin:NAT</i>	S288C	Mated GZ240 and GZ241, transformed with Whi5-tdTomato:Hyg genomic PCR, pFluorin cytosolic pH biosensor
DBY12007 + Whi5	<i>MATα/α HAP1 WHI5 / WHI5-tdTomato:HYG</i>	S288C	Transformed DBY12007 with PCR product of DLB 3640, Whi5_Tomato_Hyg_F2, Whi5_Tomato_Hyg_R1

pH-sensitive GFP pFluorin, the nourseothricin-resistance gene NrsR, and a block of homology to the HO locus. The HO locus acts as a neutral site, at which an insertion of non-metabolic genes is unlikely to affect metabolism unlike insertion at the common auxotrophy genes usually employed for this purpose [Baganz et al., 1998]. See Table 5.1 for strain details and Tables 5.2 and 5.3 for oligonucleotide and plasmid details.

5.2 Chemostat Equipment

All chemostat experiments were performed in a Multifors 6 x 1L chamber microbial system (Infors USA, Laurel, MD). In all experiments, 1L of media was stirred at 550 RPM using a Rushton impeller with airflow rate of 1L/min filtered room air at 30°C.

Oxygen saturation was measured using Broadley James oxyprobe pO_2 probes,

Table 5.2: Oligonucleotides Used for Transformation and Confirmation of Yeast.

Oligonucleotide	Sequence	Purpose
Whi5_tomato_Hyg_F2	AACCCACGGACGAAACGGAGC- CCGAGTCGGATACCGAAGTGG- AGACGTCTCGGATCCCCGGGT- TAATTAA	Fusion of WHI5 and tdTomato with hygromycin resistance using plasmid DLB 3640
Whi5_Tomato_Hyg_R1	CGCGGCTGCACTAACTCCGAG- ATTGCGGAGAAAAAACTCGTA- CTACCACAGAATTTCGAGCTCG- TTTAAAC	Fusion of WHI5 and tdTomato with hygromycin resistance using plasmid DLB 3640
WHI5_ext_F	CAAGGCAAAGAACCTGATGG	Whi5 genotyping & PCR of genomic Whi5-tdTomato:HYG locus with ≥ 500 bp flanking sequence for transformation
WHI5_ext_R	GTGGTTAACCTGGTCGATCAAC	Whi5 genotyping & PCR of genomic Whi5-tdTomato:HYG locus with ≥ 500 bp flanking sequence for transformation
HO_ext_F	ATCCATATCCTCATAAGCAG	HO locus genotyping
HO_ext_R	CAGTGCCGGTAACGC	HO locus genotyping

Table 5.3: Plasmids Used for Transformation of Yeast.

Plasmid	Purpose	Notes
DLB 3640	tdTomato:HYG tagging	Obtained from Lew lab
pNB 1161	Expressing pHluorin at HO locus	Built from pRS plasmid

models D140 or D145. pH was measured using Broadley James FermProbe pH probes, model F-695 at 225 or 325 mm lengths. All data was recorded on Iris V5.3 or Iris V6.0 process recording software. Temperature, pO_2 , pH, the cumulative volume of 1M NaOH added, the cumulative volume of 1M H_2PO_4 added, and the cumulative media volume added were recorded with a minimum frequency of once per minute when readings were constant. The frequency of recording was automatically raised

when readings were changing rapidly, but averaged in one minute increments downstream for analysis. While pH was held approximately constant by the chemostat control systems, the rate of addition of sodium hydroxide to the chamber served as a proxy readout for the rate of acidification of media by the yeast. Calibration of pO₂ sensors was performed manually by setting 100% equal to the value at full oxygen saturation before inoculation and 0% equal to the value with nitrogen gas in place of air.

The chemostat controller automatically maintained temperature at 30°C and pH at a set point ± 0.1 pH units, using peristaltic pumps to deliver 1M NaOH or 1M H₂PO₄ as needed. A third peristaltic feed pump was manually controlled so as to add fresh growth media into chemostat chambers at the desired dilution rate. Added growth media was delivered via silicone tubing inside the chamber to below the surface of the stirred liquid to avoid biofilm formation over the media port. A fourth peristaltic pump attached to a telescoping adjustable ‘antifoam’ tube inside the chemostat chamber was run at maximum speed continuously whenever the feed pump was active to remove exhausted media and cells at the same rate they were added. The telescoping antifoam tube was manually adjusted to sit at the surface height of 1L of media stirred at 550 RPM with 1L/min of airflow and thus to maintain the working volume of liquid at 1L without active control. The feed pump was calibrated by measuring the volume of liquid dispensed when run at 100% speed for 25 minutes before autoclaving.

Sealed chemostat chambers containing 1L of media base salt solution, sample ports, sensors, all tubing, and peristaltic pump heads were sterilized by autoclave for a single 45 minute cycle. They were placed back in the Multifors base station, all sensors were connected, and the chambers allowed to cool overnight before inoculation.

5.3 Growth Medium

We used minimal defined (MD) growth medium, which we adapted from several sources [Burnetti et al., 2016; Saldanha et al., 2005; Brauer et al., 2005]. After testing several glucose concentrations we chose 0.25% mass/volume for all experiments due to the ability of all strains tested to oscillate at this concentration. MD medium was prepared by first autoclaving a base salt solution of 0.1 g/L $\text{CaCl}_2 \cdot 2\text{H}_2\text{O}$, 0.5 g/L $\text{Mg}_2(\text{SO}_4)_2 \cdot 7\text{H}_2\text{O}$, 2 g/L K_2HPO_4 , 5 g/L $(\text{NH}_4)_2\text{SO}_4$, and 70 $\mu\text{L}/\text{L}$ 96% H_2SO_4 . After cooling, this solution was supplemented with 1 mL/L 1000x vitamin solution, 100 $\mu\text{L}/\text{L}$ 10,000x trace salt solution, 0.02 g/L solid $\text{Fe}_2(\text{SO}_4)_2 \cdot 7\text{H}_2\text{O}$, 100 $\mu\text{L}/\text{L}$ Sigma Antifoam 204, and 0.25% glucose mass/volume.

The 10,000x trace salt solution consisted of 10 g $\text{ZnSO}_4 \cdot 7\text{H}_2\text{O}$, 5 g $\text{CuSO}_4 \cdot 5\text{H}_2\text{O}$, 1 g $\text{MnSO}_4 \cdot 7\text{H}_2\text{O}$, and 100 mL filter-sterilized H_2O . The 1000x vitamin solution consisted of 1 mg biotin, 200 mg calcium pantothenate, 1 mg folic acid, 1000 mg inositol, 200 mg niacin, 100 mg p-aminobenzoic acid, 200 mg pyridoxine HCL, 100 mg riboflavin, 200 mg thiamine HCL, and 500 mL H_2O , which was autoclaved for 40 min to dissolve vitamins and immediately cooled to 4°C. All chemicals were purchased from Sigma Altrich (St. Louis, MO).

Chemostat chambers were autoclaved containing base salt solution only, with vitamins, trace salts, iron, antifoam, and glucose added during inoculation.

5.4 Chemostat Culture and Sampling for DNA Replication Analysis

All strains were grown from single colonies in 25 mL YPD media, spun down, and inoculated via syringe into chemostat chambers bearing 1L 0.25% glucose minimal defined media at 30° C. Cells were allowed to grow to saturation, as measured by a sudden increase in pO₂, and starved for six hours. This starvation step, while not strictly necessary to observe the YMC, ensures that an oscillation emerges rapidly

upon refeeding rather than appearing slowly [Robertson, 2009]. Flow of fresh media was then initiated at 0.1L/hr ($D=0.1h^{-1}$). If stable oscillations were not observed after 2 days, media flow was shut off for 6 hours and restarted until oscillations began. Once stable oscillations were observed, flow rate was manually adjusted to values between $D=0.13h^{-1}$ and $D=0.03h^{-1}$. No sampling was performed until any transient irregularity in oscillations caused by dilution rate shifts had damped and oscillations were regular.

Samples were taken at regular intervals of 10 or 15 minutes via a sterile syringe port, for 8 hour timecourses. Sample interval was kept constant over an individual timecourse. At each timepoint 50 μL of media containing cells were fixed on ice in 200 μL of 7:1 ethanol:H₂O fixative for a final ethanol concentration of 70%. Samples were stored at 4° C for up to two weeks before measurement and analysis.

DNA content measurement protocols [Haase and Reed, 2002] were modified for low fluid volume in 96-well plates. Cells were washed and spun down twice in 200 μL H₂O before resuspension and treatment in 100 μL RNase A solution (15 mM NaCl, 50 mM Tris pH 8.0, 2 mg/mL RNase A) for 2-6 hours. Cells were then spun down and resuspended in 100 μL pepsin solution (5 mg/mL pepsin, 4.5 $\mu\text{L}/\text{mL}$ concentrated HCl) for 10-15 minutes, and stored in 200 μL storage buffer (50 mM Tris pH 7.5) for less than one week. Before the final staining step, 30 μL of each sample was sonicated to separate cell clumps using a medium setting (CEN.PK, DBY12007, YPS670) or high setting (YJM128) for 45 s in 3x8 strips of a 96-well PCR plate floating in a Bioruptor water-bath sonicator (Diagenode, Denville, NJ). The sonicated cells were immediately added to 96-well plates containing 200 μL per well of staining buffer (1 μM Sytox Green (LifeTechnologies), 50 mM Tris pH 7.5). DNA content was measured using a MacsQuant VYB (Miltenyi Biotech, Bergisch-Gladbach, Germany) using excitation at 488 nm and a 500-550 nm emission filter. Sensitivity was adjusted as needed for each set of samples such that the peak representing cells in G2 phase

with two copies of the genome laid above the midpoint of the dynamic range, and intensity was recorded linearly. A total of 300,000 cells from each sample of each time course were recorded for each sample.

5.5 Data Analysis - DNA Replication Timing and Yeast Metabolic Cycle Analysis

Analysis of the pO_2 waveform of the yeast metabolic cycle was automated using custom Matlab scripts. A peak-finding algorithm was used to identify local maxima and minima in the pO_2 trace, and then a minimum peak-size filter was used to exclude all minima and maxima but the most extreme for each cycle. The minimum peak size was manually adjusted for each experiment to ensure that a single maximum and minimum was identified for each cycle. Entry into high oxygen consumption (HOC) phase was defined as the first timepoint after pO_2 had dropped 35% of the difference between a maximum and the next minimum. Exit from high oxygen consumption phase to low oxygen consumption phase (LOC) was defined as the first timepoint after pO_2 had risen 65% of the difference from a minimum to the next maximum.

The length of the YMC, τ_{ymc} , was defined as the time between two successive entries into HOC phase. The Length of HOC phase, τ_{loc} , was defined as the time between entry into and exit from HOC. The length of LOC phase, τ_{hoc} , was defined as the time between entry into and exit from LOC.

For analysis of the behavior of the metabolic cycle, one datapoint represented a single continuous stretch of oscillations at a particular dilution rate containing at least 3 annotated oscillations. Oscillations less than 1000 minutes after a starvation period were excluded, as well as any less than 250 minutes after a switch between dilution rates.

DNA replication analysis was performed with FlowJo and Matlab. Outlier datapoints with extremely high or low fluorescence values were manually trimmed in

FlowJo before analysis with custom Matlab scripts. Fluorescence values for all samples from a chamber during a sampling run were normalized according to the global maximum of the smoothed fluorescence distribution (corresponding to the average G1 cell fluorescence value) to correct for sample-to-sample variation. Dean-Jett-Fox and other cell-cycle parsing algorithms were unable to reliably identify the fraction of S-phase cells across all time points due to the width of G1 and G2/M peaks and asymmetrical G1 fluorescence peaks at low growth rates, possibly due to large spreads in cell size. We determined G1/S and G2/S fluorescence thresholds by averaging the fluorescence distribution across all time points for a chamber, and finding the local minimum between the G1 and G2 peaks representative of the fluorescence values of S-phase cells. The G1 threshold was chosen such that 95% of cells below the local minimum were tagged as G1, and the G2 threshold was chosen such that 95% of cells above the local minimum were tagged as G2. The fraction of cells in any timepoint's distribution above the G1 threshold was defined as its S/G2/M fraction, and the fraction between the two thresholds was defined as the S fraction.

An "average" YMC/CDC dataset was produced for each 8 hour time course. The start of each YMC, defined as entry into HOC phase, were overlaid in the pO_2 data. The cell cycle data was stacked according to the number of minutes after entry into HOC phase each data point was taken. The stacked data was then averaged in rolling 10 or 15 minute (as appropriate) bins to produce the average cell cycle figure. For each stacked dataset, we calculated the time Δ at which the S/G2/M fraction reached its midpoint between maximum and minimum and the time Δ_s at which the S-phase fraction reached its maximum.

5.6 Chemostat Culture and Sampling for Cell Cycle Start Analysis

All strains were grown and inoculated as previously described. Once stable oscillations were observed at the starting dilution rate of $D=0.1h^{-1}$, flow rate was reduced

to $D=0.05h^{-1}$ in order to slow the YMC and ensure that cell division initiated during one HOC was complete by the beginning of the next HOC. In order to induce an artificial HOC phase during a sampling experiment, 1 mL of 1M ethanol was injected via syringe through a membrane port into the chemostat chamber immediately after an early sample was taken. At each timepoint 0.5 mL of media containing cells were fixed in 1.6 mL microfuge tubes with 167 μ L of 16 % formaldehyde for a final concentration of 4% formaldehyde for 10 minutes. Cells were spun down and washed in 1 mL PBS twice, and stored in 200 μ L PBS in 96 well plates at 4° C for up to two weeks before imaging.

5.7 Microscopy and Image Segmentation

Immediately before imaging, cells were stained with AlexaFluor488-conjugated wheat germ agglutinin (WGA). WGA was added to cells at a final concentration of 33 μ g/mL in PBS in conical-bottom 96 well plates at room temperature for 10 minutes. Cells were spun down and washed in PBS 4 times before imaging. After the last wash, cells were allowed to settle at the bottom of their wells. Dense cell suspension was placed on a slide with a coverslip and sealed with petroleum jelly for imaging.

Imaging was performed on a DeltaVision Elite (GE) microscope with a 60x objective. A reference phase contrast image was taken, as well as a fluorescence Z-stack 10 microns and 25 images deep centered on the plane of the phase contrast reference image. Each plane in the z-stack contained one whi5-tdTomato image excited using a m-Chery 550-600 nm light source with a 602-662 nm emission filter, and one bud scar image excited using a GFP 452-498 nm light source with a 500-550 nm emission filter. Exposure lengths were approximately 0.3 seconds and 0.1 seconds respectively, and exposure intensities were 50% and 32% respectively. Whi5-tdTomato exposures were lengthened slightly for cells which had been in storage longer and had lost tdTomato fluorescence intensity, and GFP exposures were slightly increased

or decreased according to variable background staining intensity.

Z-stacks were deconvolved on the DeltaVision workstation immediately after capture, using aggressive 10-step deconvolution with the appropriate configuration file for the objective used. The resulting deconvolved Z-stack was processed into a 2-channel image via a maximum-intensity projection, in order to maximize the difference in fluorescence distributions between cells with localized and delocalized Whi5-tdTomato [Ball et al., 2011]. Reference images and 2-channel fluorescence images were combined into single 3-channel TIFF files before segmentation and analysis.

Images were segmented using the Matlab package CellStat [Kvarnström et al., 2008] on the phase contrast reference image, using the 2deriv and projMag algorithms as appropriate depending on the focus of the image. Buds were not segmented. Images with poor focus in the phase contrast reference were not segmented, nor were any images after approximately 400 cells were segmented per timepoint. Typical images contained up to 50 cells. At the time of segmentation, cells were noted manually as mothers or daughters based upon the presence or absence of bright green bud scars. Birth scars were identified by their large size (nearly as wide as the cell itself) and diffuse staining and were ignored. For each cell the following data were exported for further analysis: Cell ID, cell position, cell area in pixels, eccentricity (major axis / minor axis), average intensity of whi5-tdTomato channel, standard deviation of whi5-tdTomato channel.

5.8 Data Analysis - Cell Cycle Start

For each cell, the coefficient of variation (CV) of Whi5-tdTomato pixel intensity values was calculated from the mean and standard deviation. The distribution of this CV across a dataset was used to pick a CV cutoff below which a cell was considered delocalized (committed to cell cycle progression after passing Start) and above which it was considered localized (in G1 phase of the cell division cycle). This cutoff was

the local minimum in smoothed frequency of CV values between a localized high-CV and delocalized low-CV cluster (see Fig. 3.4c). Cells were automatically classified as localized if their CV was above this value and delocalized if their CV was below this value.

All timepoints were analyzed according to their time after the most recent entry into HOC. For individual datasets that contained multiple oscillations in a row, datasets were superimposed such that all entries into HOC occur at $T=0$.

Cubic splines were fit to all data series of fractions of committed cells over time using the ‘smoothingspline’ command in Matlab, with all points weighted equally. The smoothing spline s is created using the data (x_i, y_i) , the smoothing parameter p and list of weights w_i , and minimizes the following fit equation:

$$p \sum_i w_i (y_i - s(x_i))^2 + (1 - p) \int \left(\frac{d^2 s}{dx^2} \right)^2 dx \quad (5.1)$$

Datasets of the fractions of cells that have passed Start were fit for all cells, all mothers, all daughters, all cells within size bins, mothers within size bins, and daughters within size bins. The time of cell cycle commitment T_c was determined to be the closest time to entry into HOC during which the smoothing spline was increasing and reached the halfway point between the absolute minimum and absolute maximum of the spline fit of fraction of committed cells. The fraction of cell cycle commitment F_c was the calculated value of the smoothing spline at this time. Smoothing parameter p was tested at values of 0.1, 0.01, 0.001, 0.0001, and 0.00001. While F_{max} was affected by this choice, neither T_c nor F_c were strongly affected over this large parameter range due to dense data sampling during the period of most rapid change in the fraction of committed cells. A p value of 0.001 was chosen as a compromise value between overfitting and smoothing away high temporal resolution.

5.9 Measurement of Cytosolic pH With pHluorin Via Flow Cytometry

Live yeast samples bearing the ratiometric pHluorin protein were removed from cycling chemostat chambers via a sterile syringe port and immediately sampled in a MacsQuant VYB (Miltenyi Biotech, Bergisch-Gladbach, Germany). Cells were excited at 405 and 488 nm, with a 500-550 nm emission filter. The gain at each excitation was manually adjusted until the ratio of both fluorescences was close to 1. 300,000 cells were sampled per time point or calibration sample. The ratio of emission when excited at 405 nm to emission when excited at 488 nm was calculated for each cell.

In order to calibrate measurements of cytosolic pH to the ratio of fluorescence when excited at 405 and 488 nm, control samples were required. A yeast sample was permeabilized for ten minutes at 30°C in 0.1 mg/mL digitonin in PBS with shaking. Cells were spun down and washed twice with PBS at a pH of 7.0. These cells were then spun down and resuspended in PBS at a pH of 5.5, 6.0, 6.5, 7.0, 7.5, and 8.0. Multiple samples for each pH value were prepared. These controls were sampled via flow cytometry in between experimental samples.

For each run, a standard calibration curve was produced from the control samples. The following equation was fit to the average ratios (r) for each control sample, where β_h and β_l are the high and low baselines respectively, n is the hill coefficient, and pKa is the apparent pKa of pHluorin:

$$r(pH) = (\beta_h - \beta_l) \left(\frac{10^{n(pH-pKa)}}{1 + 10^{n(pH-pKa)}} \right) + \beta_l \quad (5.2)$$

Fluorescence ratios of individual cells can then be converted into pH values for live yeast samples using the following equation:

$$pH = pKa + n^{-1} \cdot \log\left(\frac{\left(\frac{r-\beta_l}{\beta_h-\beta_l}\right)}{\left(1 - \frac{r-\beta_l}{\beta_h-\beta_l}\right)}\right) \quad (5.3)$$

Appendix A

Quantification of CDC Commitment

Table A.1: Cell cycle Start commitment variables for natural oscillations in strain DBY12007, extracted from smoothing splines. Insufficient cells were classified as mothers or daughters during these runs to produce mother or daughter statistics.

T_c (min after HOC entry)	All cells
0-45 fL	24.2 ± 11.8
45-90 fL	25.7 ± 6.9
90-135 fL	22.5 ± 7.1
135-180 fL	25.6 ± 8.4
All sizes	22.6 ± 9.0
R_{max} (fraction/minute)	All cells
0-45 fL	0.0032 ± 0.0033
45-90 fL	0.0035 ± 0.0025
90-135 fL	0.0065 ± 0.00001
135-180 fL	0.0104 ± 0.0001
All sizes	0.0047 ± 0.0011
F_{max} (fraction)	All cells
0-45 fL	0.144 ± 0.158
45-90 fL	0.196 ± 0.143
90-135 fL	0.356 ± 0.067
135-180 fL	0.466 ± 0.235
All sizes	0.247 ± 0.028

Table A.2: Cell cycle Start commitment variables for natural oscillations in strain GZ240/241, extracted from smoothing splines.

T_c (min after HOC entry)	Mothers	Daughters	All cells
0-45 fL	28.4±24.5	14.7±5.4	14.2±5.7
45-90 fL	18.4±6.9	18.4±0.7	16.9±4.6
90-135 fL	15.4±0.4	8.5±2.5	14.1±0.6
135-180 fL	13.2±5.6	5.4±2.6	12.4±4.9
All sizes	14.4±4.4	13.7±2.0	14.2±3.5
R_{max} (fraction/min)	Mothers	Daughters	All cells
0-45 fL	0.0081± 0.0025	0.0020± 0.0005	0.0021± 0.0007
45-90 fL	0.0078±0.0032	0.0065±0.0014	0.0067±0.0018
90-135 fL	0.0095±0.0007	0.0057±0.0004	0.0075±0.0003
135-180 fL	0.0102±0.0004	0.0089±0.0013	0.0094±0.0002
All sizes	0.0090±0.0004	0.0041±0.0001	0.0058±0.0001
F_{max} (fraction)	Mothers	Daughters	All cells
0-45 fL	0.165±0.049	0.077±0.013	0.077±0.014
45-90 fL	0.293±0.054	0.224±0.013	0.225±0.041
90-135 fL	0.354±0.013	0.217±0.019	0.289±0.010
135-180 fL	0.437±0.062	0.278±0.022	0.408±0.054
All sizes	0.355±0.049	0.143±0.003	0.213±0.004

Table A.3: Cell cycle Start commitment variables for an induced HOC phase in strain GZ240/241, extracted from smoothing splines.

T_c (min after HOC entry)	Mothers	Daughters	All cells
0-45 fL	69.4	81.1	80.7
45-90 fL	33.1	34.3	32.5
90-135 fL	20.3	33.6	23.9
135-180 fL	20.1	19.2	19.7
All sizes	23.3	65.8	33.3
R_{max} (fraction/min)	Mothers	Daughters	All cells
0-45 fL	0.0076	0.0065	0.0068
45-90 fL	0.0108	0.0062	0.0081
90-135 fL	0.0155	0.0101	0.0123
135-180 fL	0.0105	0.0185	0.0106
All sizes	0.0103	0.0053	0.0055
F_{max} (fraction)	Mothers	Daughters	All cells
0-45 fL	0.469	0.336	0.348
45-90 fL	0.570	0.339	0.381
90-135 fL	0.644	0.442	0.588
135-180 fL	0.711	0.484	0.688
All sizes	0.576	0.334	0.393

Bibliography

- Baganz, F., Hayes, A., Marren, D., Gardner, D., and Oliver, S. (1998), “Suitability of replacement markers for functional analysis studies in *Saccharomyces cerevisiae*,” *Yeast*, 13, 1563–73.
- Ball, D. A., Marchand, J., Poulet, M., Baumann, W. T., Chen, K. C., Tyson, J. J., and Peccoud, J. (2011), “Oscillatory dynamics of cell cycle proteins in single yeast cells analyzed by imaging cytometry,” *PLoS ONE*, 6.
- Bieler, J., Cannavo, R., Gustafson, K., Gobet, C., Gatfield, D., and Naef, F. (2014), “Robust synchronization of coupled circadian and cell cycle oscillators in single mammalian cells.” *Molecular Systems Biology*, 10, 739.
- Brauer, M. and Huttenhower, C. (2008), “Coordination of growth rate, cell cycle, stress response, and metabolic activity in yeast,” *Molecular Biology of the Cell*, 19, 352–367.
- Brauer, M. J., Saldanha, A. J., Dolinski, K., and Botstein, D. (2005), “Homeostatic Adjustment and Metabolic Remodeling in Glucose-limited Yeast Cultures,” *Molecular Biology of the Cell*, 16, 2503–2517.
- Breunig, J. S., Hackett, S. R., Rabinowitz, J. D., and Kruglyak, L. (2014), “Genetic Basis of Metabolome Variation in Yeast,” *PLoS Genetics*, 10.
- Burnetti, A. J., Aydin, M., and Buchler, N. E. (2016), “Cell cycle Start is coupled to entry into the yeast metabolic cycle across diverse strains and growth rates,” *Molecular Biology of the Cell*, 27, 64–74.
- Cai, L., Sutter, B. M., Li, B., and Tu, B. P. (2011), “Acetyl-CoA induces cell growth and proliferation by promoting the acetylation of histones at growth genes.” *Molecular Cell*, 42, 426–37.
- Carter, B. L. A. and Jagdish, M. N. (1978), “The relationship between cell size and cell division in the yeast *Saccharomyces cerevisiae*,” *Experimental Cell Research*, 112, 15–24.

- Causton, H. C., Feeney, K. A., Ziegler, C. A., and O'Neill, J. S. (2015), "Metabolic cycles in yeast share features conserved among circadian rhythms," *Current Biology*, 25, 1056–1062.
- Chen, Z., Odstrcil, E. A., Tu, B. P., and McKnight, S. L. (2007), "Restriction of DNA replication to the reductive phase of the metabolic cycle protects genome integrity." *Science (New York, N.Y.)*, 316, 1916–9.
- Costanzo, M., Nishikawa, J. L., Tang, X., Millman, J. S., Schub, O., Breitkreuz, K., Dewar, D., Rupes, I., Andrews, B., and Tyers, M. (2004), "CDK activity antagonizes Whi5, an inhibitor of G1/S transcription in yeast," *Cell*, 117, 899–913.
- De Bruin, R. A. M., McDonald, W. H., Kalashnikova, T. I., Yates, J., and Wittenberg, C. (2004), "Cln3 activates G1-specific transcription via phosphorylation of the SBF bound repressor Whi5," *Cell*, 117, 887–898.
- Dimitrov, L. N., Brem, R. B., Kruglyak, L., and Gottschling, D. E. (2009), "Polymorphisms in multiple genes contribute to the spontaneous mitochondrial genome instability of *Saccharomyces cerevisiae* S288C strains," *Genetics*, 183, 365–383.
- Edgar, R. S., Green, E. W., Zhao, Y., van Ooijen, G., Olmedo, M., Qin, X., Xu, Y., Pan, M., Valekunja, U. K., Feeney, K. A., Maywood, E. S., Hastings, M. H., Baliga, N. S., Merrow, M., Millar, A. J., Johnson, C. H., Kyriacou, C. P., O'Neill, J. S., and Reddy, A. B. (2012), "Peroxisomes are conserved markers of circadian rhythms." *Nature*, 485, 459–64.
- Entian, K. D. and Kötter, P. (2007), "25 Yeast Genetic Strain and Plasmid Collections," *Methods in Microbiology*, 36, 629–666.
- Ewald, J. C., Kuehne, A., Zamboni, N., and Skotheim, J. M. (2016), "The Yeast Cyclin-Dependent Kinase Routes Carbon Fluxes to Fuel Cell Cycle Progression," *Molecular Cell*, 62, 532–545.
- Feillet, C., Krusche, P., Tamanini, F., Janssens, R. C., Downey, M. J., Martin, P., Teboul, M., Saito, S., Lévi, F. A., Bretschneider, T., van der Horst, G. T. J., Delaunay, F., and Rand, D. A. (2014), "Phase locking and multiple oscillating attractors for the coupled mammalian clock and cell cycle." *Proceedings of the National Academy of Sciences of the United States of America*, 111, 9828–33.
- Feillet, C., van der Horst, G. T. J., Levi, F., Rand, D. A., and Delaunay, F. (2015), "Coupling between the Circadian Clock and Cell Cycle Oscillators: Implication for Healthy Cells and Malignant Growth." *Frontiers in Neurology*, 6, 96.
- Gancedo, J. M. (1998), "Yeast Carbon Catabolite Repression Yeast Carbon Catabolite Repression," *Microbiology and Molecular Biology Reviews*, 62, 334–361.

- Garcia-Ochoa, F. and Gomez, E. (2009), “Bioreactor scale-up and oxygen transfer rate in microbial processes: An overview,” *Biotechnology Advances*, 27, 153–176.
- Gérard, C. and Goldbeter, A. (2012), “Entrainment of the mammalian cell cycle by the circadian clock: modeling two coupled cellular rhythms.” *PLoS Computational Biology*, 8, e1002516.
- Haase, S. B. and Reed, S. I. (2002), “Improved flow cytometric analysis of the budding yeast cell cycle.” *Cell cycle (Georgetown, Tex.)*, 1, 132–6.
- Hatzis, C. and Porro, D. (2006), “Morphologically-structured models of growing budding yeast populations,” *Journal of Biotechnology*, 124, 420–438.
- Hui, S., Silverman, J. M., Chen, S. S., Erickson, D. W., Basan, M., Wang, J., Hwa, T., and Williamson, J. R. (2015), “Quantitative proteomic analysis reveals a simple strategy of global resource allocation in bacteria.” *Molecular Systems Biology*, 11, 784.
- Isom, D., Sridharan, V., Baker, R., Clement, S., Smalley, D., and Dohlman, H. (2013), “Protons as second messenger regulators of G protein signaling,” *Molecular Cell*, 51, 531–538.
- Johnston, G. C., Prongle, J. R., and Hartwell, L. H. (1977), “Coordination of growth with cell division in the yeast {*Saccharomyces cerevisiae*},” *Experimental Cell Research*, 105, 79–98.
- Jules, M., François, J., and Parrou, J. L. (2005), “Autonomous oscillations in *Saccharomyces cerevisiae* during batch cultures on trehalose,” *FEBS Journal*, 272, 1490–1500.
- Kaspar von Meyenburg, H. (1969), “Energetics of the budding cycle of *Saccharomyces cerevisiae* during glucose limited aerobic growth.” *Archiv für Mikrobiologie*, 66, 289–303.
- Keulers, M., Suzuki, T., Satroutdinov, A. D., and Kuriyama, H. (1996), “Autonomous metabolic oscillation in continuous culture of *Saccharomyces cerevisiae* grown on ethanol.” *FEMS Microbiology Letters*, 142, 253–8.
- Klevecz, R. R., Bolen, J., Forrest, G., and Murray, D. B. (2004), “A genomewide oscillation in transcription gates DNA replication and cell cycle.” *Proceedings of the National Academy of Sciences of the United States of America*, 101, 1200–5.
- Klumpp, S., Zhang, Z., and Hwa, T. (2009), “Growth rate-dependent global effects on gene expression in bacteria.” *Cell*, 139, 1366–75.

- Kuang, Z., Cai, L., Zhang, X., Ji, H., Tu, B. P., and Boeke, J. D. (2014), “High-temporal-resolution view of transcription and chromatin states across distinct metabolic states in budding yeast.” *Nature Structural & Molecular Biology*, 21, 854–63.
- Kvarnström, M., Logg, K., Diez, A., Bodvard, K., and Käll, M. (2008), “Image analysis algorithms for cell contour recognition in budding yeast.” *Optics Express*, 16, 12943–12957.
- Lloyd, D. and Murray, D. B. (2005), “Ultradian metronome: timekeeper for orchestration of cellular coherence.” *Trends in Biochemical Sciences*, 30, 373–7.
- Lloyd, D. and Murray, D. B. (2007), “Redox rhythmicity: clocks at the core of temporal coherence.” *BioEssays : News and Reviews in Molecular, Cellular and Developmental Biology*, 29, 465–73.
- Lloyd, D., Salgado, L. E. J., Turner, M. P., Suller, M. T. E., and Murray, D. (2002), “Cycles of mitochondrial energization driven by the ultradian clock in a continuous culture of *Saccharomyces cerevisiae*.” *Microbiology*, 148, 3715–24.
- Longtine, M. S., McKenzie, A., Demarini, D. J., Shah, N. G., Wach, A., Brachat, A., Philippsen, P., and Pringle, J. R. (1998), “Additional modules for versatile and economical PCR-based gene deletion and modification in *Saccharomyces cerevisiae*,” *Yeast*, 14, 953–961.
- Lu, C., Brauer, M. J., and Botstein, D. (2009), “Slow Growth Induces Heat-Shock Resistance in Normal and Respiratory-deficient Yeast,” *Molecular Biology of the Cell*, 20, 891–903.
- Machné, R. and Murray, D. B. (2012), “The yin and yang of yeast transcription: elements of a global feedback system between metabolism and chromatin.” *PLoS one*, 7, e37906.
- Martegani, E., Porro, D., Ranzi, B. M., and Alberghina, L. (1990), “Involvement of a cell size control mechanism in the induction and maintenance of oscillations in continuous cultures of budding yeast.” *Biotechnology and Bioengineering*, 36, 453–9.
- Matsuo, T., Yamaguchi, S., Mitsui, S., Emi, A., Shimoda, F., and Okamura, H. (2003), “Control mechanism of the circadian clock for timing of cell division in vivo.” *Science (New York, N.Y.)*, 302, 255–9.
- Maxwell, C. S. and Magwene, P. M. (2017), “The quick and the dead: microbial demography at the yeast thermal limit,” *Molecular Ecology*.
- McCusker, J. H., Clemens, C. V., Stevens, D. A., and Davis, R. W. (1994), “*Saccharomyces cerevisiae*,” *Genetics*, 136, 1261–1269.

- Miesenböck, G., De Angelis, D. A., and Rothman, J. E. (1998), “Visualizing secretion and synaptic transmission with pH-sensitive green fluorescent proteins.” *Nature*, 394, 192–5.
- Mochan, E. and Pye, E. K. (1973), “Respiratory oscillations in adapting yeast cultures,” *Nature: New Biology*, 242, 177–179.
- Murphy, H. A., Kuehne, H. A., Francis, C. A., and Sniegowski, P. D. (2006), “Mate choice assays and mating propensity differences in natural yeast populations.” *Biology Letters*, 2, 553–6.
- Murray, D. B., Engelen, F., Lloyd, D., and Kuriyama, H. (1999), “Involvement of glutathione in the regulation of respiratory oscillation during a continuous culture of *Saccharomyces cerevisiae*,” *Microbiology*, 145, 2739–2745.
- Murray, D. B., Roller, S., Kuriyama, H., and Lloyd, D. (2001), “Clock control of ultradian respiratory oscillation found during yeast continuous culture,” *Journal of Bacteriology*, 183, 7253–7259.
- Murray, D. B., Klevecz, R. R., and Lloyd, D. (2003), “Generation and maintenance of synchrony in *Saccharomyces cerevisiae* continuous culture,” *Experimental Cell Research*, 287, 10–15.
- Nagoshi, E., Saini, C., Bauer, C., and Laroche, T. (2004), “Circadian gene expression in individual fibroblasts: cell-autonomous and self-sustained oscillators pass time to daughter cells,” *Cell*, 119, 693–705.
- Nasmyth, K. and Dirick, L. (1991), “The role of SWI4 and SWI6 in the activity of G1 cyclins in yeast.” *Cell*, 66, 995–1013.
- Nijkamp, J. F., van den Broek, M., Datema, E., de Kok, S., Bosman, L., Luttk, M. A., Daran-Lapujade, P., Vongsangnak, W., Nielsen, J., Heijne, W. H. M., Klaassen, P., Paddon, C. J., Platt, D., Kötter, P., van Ham, R. C., Reinders, M. J. T., Pronk, J. T., de Ridder, D., and Daran, J.-M. (2012), “De novo sequencing, assembly and analysis of the genome of the laboratory strain *Saccharomyces cerevisiae* CEN.PK113-7D, a model for modern industrial biotechnology.” *Microbial Cell Factories*, 11, 36.
- Ogas, J., Andrews, B., and Herskowitz, I. (1991), “Transcriptional Activation of CLN1, CLN2, and a Putative New G1 Cyclin (HCS26) by SWI4, a Positive Regulator of G1 -Specific Transcription,” *Cell*, 66, 1015–1026.
- O’Neill, J. S. and Reddy, A. B. (2011), “Circadian clocks in human red blood cells.” *Nature*, 469, 498–503.

- Papagiannakis, A., Niebel, B., Wit, E. C., and Heinemann, M. (2016), “Autonomous Metabolic Oscillations Robustly Gate the Early and Late Cell Cycle,” *Molecular Cell*, pp. 1–11.
- Porro, D., Martegani, E., Ranzi, B. M., and Alberghina, L. (1988), “Oscillations in continuous cultures of yeast: A segregated parameter analysis,” *Biotechnology and Bioengineering*, 32, 411–417.
- Robertson, J. B. (2009), “Shedding light on the yeast respiratory oscillation: using luciferase and visible light to investigate biological rhythms in yeast,” Ph.D. thesis, Vanderbilt University.
- Robertson, J. B., Stowers, C. C., Boczko, E., and Johnson, C. H. (2008), “Real-time luminescence monitoring of cell-cycle and respiratory oscillations in yeast.” *Proceedings of the National Academy of Sciences of the United States of America*, 105, 17988–93.
- Rolland, F., Winderickx, J., and Thevelein, J. M. (2002), “Glucose-sensing and-signalling mechanisms in yeast,” *FEMS Yeast Research*, 2, 183–201.
- Saldanha, A. J., Brauer, M. J., and Botstein, D. (2005), “Nutritional homeostasis in batch and steady-state culture of yeast,” *Molecular Biology of the Cell*, 16, 1–13.
- Satroutdinov, A. D., Kuriyama, H., and Kobayashi, H. (1992), “Oscillatory metabolism of *Saccharomyces cerevisiae* in continuous culture.” *FEMS Microbiology Letters*, 77, 261–7.
- Schaechter, M., Maaløe, O., and Kjeldgaard, N. O. (1958), “Dependency on Medium and Temperature of Cell Size and Chemical Composition during Balanced Growth of *Salmonella typhimurium*,” *Journal of General Microbiology*, 19, 592–606.
- Scheving, L. E., Burns, E. R., Pauly, J. E., and Tsai, T. H. (1978), “Circadian variation in cell division of the mouse alimentary tract, bone marrow and corneal epithelium.” *The Anatomical Record*, 191, 479–86.
- Schmoller, K. M., Turner, J. J., Koivomagi, M., and Skotheim, J. M. (2015), “Dilution of the cell cycle inhibitor Whi5 controls budding-yeast cell size,” *Nature*, 526, 268–272.
- Scott, M. and Hwa, T. (2011), “Bacterial growth laws and their applications,” *Current Opinion in Biotechnology*, 22, 559–565.
- Scott, M., Mateescu, E. M., Zhang, Z., and Hwa, T. (2010), “Interdependence of Cell Growth and Gene Expression: Origins and Consequences,” *Science*, 330, 1099–1102.

- Scott, M., Klumpp, S., Mateescu, E. M., and Hwa, T. (2014), “Emergence of robust growth laws from optimal regulation of ribosome synthesis.” *Molecular Systems Biology*, 10, 747.
- Shi, L. and Tu, B. P. (2013a), “Acetyl-CoA induces transcription of the key G1 cyclin CLN3 to promote entry into the cell division cycle in *Saccharomyces cerevisiae*.” *Proceedings of the National Academy of Sciences of the United States of America*, 110, 7318–7323.
- Shi, L. and Tu, B. P. (2013b), “Acetyl-CoA induces transcription of the key G1 cyclin CLN3 to promote entry into the cell division cycle in *Saccharomyces cerevisiae*.” *Proceedings of the National Academy of Sciences of the United States of America*, 110, 7318–7323.
- Shi, L., Sutter, B. M., Ye, X., and Tu, B. P. (2010), “Trehalose Is a Key Determinant of the Quiescent Metabolic State That Fuels Cell Cycle Progression upon Return to Growth,” *Molecular Biology of the Cell*, 21, 1982–1990.
- Sidorova, J. and Breeden, L. (1993), “Analysis of the SWI4/SWI6 protein complex, which directs G1/S-specific transcription in *Saccharomyces cerevisiae*.” *Molecular and Cellular Biology*, 13, 1069–77.
- Silverman, S. J., Petti, A. a., Slavov, N., Parsons, L., Briehof, R., Thiberge, S. Y., Zenklusen, D., Gandhi, S. J., Larson, D. R., Singer, R. H., and Botstein, D. (2010), “Metabolic cycling in single yeast cells from unsynchronized steady-state populations limited on glucose or phosphate.” *Proceedings of the National Academy of Sciences of the United States of America*, 107, 6946–51.
- Skotheim, J. M., Di Talia, S., Siggia, E. D., and Cross, F. R. (2008), “Positive feedback of G1 cyclins ensures coherent cell cycle entry.” *Nature*, 454, 291–6.
- Slavov, N. and Botstein, D. (2011), “Coupling among growth rate response, metabolic cycle, and cell division cycle in yeast.” *Molecular Biology of the Cell*, 22, 1997–2009.
- Slavov, N., Macinskas, J., Caudy, A., and Botstein, D. (2011), “Metabolic cycling without cell division cycling in respiring yeast.” *Proceedings of the National Academy of Sciences of the United States of America*, 108, 19090–19095.
- Slavov, N., Airoidi, E. M., van Oudenaarden, A., and Botstein, D. (2012), “A conserved cell growth cycle can account for the environmental stress responses of divergent eukaryotes.” *Molecular Biology of the Cell*, 23, 1986–97.
- Sohn, H. Y., Murray, D. B., and Kuriyama, H. (2000), “Ultradian oscillation of *Saccharomyces cerevisiae* during aerobic continuous culture: hydrogen sulphide mediates population synchrony.” *Yeast (Chichester, England)*, 16, 1185–90.

- Tu, B. P. and McKnight, S. L. (2007), “The yeast metabolic cycle: insights into the life of a eukaryotic cell.” *Cold Spring Harbor Symposia on Quantitative Biology*, 72, 339–43.
- Tu, B. P., Kudlicki, A., Rowicka, M., and Mcknight, S. L. (2005), “Logic of the Yeast Metabolic Cycle: Temporal Compartmentalization of Cellular Processes,” *Science*, 310, 1152–1159.
- Tu, B. P., Mohler, R. E., Liu, J. C., Dombek, K. M., Young, E. T., Synovec, R. E., and McKnight, S. L. (2007), “Cyclic changes in metabolic state during the life of a yeast cell.” *Proceedings of the National Academy of Sciences of the United States of America*, 104, 16886–91.
- Turner, J. J., Ewald, J. C., and Skotheim, J. M. (2012), “Cell size control in yeast,” *Current Biology*, 22, R350–R359.
- Tyson, C. B. and Lord, P. G. (1979), “Dependency of size of *Saccharomyces cerevisiae* cells on growth rate.” *Journal of Bacteriology*, 138, 92–98.
- van Dijken JP, Bauer, J., Brambilla, L., Duboc, P., Francois, J., Gancedo, C., Giuseppin, M., Heijnen, J., Hoare, M., Lange, H., Madden, E., Niederberger, P., Nielsen, J., Parrou, J., Petit, T., Porro, D., Reuss, M., van Riel N, Rizzi, M., Steensma, H., Verrips, C., Vindeløv, J., and Pronk, J. (2000), “An interlaboratory comparison of physiological and genetic properties of four *Saccharomyces cerevisiae* strains.” *Enzyme And Microbial Technology*, 26, 706–714.
- Van Maris, A. J. A., Bakker, B. M., Brandt, M., Boorsma, A., Teixeira De Mattos, M. J., Grivell, L. A., Pronk, J. T., and Blom, J. (2001), “Modulating the distribution of fluxes among respiration and fermentation by overexpression of HAP4 in *Saccharomyces cerevisiae*,” *FEMS Yeast Research*, 1, 139–149.
- Wang, G. Z., Hickey, S. L., Shi, L., Huang, H. C., Nakashe, P., Koike, N., Tu, B. P., Takahashi, J. S., and Konopka, G. (2015), “Cycling Transcriptional Networks Optimize Energy Utilization on a Genome Scale,” *Cell Reports*, 13, 1868–1880.
- Wang, T. A., Yu, Y. V., Govindaiah, G., Ye, X., Artinian, L., Coleman, T. P., Sweedler, J. V., Cox, C. L., and Gillette, M. U. (2012), “Circadian rhythm of redox state regulates excitability in suprachiasmatic nucleus neurons.” *Science (New York, N.Y.)*, 337, 839–42.
- Xu, Z. and Tsurugi, K. (2007), “Destabilization of energy-metabolism oscillation in the absence of trehalose synthesis in the chemostat culture of yeast,” *Archives of Biochemistry and Biophysics*, 464, 350–358.
- You, C., Okano, H., Hui, S., Zhang, Z., Kim, M., Gunderson, C. W., Wang, Y.-P., Lenz, P., Yan, D., and Hwa, T. (2013), “Coordination of bacterial proteome with metabolism by cyclic AMP signalling,” *Nature*, 500, 301–306.

Zhao, G., Chen, Y., Carey, L., and Futcher, B. (2016), “Cyclin-Dependent Kinase Coordinates Carbohydrate Metabolism and Cell Cycle in *S. cerevisiae*,” *Molecular Cell*, 62, 546–557.

Biography

Anthony James Burnetti was born in Washington, D.C. on May 26, 1989. He obtained his B.S. degree in Cell Biology and Molecular Genetics with a minor in Astronomy from the University of Maryland at College Park in May 2011. Anthony began his PhD studies in the Cell and Molecular Biology program at Duke University in August 2011, participating in the James Duke Fellowship and the Chancellor's Scholar program. He joined the University Program in Genetics and Genomics and the laboratory of Dr. Nicolas Buchler, studying the relationship between the yeast metabolic cycle and cell division cycle in budding yeast as a model for coupled biological oscillations. He is interested in how multiple biological oscillators with varied periods and functions coexist within the same cell, influencing and coupling to each other.

Publications: Burnetti, A.J., Aydin, M. & Buchler, N.E. Cell cycle Start is coupled to entry into the yeast metabolic cycle across diverse strains and growth rates. *Mol. Biol. Cell* 27, 6474 (2016).